

AUG 24 1992

RIFTING AND VOLCANISM IN THE NORTHERN MARIANA TROUGH:

A SeaMARC II AND SEISMIC REFLECTION STUDY

A thesis submitted to the Graduate Division of the University of Hawaii
in partial fulfillment of the requirements for the degree of

MASTER OF SCIENCE

IN

GEOLOGY AND GEOPHYSICS

MAY 1992

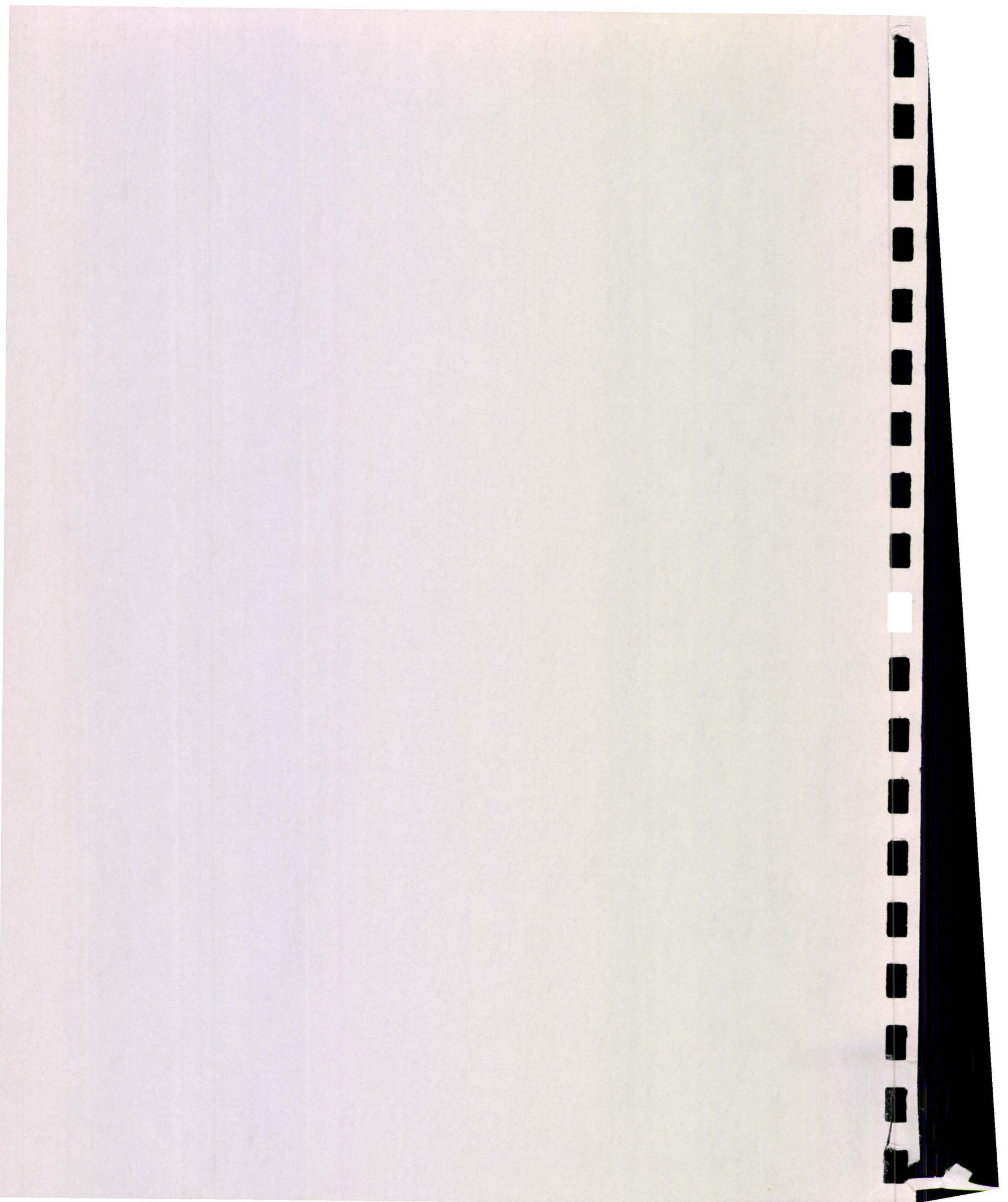
by

Nancy Allison Baker

Thesis Committee:

Patricia Fryer, Chairperson
Frederick K. Duennebier
Fernando Martinez
Alexander N. Shor

Return to
School of Ocean and
Earth Science and Technology
LIBRARY





RIFTING AND VOLCANISM IN THE NORTHERN MARIANA TROUGH:

A SeaMARC II AND SEISMIC REFLECTION STUDY

A thesis submitted to the Graduate Division of the University of Hawaii
in partial fulfillment of the requirements for the degree of

MASTER OF SCIENCE

IN

GEOLOGY AND GEOPHYSICS

MAY 1992

by

Nancy Allison Baker

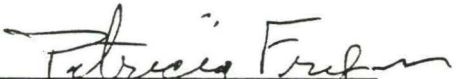
Thesis Committee:

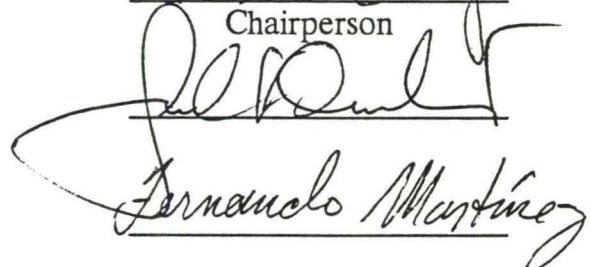
Patricia Fryer, Chairperson
Frederick K. Duennebier
Fernando Martinez
Alexander N. Shor

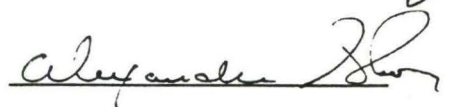
Return to
School of Ocean and
Earth Science and Technology
LIBRARY

We certify that we have read this thesis and that, in our opinion, it is satisfactory in scope and quality as a thesis for the degree of Master of Science in Geology and Geophysics.

THESIS COMMITTEE


Chairperson





DEDICATION

This thesis is dedicated to the memory of my father,

Bill Cosdon,

whose playful spirit
and love of life

even in the face of death,

gave me both the courage
and the strength

to finally finish
what I had started.

ACKNOWLEDGEMENTS

The completion of this thesis has been a long and arduous trail, as Frank Trusdell put it so well. I wish to thank first the people who started me on this path: Isador Elias, my community college physics professor, for teaching me that science can be fun; my little big sister Terri, for my first introduction to geology (against my own will at first!); and my husband Mike, for choosing Hawaii as his favorite graduate school. After my arrival in Hawaii, George Walker's quest to understand volcanoes, and Fred Duennebier's enthusiasm for research at sea infected me with the desire to go on to grad school after I finished my B.S.

Many people deserve thanks for influencing and funding my graduate work. Mike Garcia provided me with National Science Foundation (NSF) funds for my first research experience, and gave me the opportunity to fulfill my fantasy of playing along hot lava flows. Dick Hey sponsored my first presentation at a scientific meeting, and Rick Hagen saw to it that "the paper that wouldn't go away" was finally published. The geology department allowed me to try my hand at teaching for a year, satisfying one important goal of my graduate education. Rachel Laudan's expertise in the history of geology added an important new perspective to my views of geological research. Sandy Shor and the SeaMARC II group kept me employed during several research cruises, and at the same time allowed me the opportunities to practice celestial navigation, be the first woman to carry "the can", experience a hurricane at sea, and go

on an excellent adventure in Europe with my husband. An ARCS (Achievement Rewards for College Scientists) Scholarship kept me from starving when no other funds were available to me. And finally, NSF funding through my advisor Patty Fryer saw this project to its completion.

Karen Sender's dedication to helping SeaMARC II data users ensured that the SeaMARC II side-scan data were reprocessed, along with the help of Les Kajiwara. Many thanks to Clyde Nishimura during our marathon magnetic tape reading week, and for providing his computer wizardry in producing a new flat bottom table for reprocessing the SeaMARC II phase data; to Steve Miller of UCSB for use of his bathymetry gridding and contouring routines; to Paul Wessel for the use of the GMT (Generic Mapping Tool) programs; to Fernando Martinez, Bruce Applegate, Devi Joseph, Adam Klaus and Jill Wessel for helping me learn to use these programs; to Jill Wessel for use of the AZFAR program for computing the length and azimuth of digitized fault data; and to Margo Edwards for mean, variance and high/low values routines. Thanks to Brooks Bays, who drafted the final hand-contoured bathymetry maps, Tom Tatnall and Ev Wingert for photographing the side-scan images, Ruth Wilmoth (and Rachel too!) for help with drafting, photography and paste-up, to my sister Terri for rescuing me the night before my defense, and to Wendy Zayac for helping me finish.

I am grateful to Fernando Martinez, Patty Fryer, Fred Duennebier, Sandy Shor, Adam Klaus, Brian Taylor, Dick Hey, Greg Moore, Rodey Batiza, Margo Edwards, Wendy Zayac, Rick Hagen, Mary MacKay, Glenn Brown, and Toshitsugu Yamazaki for many helpful discussions about rifting and spreading processes in general, and the interpretation of my data. A very special thanks to Toshitsugu Yamazaki and the Geological Survey of Japan for allowing us unrestricted use of their 3.5 kHz data.

My mental health was maintained by many friends and students, and with the fear of accidentally omitting someone, I will say thank you to everyone (especially my house mates, office mates and other inmates of the zoo) who listened to me rant and rave about life as a grad student; and thanks to the ferocious bunny (I mean you, rabbit!) for not killing me. Thanks to Diane and to Hospice, for helping me through my most difficult hours this last year. I am most grateful to the innkeepers at the Manoa Hilton for the upkeep of my physical, and more importantly, emotional well being. My utmost appreciation goes to my family: to my husband Mike, both for his help and for having faith that I would finally make it all the way to the beach, to Bill, Judy, Phyllis, Terri, Eric, Marilyn, Kevin and Ken for their love, support and understanding during my more-than-a-decade as a college student.

ABSTRACT

Reprocessed SeaMARC II imagery and seismic reflection profiles of the northern Mariana Trough from 21°30'N to 23°15'N show a progressive evolution of rifting in this backarc basin. Near 24°N the West Mariana Ridge (the remnant arc) and the Mariana Ridge (the active arc) meet, whereas near 21°30'N the trough separating the arcs is about 135 km wide.

In plan view, the structural style of rift boundary faults differs along strike; *en echelon*, zig-zag and curvilinear fault geometries are all observed along the rift boundary. Fault traces on the basin floor have one preferred orientation along strike of the rift basin. The basin is broken into 10 to 15 km wide blocks by large-offset (>100m) normal faults. Small offset faults (<100m) are superimposed onto this fault block terrain, producing both *en echelon* and anastomosing lineaments in the acoustic image.

Recent volcanism is nearly continuous along and generally restricted to a 6 to 20 km wide, rift-parallel zone on the east (arc) side of the basin. A high diversity of volcanic landforms, including arc volcanoes and elongate ridges, is found along this zone. A model of asymmetric extension is proposed for the opening of the basin, contrary to an earlier model which described this area as the transition from rifting to seafloor spreading. This transition is now proposed to occur more than 100 km south of this location.

TABLE OF CONTENTS

Acknowledgements	iv
Abstract	vii
List of Tables	x
List of Figures	xi
CHAPTER 1: Introduction	1
CHAPTER 2: Data Acquisition and Analysis Methods	7
Data Acquisition	7
Data Processing	8
Bathymetry	8
Side-Scan	11
Seismic Data	16
Geologic Map Construction	16
Analysis of Fault and Lineament Orientations	23
Bias in SeaMARC II Data arising from look-direction	25
CHAPTER 3: Data Description and Geologic Interpretation	28
The survey area	28
Major Structural Provinces	28
Remnant Arc Margin	31
Active Arc Margin	32
East Boundary Fault Zone	33
Nikko Seamount	34

Basin Floor	41
North Province	41
Central Province	45
South Province	51
Southwest Basin	51
Central fault-block terrain	51
Volcanic-tectonic zone	55
CHAPTER 4: Analysis of Faulting Patterns	58
Azimuth orientations	58
Faulting models	67
Estimating extension direction	69
CHAPTER 5: Implications for Models of Structural Development	71
The volcanic-tectonic zone	71
Elevation of Central Province	76
On the Rift to Spreading transition	79
A tectonic cartoon	88
Conclusions	90
References	93

LIST OF TABLES

1. Fault azimuth analysis results (8 zones) 59

2. Fault azimuth analysis results (combined zones) 61

LIST OF FIGURES

1. Location and tectonic setting of the Mariana Island Arc	2
2. Bathymetry of the Northern Mariana Island Arc	3
3. Distribution of bathymetry data points	10
4A. Color bathymetric map of the survey area	12
4B. Location map of profiles and rock dredges	13
5A. "Normalized" SeaMARC II side-scan sonar acoustic image	14
5B. "Ramped" SeaMARC II side-scan sonar acoustic image	15
6A. Mixed frequency single-channel seismic reflection profiles 1-10	17
6B. Mixed frequency single-channel seismic reflection profiles 11-21	18
7. Profiles across the Northern Mariana Trough traced from 3.5 kHz data .	19
8. Geologic interpretation map of the area surveyed.	20
9. Effect of SeaMARC II look-direction on fault interpretations	26
10. Location map of structural provinces and place names	29
11. Perspective block diagram of the survey area	30
12A. Bathymetry of Fukuyama Seamount and the East Border Fault Zone .	35
12B. Side-scan and interpretation of Fukuyama Seamount and the EBFZ . .	36
13A. Bathymetry of Nikko Seamount and surrounding area	37
13B. Side-scan and interpretation of Nikko Seamount	38
14A. Bathymetry of North Province and Seamount A	42
14B. Side-scan and interpretation of North Province and Seamount A	43
15A. Bathymetry of Central Province volcanic-tectonic zone.	46

15B. Side-scan and interpretation of Central Province	47
16A. Bathymetry of South Province fault-block terrain	52
16B. Side-scan of South Province fault-block terrain	53
16C. Interpretation of South Province fault-block terrain	54
17. Percent frequency histograms of fault azimuth data	62
18. Sector diagrams of West Boundary Fault Zone (WBFZ)	64
19. Sector diagrams of East Boundary Fault Zone (EBFZ)	65
20. Sector diagrams of basin floor faults	66
21. Lithospheric strength model of Kusznir and Park (1987)	75
22. Rift to spreading transition model of the Northern Red Sea	81
23. A tectonic cartoon of the rifting of the Northern Mariana Trough	89
24. Tectonic sketch map of the survey area	91

CHAPTER 1: Introduction

The processes and mechanisms associated with the opening of backarc basins are not fully understood. The Mariana Trough is one of the few backarc basins that shows a transition from rifting (extensional faulting) to seafloor spreading (crustal accretion). The transition was previously proposed to occur in the northern part of the basin, near 22°N. This study, based on SeaMARC II side-scan images and bathymetry, single-channel seismic profiles, and 3.5 kHz echo soundings, proposes a new interpretation of the region. Instead, an asymmetric rifting model is preferred.

The Mariana arc-trench system is located south of Japan, where the western edge of the Pacific plate is subducting beneath the Philippine sea plate (Figure 1). The West Mariana Ridge (a remanent arc) and the Mariana Island Arc (an active volcanic arc) bound the crescent-shaped backarc basin known as the Mariana Trough (Figure 2). The trough is widest at about 18°N, and narrows northward to 24°N where the remanent arc and active arc join at the Bonin Arc. Thick volcanoclastic sediments (locally up to 2 km) shed from the arc cover the eastern part of the trough, and the western region is characterized by complex topography (Karig et al., 1978; Bibee et al., 1980).

Karig (1971) presented the first geological evidence for extension in the Mariana Trough at 18°N: (1) an axial bathymetric high with comparatively little

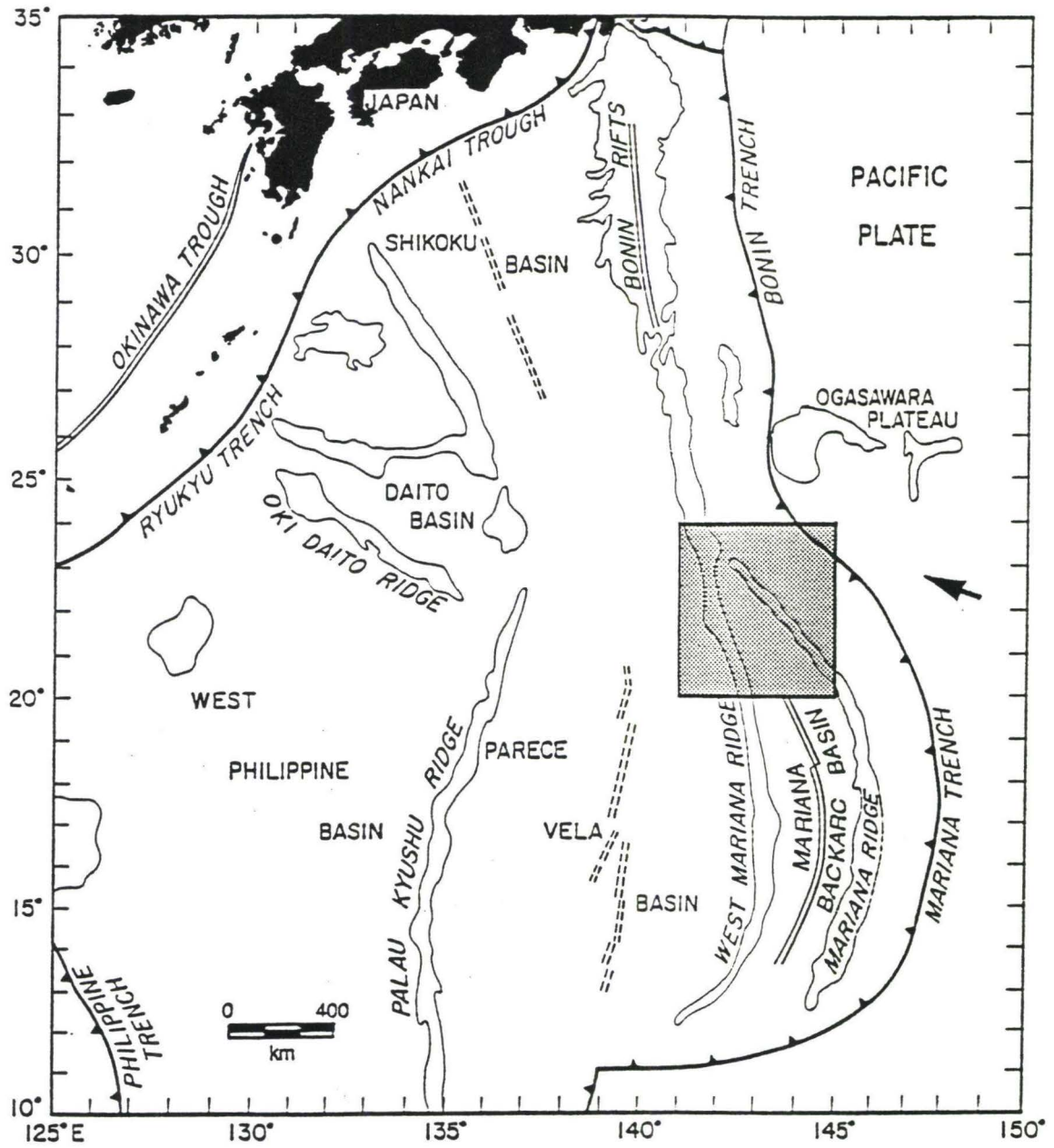


Figure 1 Location and tectonic setting of the Mariana Island Arc (from Wessel, 1991). The arrow shows the relative motion of the Pacific plate subducting beneath the Philippine plate (Moore, 1984). The location of Figure 2 is indicated by the shaded region.

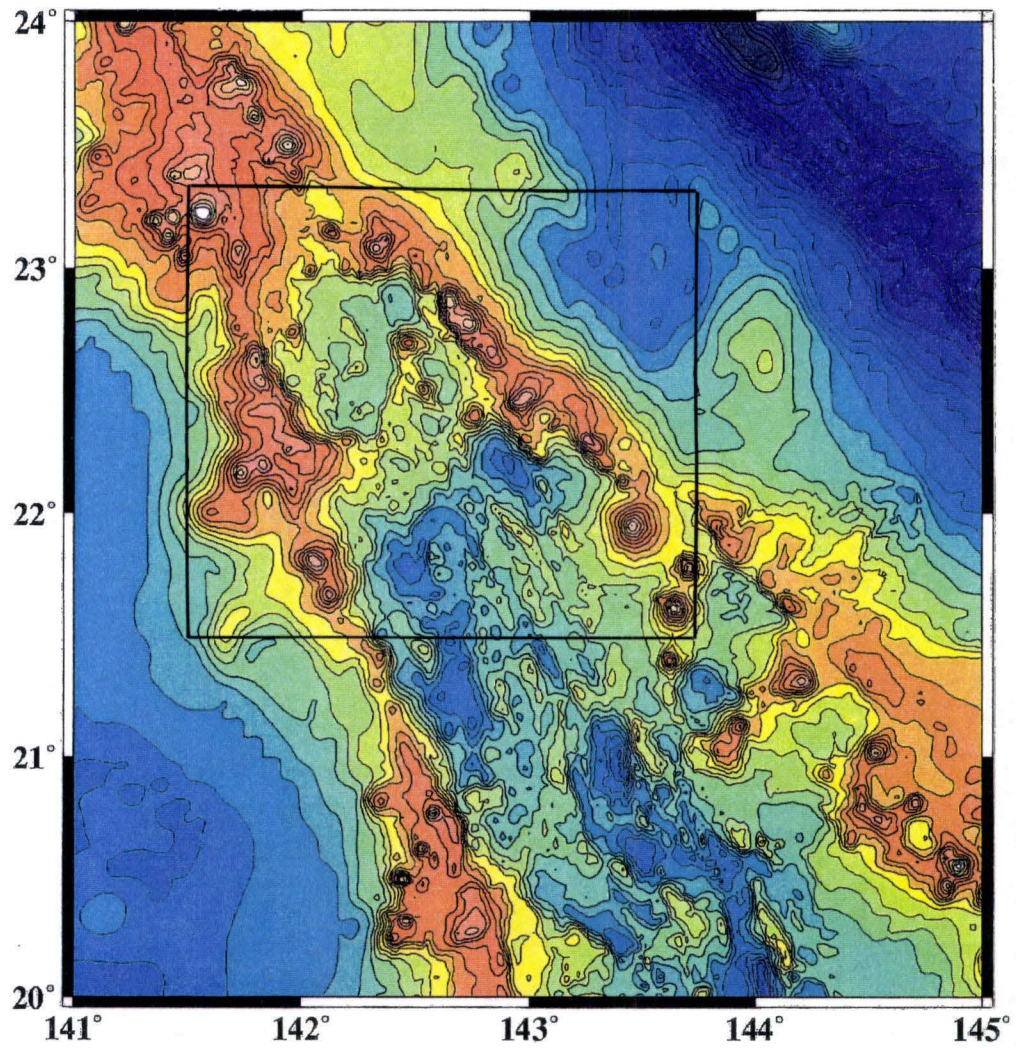


Figure 2 Bathymetry of the Northern Mariana Island Arc compiled from SeaMARC II data and 3.5 kHz soundings, gridded at 1 km spacing, and contoured at 200 meter interval. Location of Figure 3 is indicated by the box.

sediment cover, and (2) sampling of young pillow basalts on the axis. The first attempts to identify symmetric spreading anomaly patterns (Karig, 1971; Anderson, 1975; Karig et al., 1978) were unsuccessful. Later, Bibee et al. (1980) successfully correlated observed and synthetic magnetic anomalies near 18°N assuming a half-rate of 1.5 cm/yr for the last 3 million years, though Eguchi (1984) argued that their fit was "not totally convincing". Results from the Deep Sea Drilling Project Leg 60 imply a symmetric spreading rate of 2.15 cm/yr from three drill holes across the trough at latitude 18°N (Hussong and Uyeda, 1981). Hussong and Uyeda (1981) suggest the rifting of the old Mariana arc began in the latest Miocene, and continued at a constant rate. Other ages proposed for the opening of the Mariana Trough are 3 Ma (Karig et al., 1975), 8 Ma (Bibee et al., 1980), and less than 10 Ma (Eguchi, 1984).

The morphology of the central trough has been described as analagous to a slow-spreading mid-ocean ridge (Hussong and Fryer, 1981). Extremely variable heat flow measurements, a pattern characteristic of active oceanic spreading ridges, have been recorded in the trough (Anderson, 1975; Hobart et al., 1979). However, the axial spreading zone is difficult to characterize because it is quite variable along the axis of the basin, and topographic symmetry adequate to identify a central zone of rifting and volcanism is seldom observed (Karig, 1978). In more recent studies, a well-defined spreading axis has been documented near 18°N (Fryer and Hussong, 1982; Lonsdale and Hawkins, 1985). A Sea Beam

investigation mapped seven discrete ridges interpreted as spreading segments separated by lateral offsets and transforms between 15°N and 17°30'N (Barone et al., 1990). Based on multi-beam bathymetry data collected throughout the trough, Smoot (1990) concluded the spreading system is diffuse because of the absence of a well-defined topographic feature identifiable as a spreading center. However, Hagen et al. (1992) have recently published new SeaMARC II evidence for the locus of a discrete spreading axis in the southern Mariana Trough (near 13°45'N). Martinez et al. (1992) suggest from new sampling, narrow-beam bathymetry, echo soundings, and preexisting SeaMARC II data, that seafloor spreading may be well-organized within some locations of the trough between 19°30'N and 14°50'N.

Hussong and Fryer (1982) postulated that the Mariana Trough has undergone an early stage of stretching, resulting in a 60 km wide region of fault-controlled terraces on both sides of the basin. The trough narrows to the north as the arcs converge. In this northern region of the trough, early stages of rifting are suggested (Stern et al., 1984; Beal, 1987). Since this region shows evidence of extension (Beal, 1987; Baker et al., 1989) but not formation of new lithosphere (Murakami et al., 1989), a transition between rifting and spreading must exist somewhere between 24°N and 18°N. The location of this transition has been subject to debate. In a previous analysis of the SeaMARC II survey used in this study, Beal (1987) proposed the transition to be at 22°N. Based on

magnetic modeling, Yamazaki et al. (1991) conclude that the trough develops from a rifting stage to a spreading stage at about 22°N , in agreement with Beal's (1987) hypothesis. The evidence presented in this paper suggests that the transition is south of $21^{\circ}30'\text{N}$. In fact, the transition has recently been postulated to occur between $19^{\circ}30'\text{N}$ and 20°N (Martinez et al., 1992; Fryer et al., 1992).

CHAPTER 2: Data Acquisition and Analysis Methods

Data Acquisition

The primary data set for this study was collected by the Hawaii Institute of Geophysics from May 21 to 25, 1984, on the Research Vessel Kana Keoki (cruise KK84/04/28-01). A geophysical survey was conducted in the Northern Mariana Trough between 21°35'N 142°E and 23°15'N 143°20'E, collecting SeaMARC II data, 3.5 kHz profiles, analog mixed-frequency single channel seismic profiles (using a 120 in³ air gun), gravity, and magnetics data. SeaMARC II is a long-range seafloor mapping system capable of collecting side-scan sonar and bathymetric data simultaneously. Detailed system description, data logging and processing information (Blackinton, et al., 1983; Hussong and Fryer, 1983; Sender et al., 1989; Matsumoto, 1990; Shor, 1990; Hagen et al., 1991; Naar et al., 1991; Bergersen, 1991) and comparison to other seafloor mapping systems (Vogt and Tucholke, 1986; Davis et al., 1987; Tyce, 1987) have previously been described.

Navigation during the survey was based on Loran C and Sat Nav transit satellite fixes. Post-cruise navigation adjustments were made by checking the SeaMARC II data for coregistration of recognizable features on overlapping data swaths, and continuity of features along adjacent shiptracks. Significant adjustments were required because of a problem with time logged on Loran C

navigation. Shiptracks without overlapping swaths may therefore have navigational errors of a kilometer or more.

All data from this survey, with the exception of the gravity and magnetics (presented in a separate paper by Martinez) were examined for this study. In addition to data collected by HIG, the Geological Survey of Japan (GSJ) supplied 3.5 kHz data (both analog profiles and digitized depth data) collected aboard the R/V Hakurei-maru on five separate cruises (GH79-2, GH85-3, GH87-1, GH88-1, GH88-3) in the Northern Mariana region. Sources for rock dredge information used for the purpose of ground truth of the acoustic image are: Jackson, 1989; Bloomer et al., 1989; and P. Fryer, unpublished data, Kana Keoki cruise KK84/04/28-1.

Data Processing

Bathymetry

SeaMARC II phase data were reprocessed in 1991. Flat areas within the survey region were selected, and data from these areas were used to create 14 new angle-angle tables that relate phase angle differences and travel times to depth-range pairs by geometrical ray path approximation, assuming a flat bottom. These tables were created and averaged together by Clyde Nishimura and the resultant table was used to process the entire data set. The data were filtered (by median and frequency input response) to reduce the excessive noise before

merging with the navigation, and then plotted on a Tektronix color plotter at 1:200,000 scale for manual construction of the mosaic. Both SeaMARC II swath bathymetry and GSJ 3.5 kHz soundings were hand contoured using a 100 meter contour interval to aid in structural interpretation of the side-scan data. The close-up bathymetry figures in Chapter 3 were drafted from the hand-contoured map.

The filtered SeaMARC II bathymetry data were gridded (125 m spacing) using a nearest neighbor algorithm (Davis, 1986; code written by S. Miller of UC Santa Barbara) for incorporation into a digital bathymetric data base. The final digital bathymetry was compiled and filtered by Fernando Martinez using the SeaMARC II grid, shiptrack data from the Lamont-Doherty Geophysical Data Base, and GSJ 3.5 kHz data. The data were filtered and smoothed using a Fourier transform technique to remove noise with wavelengths less than 4 km. The "noise" grid was then truncated to include only those signals less 40 m; the 40 m cut-off was determined by examining the mean and standard deviations of the "noise" grid. This truncated "noise" grid was then added back to the smoothed version to produce the final 0.5 minute bathymetric grid. GSJ navigation points were adjusted by the difference between Tokyo and North American datums before combining the data sets. Location and distribution of data points from the two main data sets are shown in Figure 3. The data base was compiled, filtered, gridded and contoured using GMT V.2 (Generic Mapping

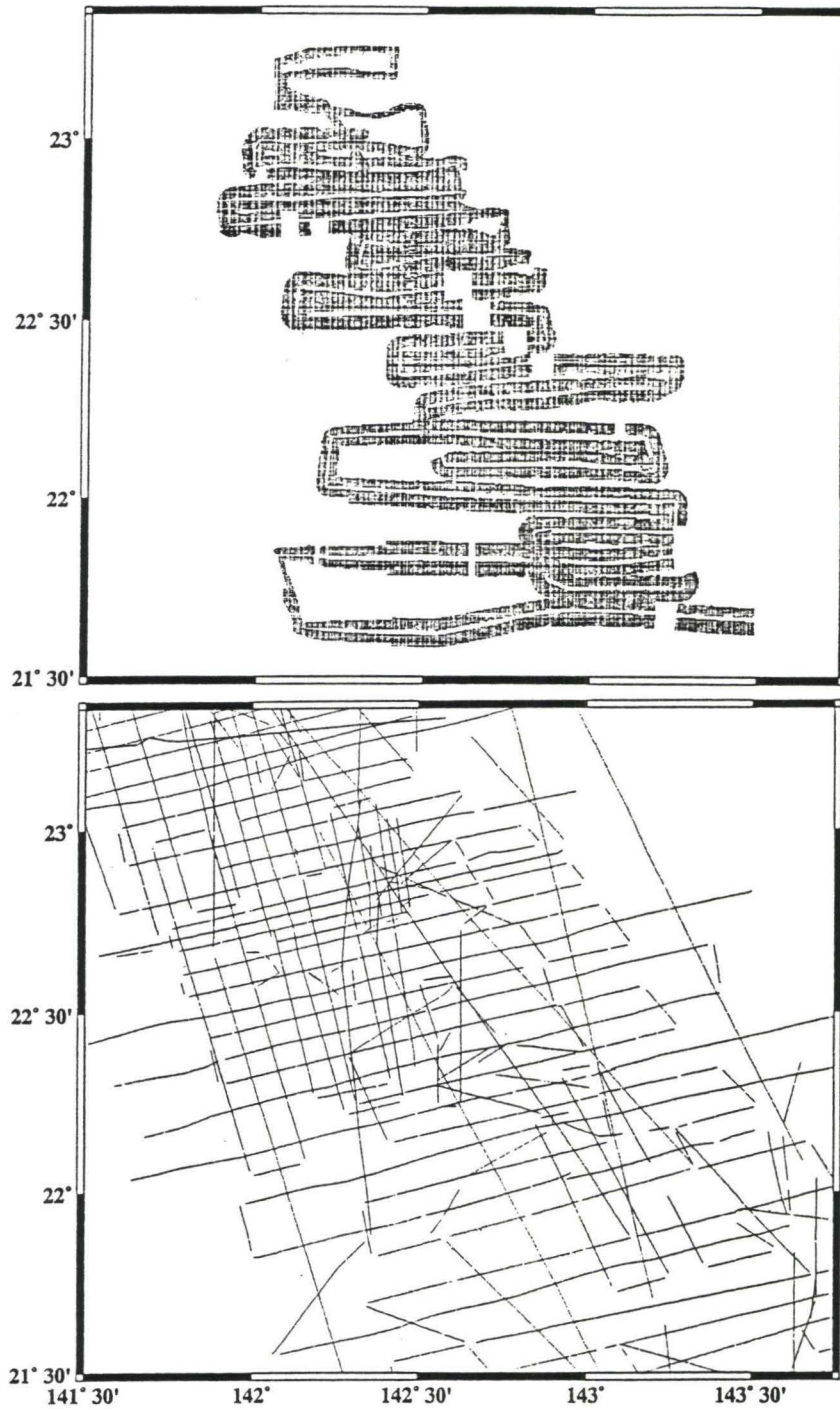


Figure 3 Distribution of bathymetry data points used to create the contour map shown in Figure 4. Top figure shows gridded SeaMARC II swath data. Blank stripes down the center of each swath represent the inner 10 degrees on each side of nadir where data are not collected; square data gaps resulted from 9-track tape read failures; the four northernmost shiptracks have data only on the starboard side because of a malfunction during data collection. The lower figure shows location of GSJ 3.5 kHz soundings.

Tool) software (Wessel and Smith, 1991) on a Sun workstation. The final 100m contour map of the gridded data set is illustrated in Figure 4.

Side-scan

The SeaMARC II data were first processed in 1986 and presented in a Master's Thesis by Beal (1987). The side-scan data were reprocessed for this study in 1990 and 1991 by SeaMARC II data manager Karen Sender, assisted by data technician Les Kajiwara. Two processing techniques, referred to as the "normalized" and "ramped" techniques, were both applied to the side-scan data (Figure 5). The "normalized" technique is used to compare regional-scale changes in bottom roughness by attempting to preserve true relative amplitude levels throughout the survey (i.e. removal of gain level changes introduced during collection and processing). The "ramped" technique maximizes local contrasts in backscatter intensities by applying the full range of grey tones available on the Raytheon plotter to the intensity-level changes within 15 minutes of data. This process improves the user's ability to resolve local structures of the ocean floor, however, it makes the comparison of absolute backscatter intensities throughout the entire survey impossible (Sender et al., 1989). Side-scan data were merged with navigation, gridded at 50 m spacing, and plotted at 1:400,000 scale for the final images. The working mosaic used for interpretation was constructed by hand at 1:200,000.

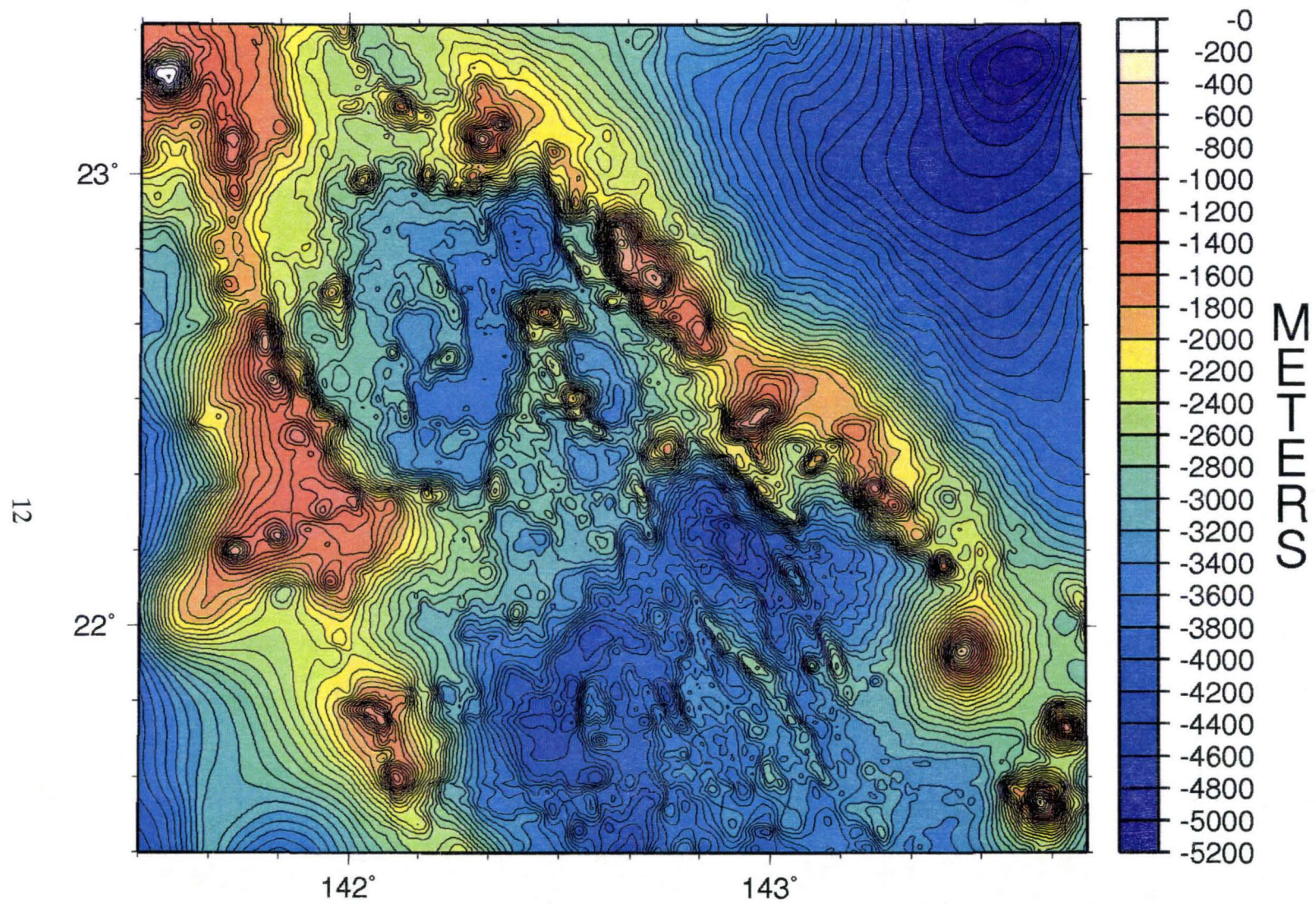


Figure 4A Color bathymetric map of the survey area compiled from SeaMARC II data and 3.5 kHz soundings, gridded at 500m spacing and contoured at 100 meter interval. Color change is every 200 meters.

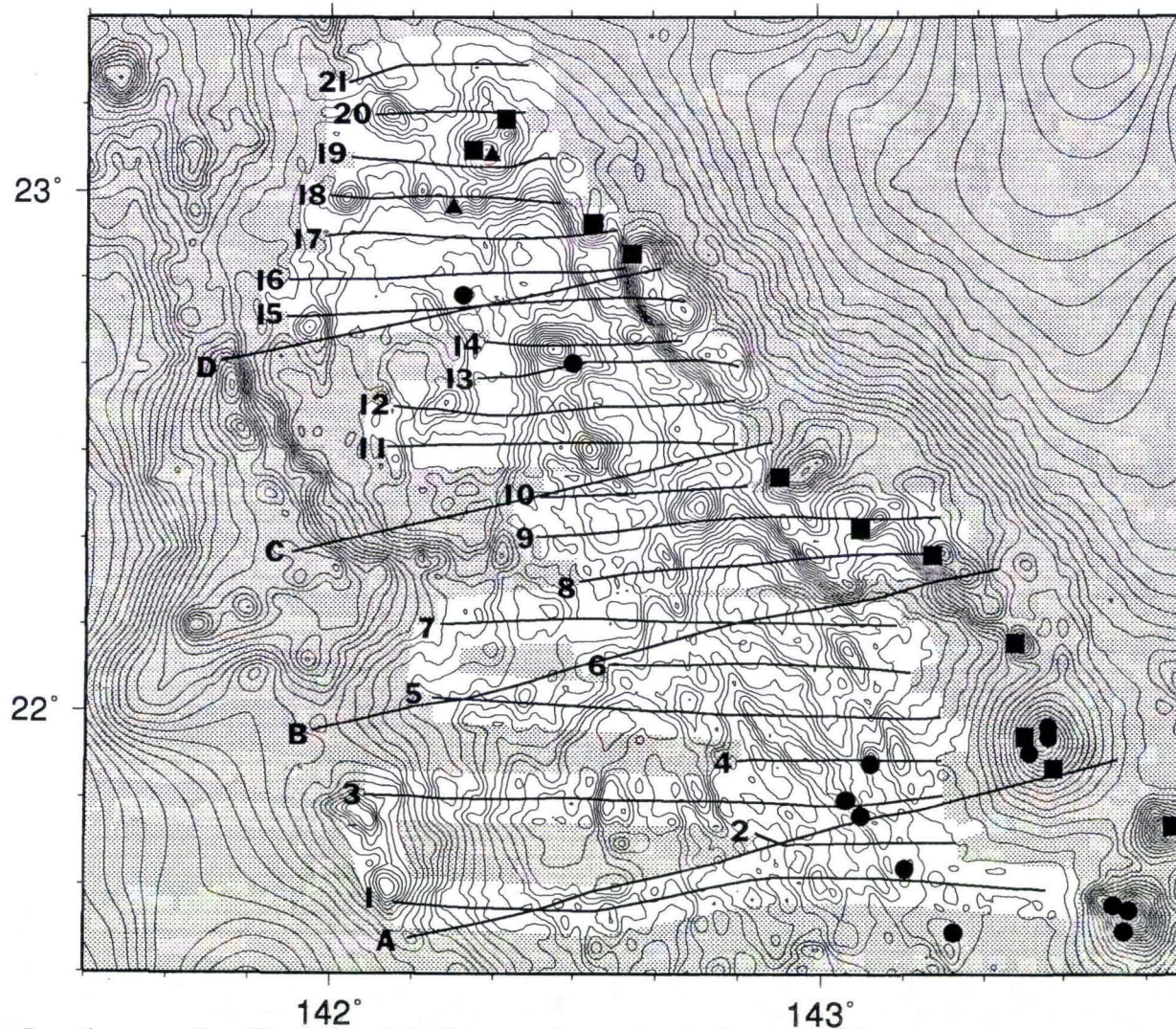


Figure 4B Location map of profiles and rock dredges superimposed on bathymetry of the survey area, contoured as in figure 4A. Lines numbered 1-21 show location of HIG single-channel seismic reflection and 3.5 kHz profiles in Figure 6. Lines lettered A-D show the location of GSI 3.5 kHz profiles in Figure 7. The non-shaded region indicates coverage of SeaMARC II backscatter data. Black symbols illustrate rock dredge locations. Dredge data sources: circles--Jackson, 1989; squares--Stern and Bloomer, 1989; triangles--P. Fryer, unpublished data.

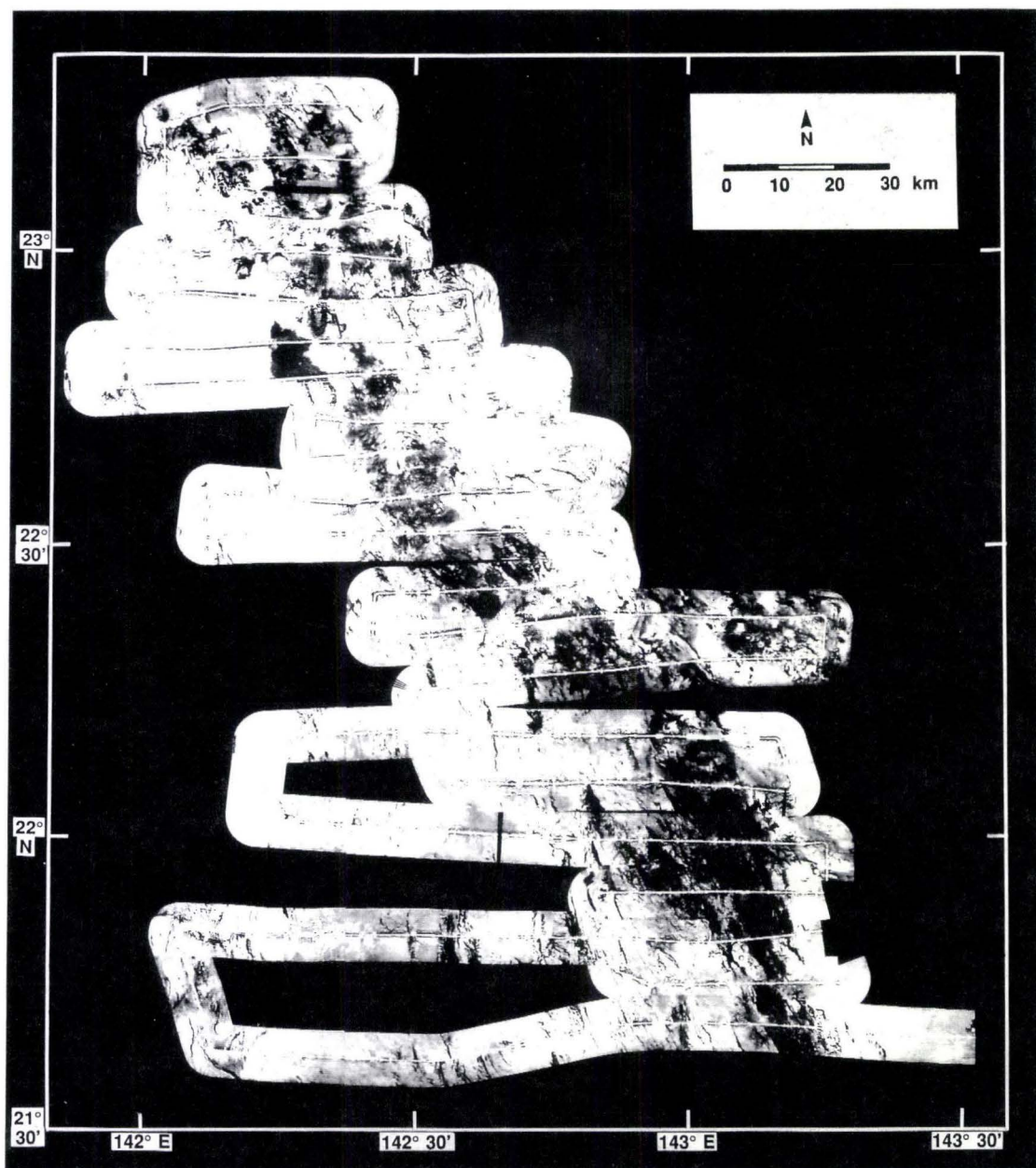


Figure 5A "Normalized" SeaMARC II side-scan sonar acoustic image. Data are plotted so that acoustic signals with strong amplitudes are dark. The shiptrack is represented by the blank stripe down the center of each 10 km wide swath. The normalized processing scheme preserves true relative amplitude levels throughout the survey.

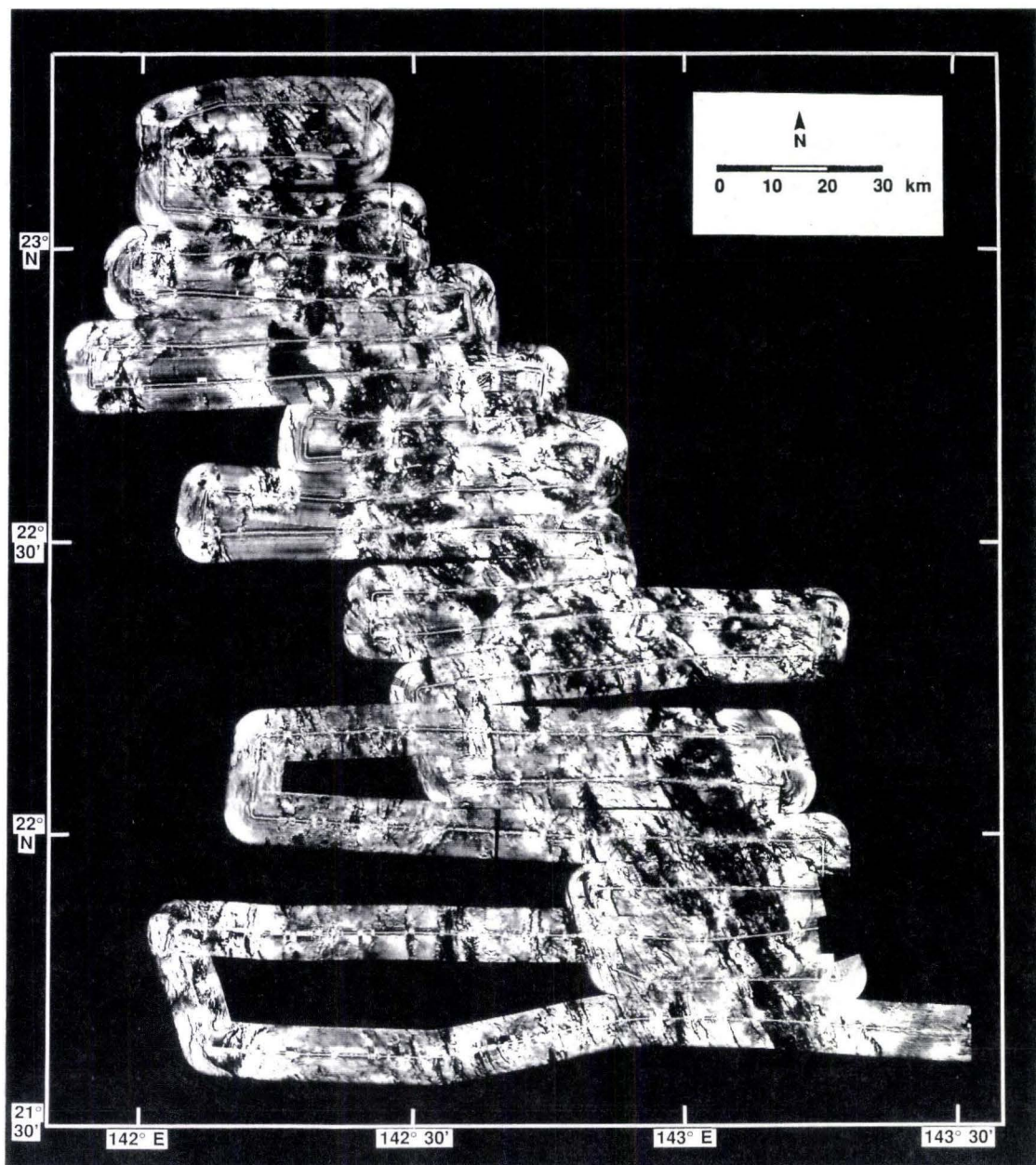


Figure 5B "Ramped" SeaMARC II side-scan sonar acoustic image. Data are plotted so that acoustic signals with strong amplitudes are dark. The shiptrack is represented by the blank stripe down the center of each 10 km wide swath. The ramped processing scheme maximizes grey level contrast to enhance local structural details.

Seismic Data

The seismic profiles were collected using analog techniques, and as such, no post-cruise processing was possible. All fault measurements were made using the original analog records of HIG data, and photocopy reproductions of the GSJ profiles. Photocopies with variable X-Y scaling were made to adjust vertical exaggerations to approximately 10:1 at 1:200,000 horizontal scale for interpretive purposes (Figure 6). Sweep changes were removed from 3.5 kHz profiles by the manual "cut and paste" method. Four profiles across the backarc (Figure 7) are representative of the GSJ 3.5 kHz data. The large number of profiles available (Figure 3) of varying quality are impractical to reproduce here.

Geologic map construction

The geological map (Figure 8) was constructed beginning with interpretation of the side-scan data. Lineaments and areas with distinct backscatter characteristics on the "ramped" 1:200,000 acoustic image were identified and mapped. The bathymetric and seismic data, and rock dredge information were then examined to interpret and label the identified acoustic features.

Fault picks were made if the following criteria were observed in the 3.5 kHz records and seismic reflection profiles: 1) an abrupt change in the depth of the water/bottom interface, 2) presence of a series of hyperbolic diffractions with

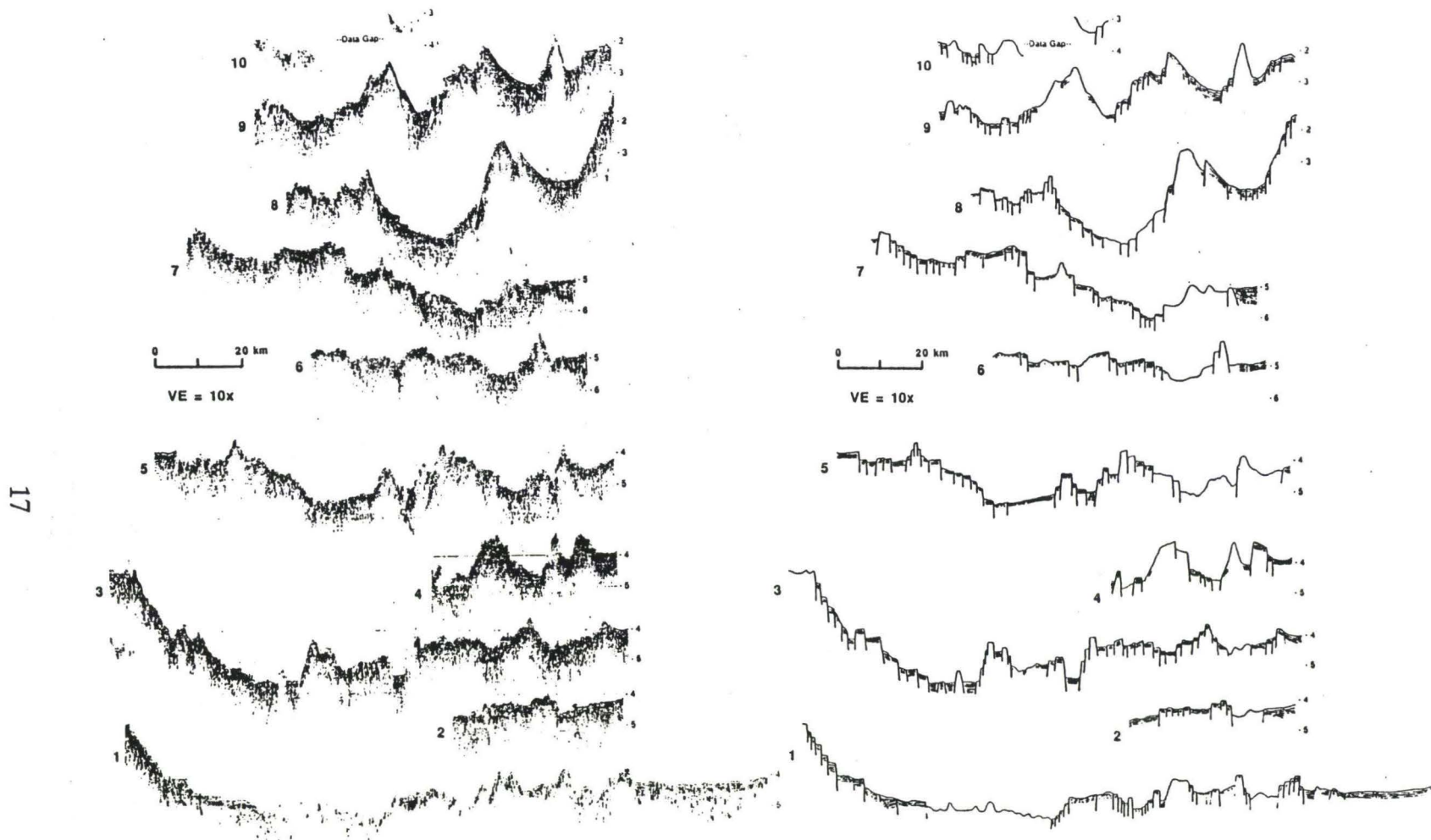


Figure 6A Mixed frequency (25-55/65-180 Hz) single-channel seismic profiles, lines 1-10. Interpretive line drawings are somewhat schematic for the southernmost lines because distinguishing between volcanic and fault-derived point sources proved difficult. Vertical scale labeled in seconds of two-way travel time. Vertical exaggeration is approximately 10x. Profiles are stacked in their approximate longitudinal positions; locations of profiles are shown in Figure 4B.

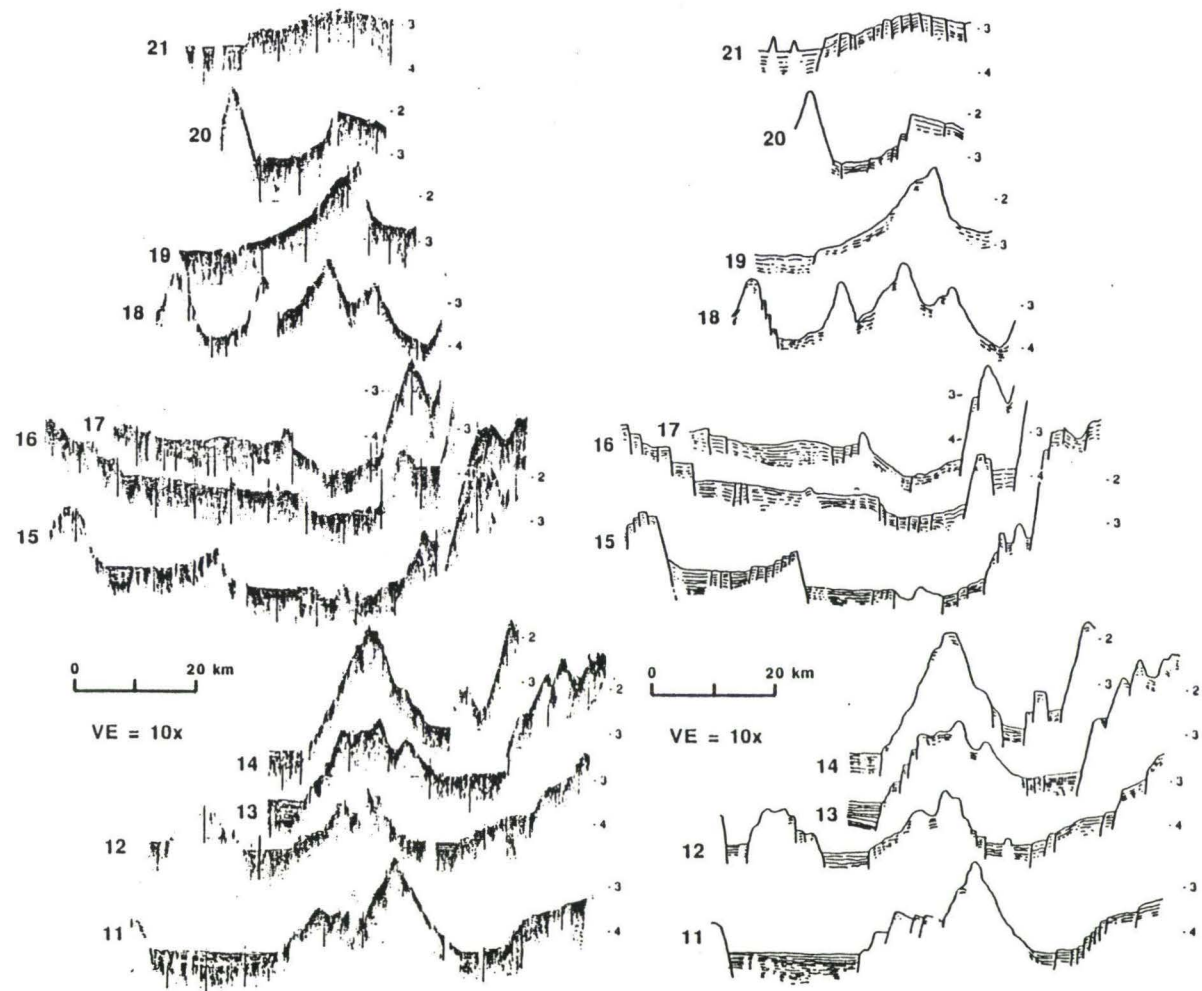


Figure 6B Mixed frequency single-channel seismic profiles, lines 11-21. Vertical scale labeled in seconds of two-way travel time. Vertical exaggeration is approximately 10x. Note these profiles have not been reduced to the same scale as those in Figure 6A.

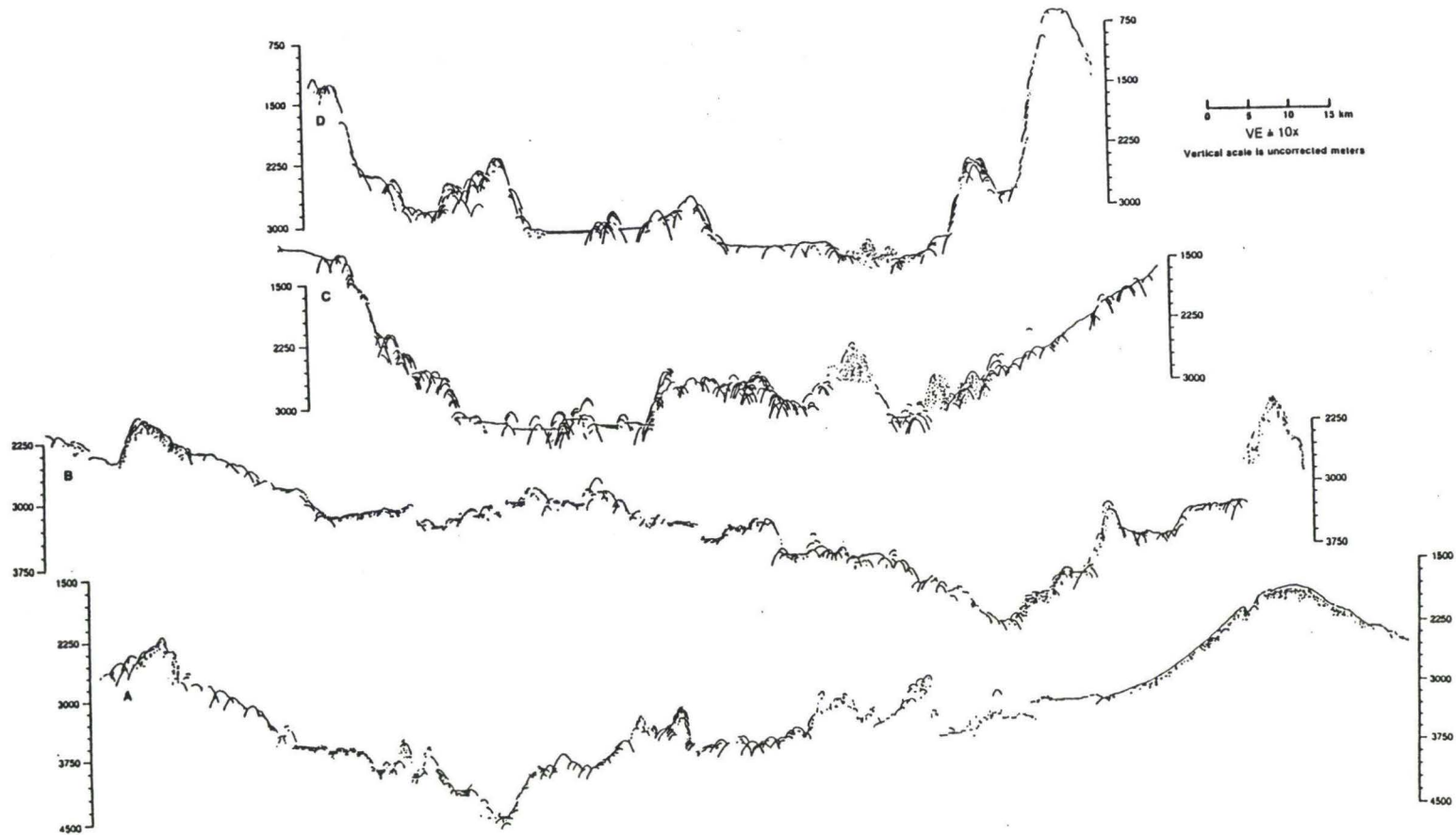


Figure 7 Profiles across the Northern Mariana Trough traced from GSJ 3.5 kHz data. Profile locations are shown in Figure 4B. These profiles illustrate the change in width and morphology of the basin from north (profile D) to south (profile A). Large tilted fault blocks characterize the north part of the basin, volcanic seamounts and fault blocks in the central region, and an increasing intensity of hyperbolic echoes resulting from intensely faulted terrain and volcanism in the south. The east end of profile A crosses the south flank of the arc volcano, Fukujin.

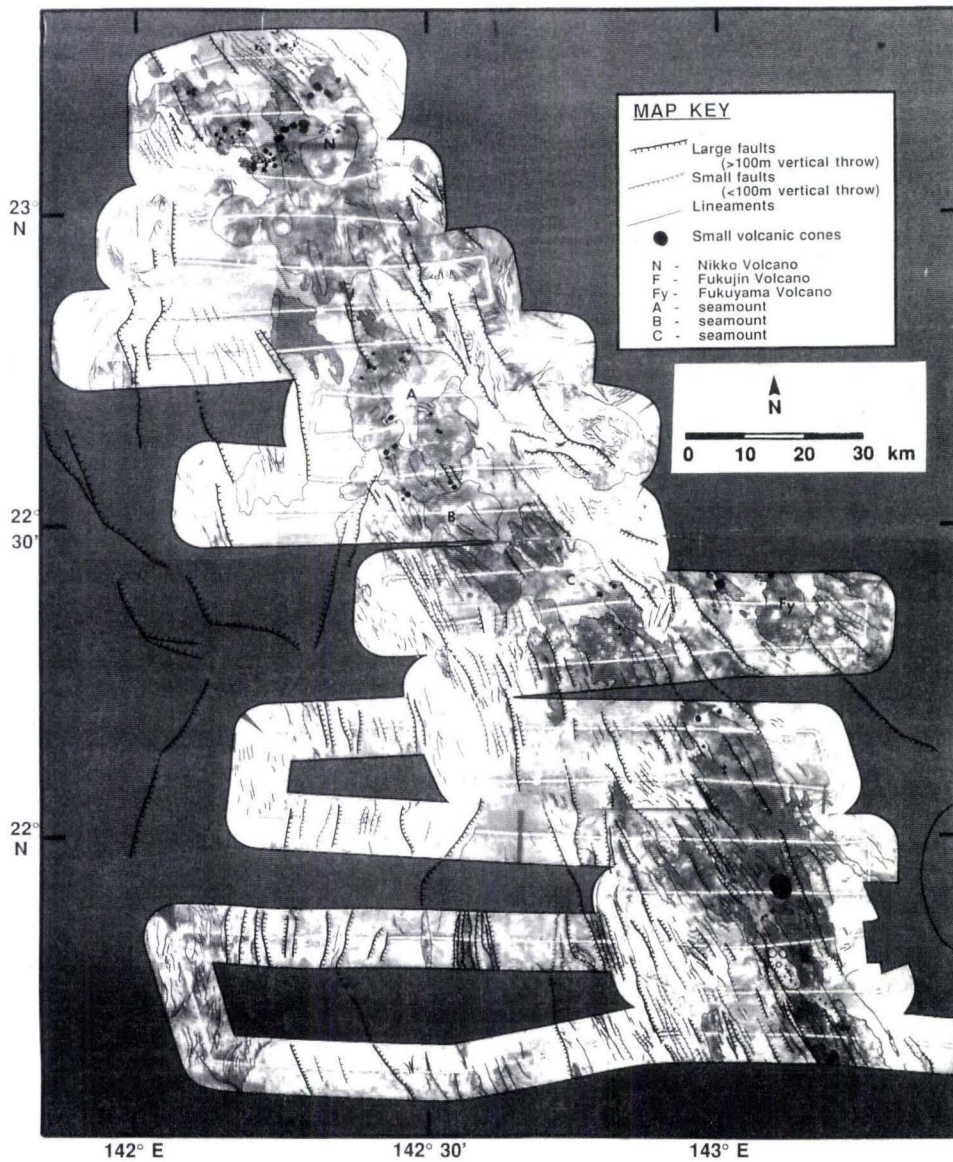


Figure 8 Geologic interpretation map of the area surveyed based on the combination of side-scan sonar, bathymetric, single-channel seismic and 3.5 kHz data. This figure was produced by placing an overlay on the "ramped" side-scan image in Figure 5B. Changes in grey tone are a result of the data, not interpretive symbols. Close-up views of key areas are shown in Figures 12-16.

aligned apices, and/or 3) interruption or offset of sub-seafloor reflectors. Fault traces were drafted on the map at the base of the scarp. The combination of the seafloor morphology (rugged, similar to that of abyssal hill fabric) and poor to fair quality of the unmigrated seismic reflection data made the distinction between faults and volcanic features difficult to determine in the southern part of the survey area. The interpretive line drawings in Figure 6 are thus subjective. Dip and depth of fault planes are sketched schematically.

The vertical throw of each fault was determined in milliseconds by measuring the orthogonal distance of the surface offset between interrupted reflectors (or between the apex of diffraction hyperbolae) directly from the original analog records. These values were later converted to meters assuming a velocity of 1500m/s. SeaMARC II bathymetry was used to check that values calculated were reasonable. Subsurface offsets were not measured because bubble pulse reverberations mask subsurface reflection characteristics in much of the data. Since all of my measurements are of surface offsets, the faults are presumably active, or at least recent enough that burial by sediment accumulation has not obscured them.

Dip directions were determined with the aid of seafloor backscatter characteristics. Faults planes facing toward the transducer array should create high intensity acoustic returns, while those facing away should produce low intensity returns, or white shadows. This is a simplified assumption, however,

and is not always observed in the data. Other factors such as the angle of the shiptrack relative to the strike of structural features (see last section in this chapter), roughness (microtopography) of the fault scarp, size and dip of the scarp also add to the total observed backscatter characteristics. These complications made determination of facing direction of small faults ambiguous in some cases, and these were mapped as lineaments. Bathymetry data were used to aid determination of facing direction of large faults. Faults were placed into categories "large" and "small" according to amount of vertical offset (greater than or less than 100 meters respectively). Lineaments visible in side-scan data that were not identifiable as faults with a reasonable degree of confidence on seismic profiles were mapped with a separate symbol and were combined with the small offset faults for analysis of fault and lineament orientation. Dip angles were not systematically calculated, though most faults are likely high angle at the surface. A few measurements made from 3.5 kHz records yielded angles of 56° to 77° . Whether the faults are planar or listric is not possible to determine from this data set.

Other features on the geologic map include volcanic seamounts, cones and ridges, fault blocks, and sedimented basins. Fault blocks were distinguished from volcanic seamounts on side-scan imagery by 1) a predominantly low backscatter intensity, broken by very highly reflective lineaments, and 2) lack of radiating, wispy patterns of relatively low backscatter that have been observed emanating

from the summit areas of the Kasuga seamounts (Hussong and Fryer, 1983), attributed to volcanoclastic debris flows. An alternative interpretation of features fitting these criteria are older, sedimented volcanics that were subsequently faulted. I prefer the former interpretation when both side-scan and seismic evidence are considered. Seamounts exhibiting wispy, radiating backscatter characteristics I have classified as volcanic in origin. Some fault blocks also exhibit acoustic characteristics (non-linear high backscatter returns) possibly indicating localized volcanic activity. On seismic reflection records, bathymetric highs were considered to be fault blocks if asymmetric, and if the echo character consisted of irregularly spaced and overlapping hyperbolae with strong indistinct bottom echoes at vertices. Internal reflectors were clearly visible in all fault blocks in lines 11-21 (Figure 6B), and only a few in lines 1-10. Symmetric highs with a smooth, continuous bottom echo were classified as volcanic seamounts. Bathymetry, rather than distribution of backscatter characteristics, was used to define the shape and size of seamount edifices. Volcanic ridges were recognized as elongate bathymetric highs with moderate to high backscatter corresponding to a distinct diffraction above the surrounding seafloor on 3.5 kHz records.

Analysis of Fault and Lineament Orientations

Azimuths and lengths of large and small offset faults and lineaments were determined using a computer program written by Wessel (1991). Each fault or

lineament was digitized from ozalid reproductions of the final 1:200,000 geologic interpretation map as a series of points representing straight line segments. The program calculates both the azimuth and the distance between the points based on position and map projection. Using this method, fault and lineament traces with variable azimuths are represented by a sum of straight segments with unique azimuths, rather than an average strike determined visually.

The procedure for estimating the errors in lineament azimuth measurements of from SeaMARC II data has been described in detail by Wessel (1991). The most significant error results from the "layover effect" in plotting of the acoustic data. This effect arises from the assumption that the seafloor is flat during calculation of across-track pixel placement, and results in distortions over terrain with bathymetric relief. The greatest distortion occurs when there is a significant across-track gradient; acoustic targets are displaced toward the shiptrack on positive slopes, and away from the shiptrack on negative slopes. Other errors include those in navigation, location picked by the interpreter, distortion in drafting and reproduction, and accuracy of digitizing. A five degree bin width was selected for analysis and presentation of the data to keep azimuthal errors smaller than bin size. The digitized data were converted to GMT format for plotting of histograms and sector diagrams.

Bias in SeaMARC II data arising from look-direction

One of the factors effecting the appearance of acoustic targets on a side-scan image is the direction of ensonification of the feature during collection of the data. Figure 9 illustrates the difference between crisp and diffuse lineaments observed on swaths of data covering the same area of the seafloor, but collected at different ship headings. The large white stripe down the center of swath A is the shiptrack, noted by the large arrow at the top. The small arrows point to sharp, dark lineaments observed at a roughly 20° angle (measured clockwise) to the shiptrack. In swath B, large arrows point in the direction of the ship's heading along the three white diagonal lines. The vertical shiptrack line from Swath A has been superimposed on Swath B for this comparison. Small arrows are placed at the same locations as Swath A. Notice the strikes of the lineaments in Swath B are nearly perpendicular to these shiptracks, and the resultant broad, diffuse and discontinuous character of the features from this look-direction.

This data set was collected during an engineering test early in the development of SeaMARC II, and the survey pattern was not planned with a structural study in mind. The long shiptracks of the survey trend in the direction of those in Swath B, and the short dog-legs at each turn-around trend as in Swath A (Figure 9). The survey pattern results in three interpretive limitations in this data set. (1) The total number of faults interpreted is considered a

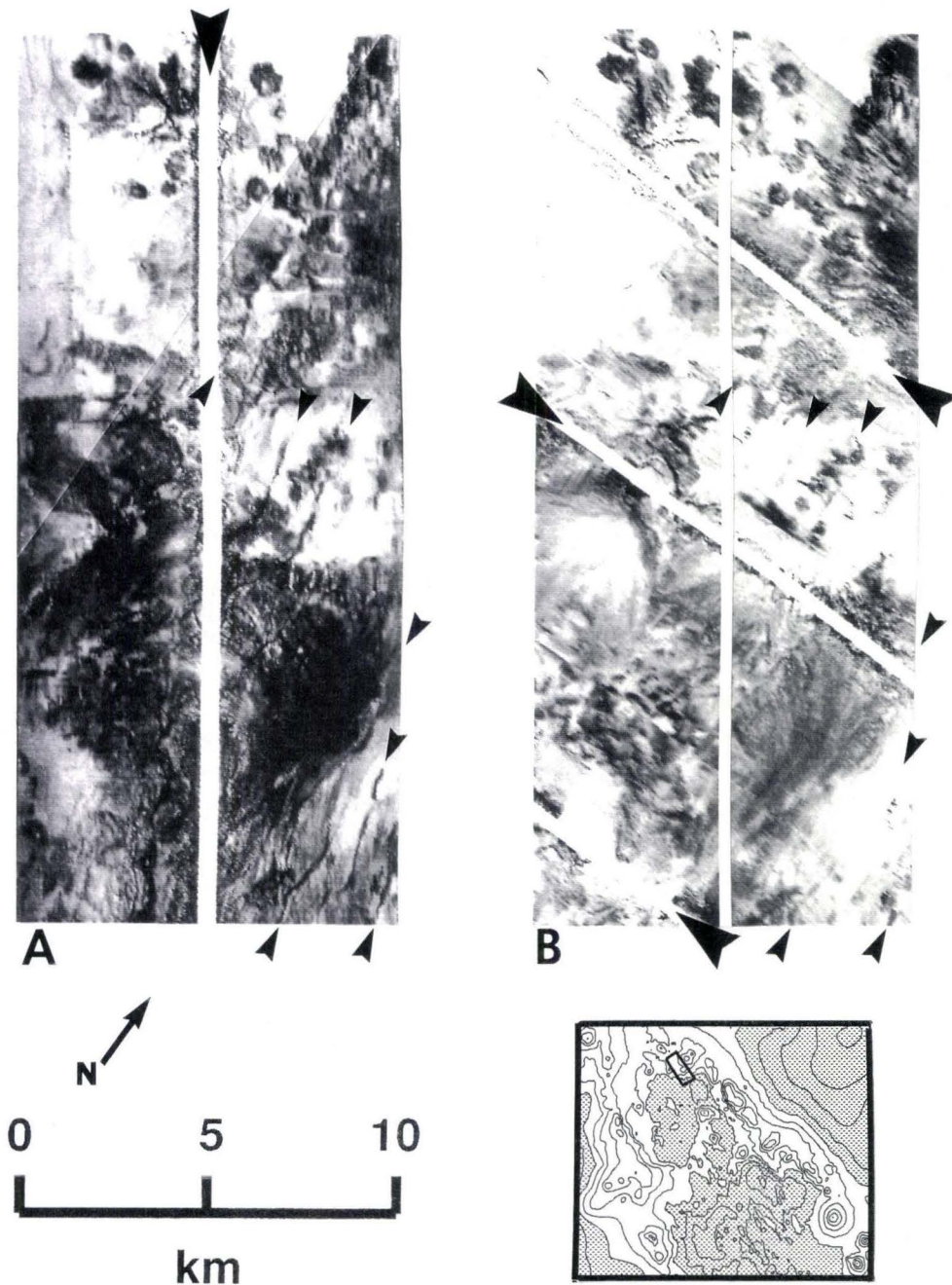


Figure 9 Effect of SeaMARC II look-direction on fault interpretations. Swaths A and B were collected over the same area of seafloor at different ship headings, indicated by the large arrows. The shiptrack of swath A has been superimposed on swath B for comparison of locations. Small arrows point to sharp, high backscatter lineaments in Swath A, which appear more diffuse and discontinuous in Swath B. Swath B represents the ship headings used in the survey pattern. The box in the small bathymetric map in the lower right corner shows the location of these data.

minimum number. If the fault planes are nearly orthogonal to the shiptrack, acoustic energy may travel along the scarp and as a result will not be reflected back to the transducer array. This problem is greatest in sedimented areas, where the terrain and the fault plane may have similar low backscatter intensities. Failure to observe some faults in the data effects (2) spacing measured between faults, exaggerating the distance between supposedly adjacent faults. Finally, (3) faults may actually be longer and more continuous than they have been mapped.

Since the survey pattern has resulted in an inherent bias in this data set, a rigorous statistical study of fault lengths and spacings was not conducted as planned. More recent SeaMARC II studies of oriented fault structures on the East Pacific Rise have been conducted roughly 45° to the strike of local seafloor features in order to minimize these problems (Edwards et al., 1991).

CHAPTER 3: Data Description and Geologic Interpretation

The Survey Area

The survey area ($\sim 17,500 \text{ km}^2$) covers the West Mariana Ridge (a remnant arc), the Northern Mariana Trough, and the active Mariana volcanic arc between $21^{\circ}30'N$ and $23^{\circ}20'N$ (Figures 4,10,11). The two ridges bounding the trough are structural and volcanic highs, asymmetric in cross-section. The steep sides of the ridges are formed by rift boundary fault zones. The backarc basin widens as the two ridges diverge southward, from 70 km near Nikko Seamount to 135 km near Fukujin Seamount.

Major Structural Provinces

Bathymetry data reveal three distinct morphological provinces on the floor of the basin (Figure 4, 10, 11); these three provinces will be referred to herein as North, Central, and South Provinces. Central Province is a shoal area relative to the other two; steep scarps with relief of at least 700 m that are oblique to the trend of the rift (020° on north, and 045° on the south), form the boundaries between provinces. The acoustic image (Figure 5A) reveals a 20 km wide zone of high backscatter on the east side of the basin that trends roughly parallel to the active arc. This zone will be referred to as the volcanic-tectonic zone (Figures 10, 11). North Province is characterized by a relatively flat-lying

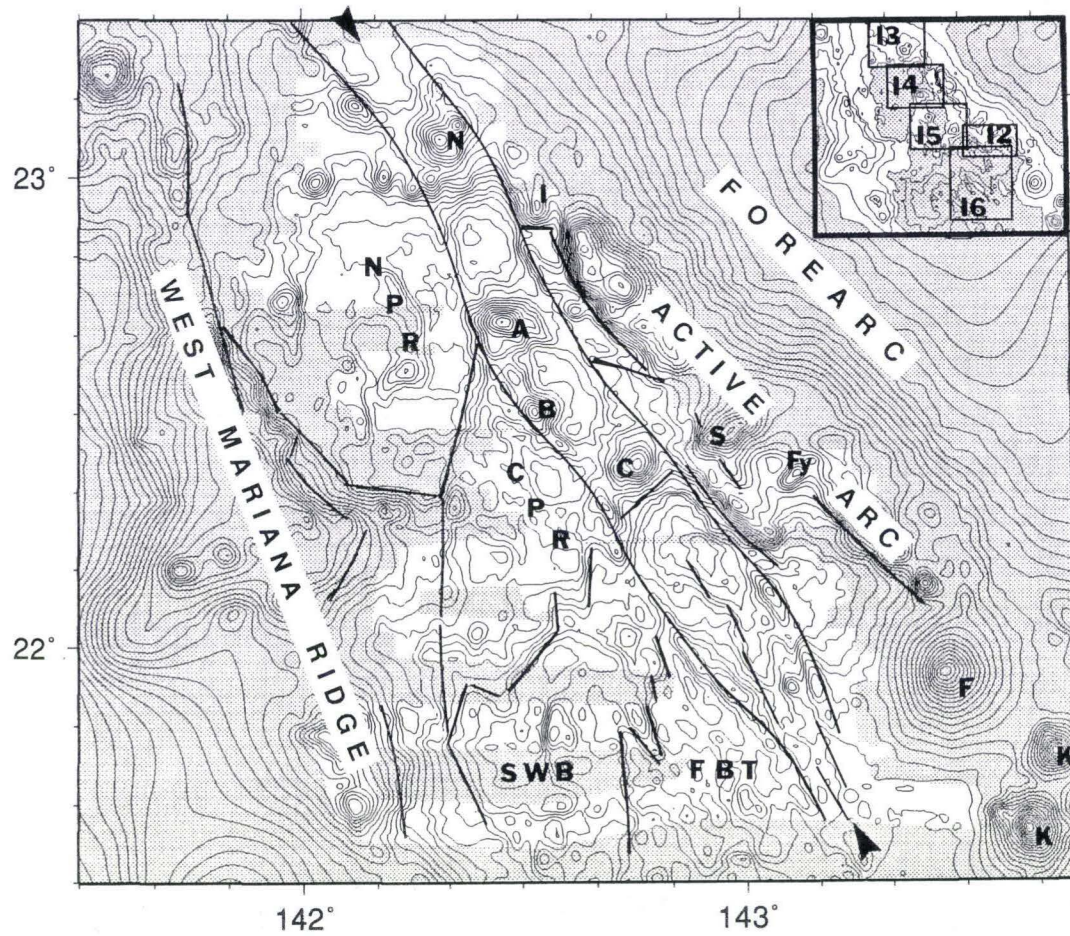


Figure 10 Location map of structural provinces and place names referred to in text, superimposed on the same bathymetric map of Figure 4. NPR-North Province; CPR-Central Province; SWB-Southwest basin in South Province; FBT-fault block terrain in South Province. The long narrow region between the two arrows is the volcanic-tectonic zone, an area of concentration of recent faulting and volcanism within the trough. Seamounts of the volcanic arc are: N-Nikko, I-Ichiyo, S-Syoyo, Fy-Fukuyama, F-Fukujin. K-Kasuga crosschain seamounts. Backarc volcanic seamounts are informally named in this thesis as A, B and C. Small inset in upper right shows locations of Figures 12-16.

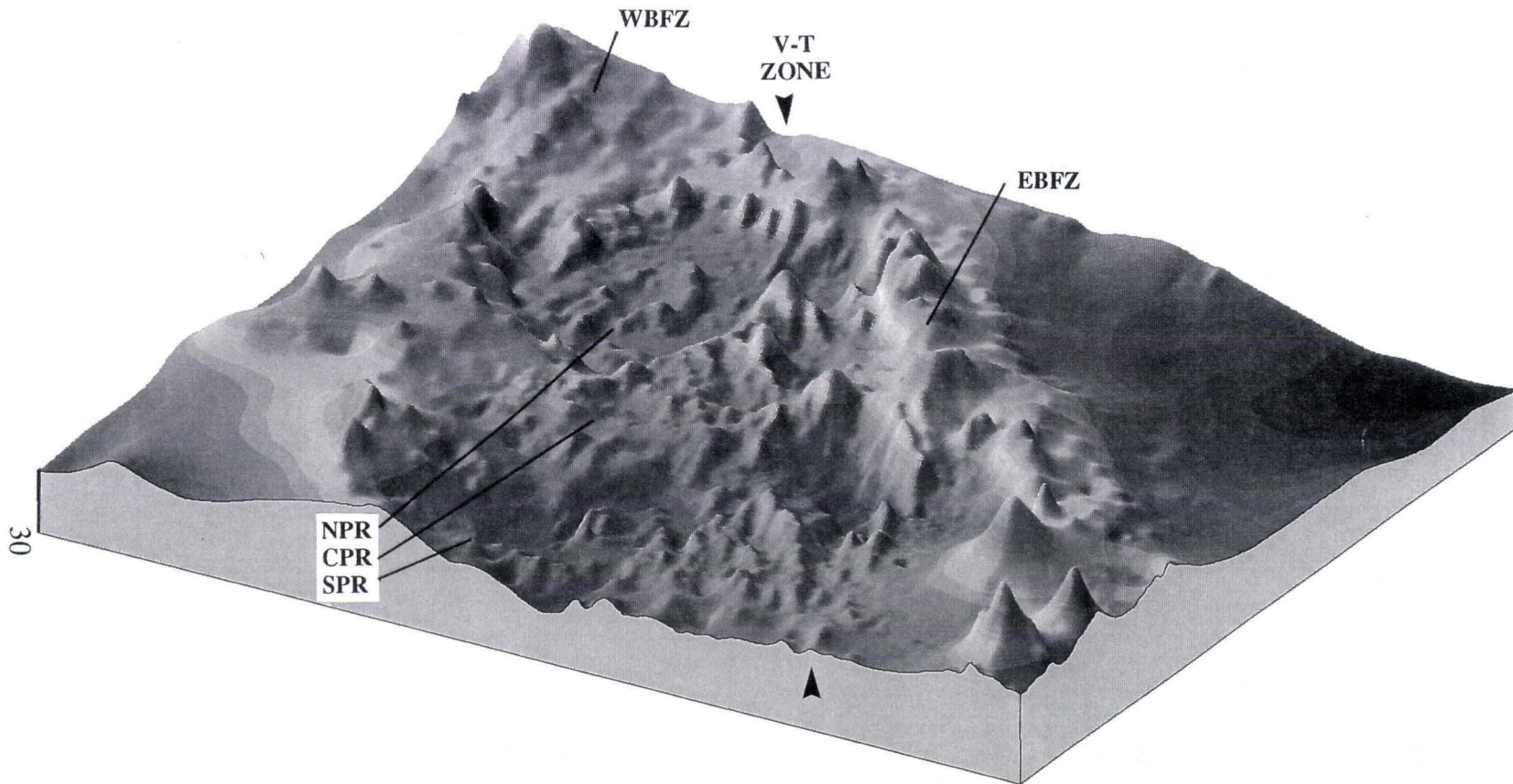


Figure 11 Perspective block diagram of the survey area viewed from the southeast, and illuminated from the west. The remnant arc lines the western edge of the Mariana Trough, and peaks of the active volcanic arc are aligned along the eastern edge. The northeast corner slopes gently into the forearc. The steep cliffs that bound both sides of the trough are the rift boundary fault zones, formed by the splitting of the arc. This view highlights the three morphologic regions within the survey area, the large tilted fault blocks in the northern basin, the elevated central region, and irregular ridges and valleys in the south. A series of basins and volcanoes along the eastern side of the trough is aligned sub-parallel to the active arc. Active faulting and volcanism within the trough is concentrated along this volcanic-tectonic zone. Abbreviations: WBFZ-west boundary fault zone; EBFZ-east boundary fault zone; NPR-North Province; CPR-Central Province; SPR-South Province; V-T zone-volcanic-tectonic zone. This illustration was generated from the same data grid used to create the bathymetric map in Figure 4.

sedimented rift valley floor (3500m depth) broken by large, backtilted fault blocks (Figures 4,5,6B,11). The generally rugged Central Province has abundant evidence of recent volcanic activity superimposed on block-faulted seafloor (Figures 4,5,6B,11). In South Province, a sedimented basin on the west is broken by normal faults and horst blocks (southwest basin), structural lineaments and a series of rugged ridges and valleys characterize the central portion (central fault-block terrain), and a fault-bound valley featuring recent volcanic flows and cones is found on the east side (high backscatter zone) (Figures 4,5,6A,11).

In this chapter, I describe the major geologic features of the Remnant Arc Margin, the active Arc Margin, and the North, Central and South Provinces in light of the reprocessed acoustic imagery, newly compiled bathymetric map, and seismic reflection data. These structures characterize the progressive evolution of rifting and volcanism in this backarc basin.

Remnant Arc Margin

The West Mariana Ridge (WMR) marks the western boundary of the rift basin (Figure 4A,10,11). Coverage of the WMR by the SeaMARC II survey is restricted to the area between 21°40'N and 21°50'N near 142°10'E, where anastomosing lineaments are found in a region with predominantly subdued backscatter characteristics (Figures 5,8). Single-channel profiles (line 1, Figure 6A) and GSJ 3.5 kHz records (Figure 7) indicate that these lineaments are the

result of the edges of tilted fault blocks, forming terraces that step down to the basin floor. These fault blocks are the result of normal extensional faulting of the West Boundary Fault Zone (WBFZ) (Figure 11). Vertical offsets of individual faults vary from 83 to 626 meters. On a regional scale, the general trend of the WBFZ is 335° in the vicinity of 20°N , and changes to 345° north of an unusually wide region of the ridge near 22°N (Figures 4A,10,11). On a local scale, fault traces form variable curvilinear or zig-zag patterns with trends ranging from 010° to 330° , traceable for 10 to 30 km lengths.

Active Arc Margin

The volcanoes Nikko ($23^{\circ}05'\text{N}$, $142^{\circ}20'\text{E}$) and Fukujin (22°N , $143^{\circ}25'\text{E}$) are the sites of active volcanism along the frontal arc (Figures 10,11). Fukujin is a 30 km diameter conical edifice rising to 50 m below sea level (Bloomer et al., 1989) from a platform depth of 3000m. Reports of discolored water, floating pumice and seismic activity have been documented by the Scientific Event Alert Network (SEAN) Bulletin in the vicinity of this volcano during the last decade. Current eruptive activity appears to be concentrated on the south and southwest flanks, where dredging has recovered fresh plagioclase phyric andesites (Fig. 4b; Wood et al., 1981; Jackson, 1987, 1989; Bloomer et al, 1989a,b); dredges near the summit in 1977 and 1985 recovered mainly altered volcanic rocks and rounded coral boulders with thin Mn oxide coatings (Wood et al., 1981; Jackson

and Fryer, 1991), indicating it has been at or near the surface for some time. Located 170 km northwest of Fukujin, Nikko has also erupted during the last decade (SEAN Bulletin). In contrast to the single conical edifice of Fukujin, Nikko has a complex morphology discussed in detail later.

East Boundary Fault Zone (EBFZ)

Between Nikko and Fukujin volcanoes, several elongate ridges trending northwest slope gradually eastward into the forearc basin, and slope steeply westward into the backarc as large scarps of the East Boundary Fault Zone (EBFZ) (Figure 4A,10,11). Based on the highly asymmetric morphology of this ridge, and the recovery of greenschist metavolcanic rocks from dredges along it (Figure 4B), Bloomer et al. (1989) concluded the ridge is formed primarily by faulted basement blocks, with three volcanoes superimposed on the blocks; two are classified extinct (Ichiyo and Syoyo) and one dormant (Fukuyama) (Figure 10).

Three predominant planar and convex-curvilinear fault zone segments in the EBFZ are discernable as steep cliffs in the regional bathymetry (Figures 2,4,10,11). In plan view, the scarp segments are 30 to 45 km in length, and are left-laterally offset from one another by 7 to 19 km, forming an *en echelon* pattern. Figure 12 shows the offset between two *en echelon* segments near 22°15'N. Fukuyama Volcano (1500m), located between the tips of two major

fault segments, appears more youthful than postulated by Bloomer et al. (1989). The volcano is a steep-sided elongate cone with moderate to high backscatter (Figure 12). Lobate patches of high backscatter (possibly young lava flows) can be found within 5 km of the cone. Volcanic activity accomodates the strain between adjacent border fault segments in continental rift border fault systems (Morley, 1988; Ebinger, 1989), and also in arc rift systems (Klaus, 1991). The growth of a connecting fault between border fault segments has been inhibited by volcanism on this section of the EBFZ.

Nikko Seamount

Nikko Seamount is quite complex in contrast to the generally simple cones of the volcanoes further south along the Mariana Arc (Figures 4,10,11,13). The 1500m contour encloses an 11 km diameter edifice (Figure 13A). Nikko was shown by a 1971 SASS survey to have two peaks (Smoot, 1988). The larger southwestern peak (142°20'E 23°05'N) has a diameter of 4 km. Smoot (1988) reported the bathymetry could also be interpreted to include both this peak and a smaller one located 7 km northeast as part of one large summit rim having an opening to the northwest. Unfortunately, our bathymetric data cannot verify either interpretation of the 1971 SASS data. A malfunction in the port side during the SeaMARC II survey caused the collection of bathymetric data on only half of the swath. This data loss, combined with the reduced swath width in

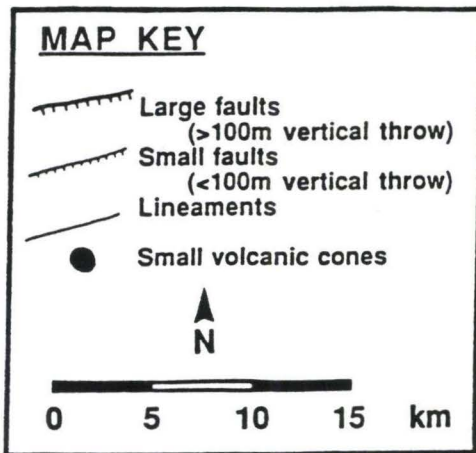
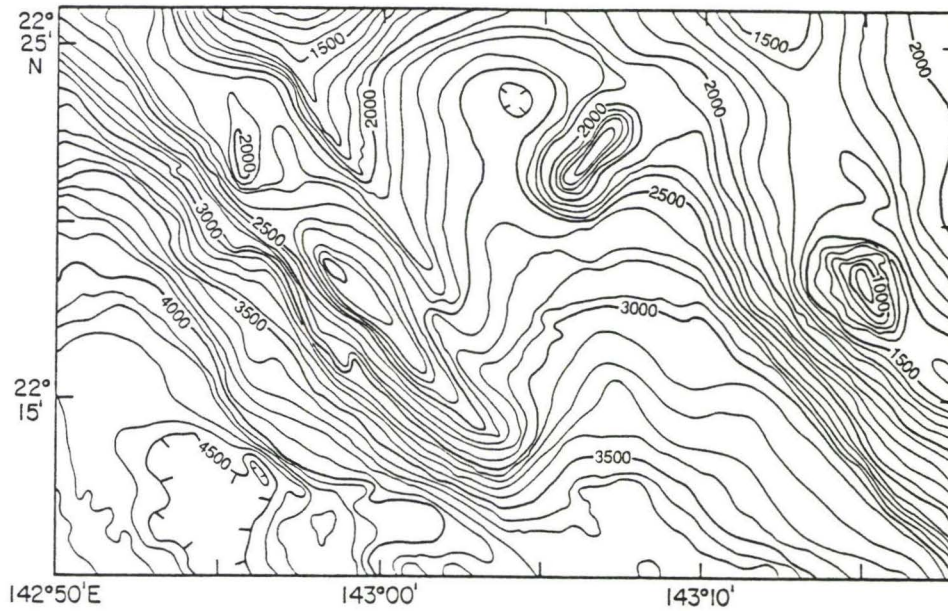


Figure 12A Bathymetry of Fukuyama Seamount and the East Border Fault Zone (EBFZ). Fukuyama is located at the tip of left-stepping *en echelon* border fault segments. Volcanism accommodates the strain between adjacent segments of the EBFZ. Contour interval is 100 meters. Map key explains symbols in Figure 12B. Location of this figure is shown in Figure 10 inset.

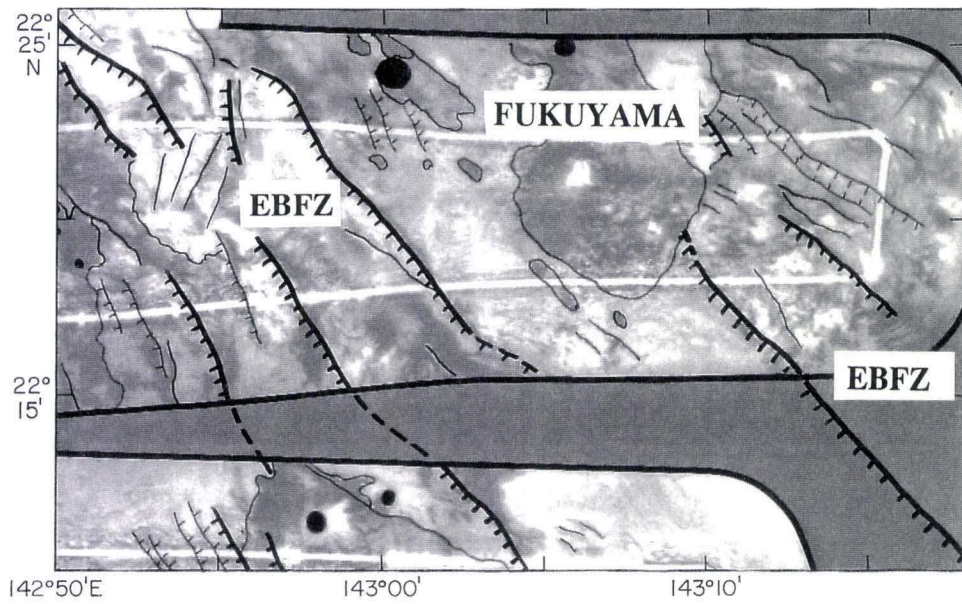
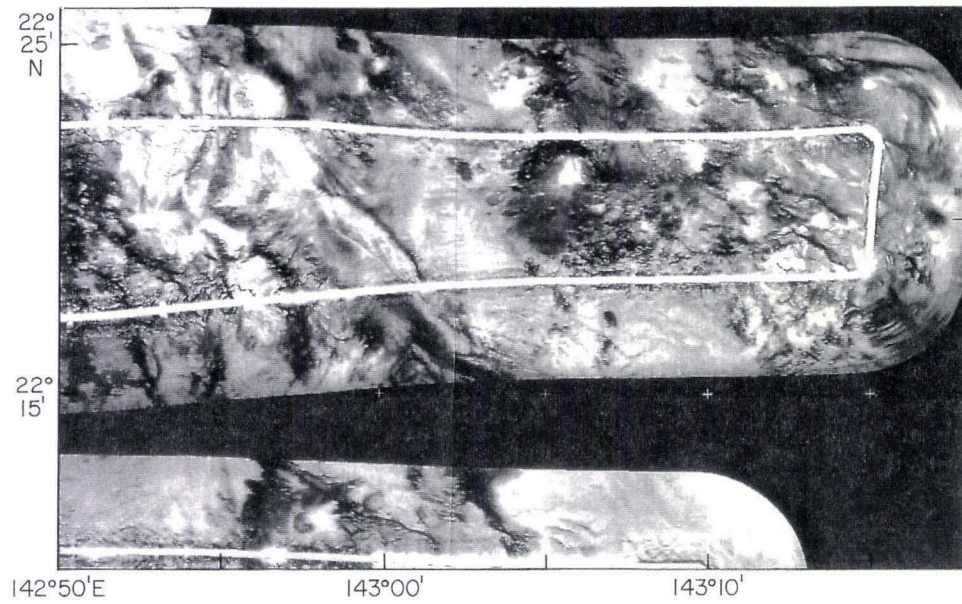


Figure 12B Side-scan and interpretation of Fukuyama Seamount and the EBFZ. Symbols are explained in Figure 12A

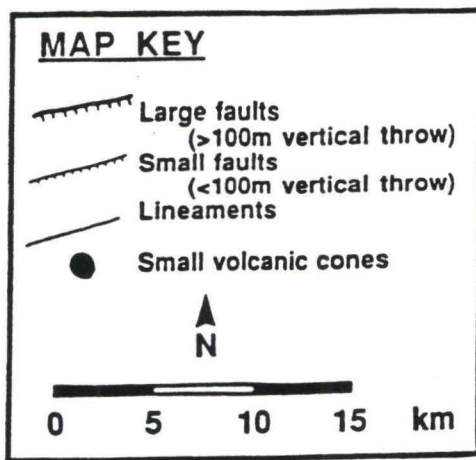
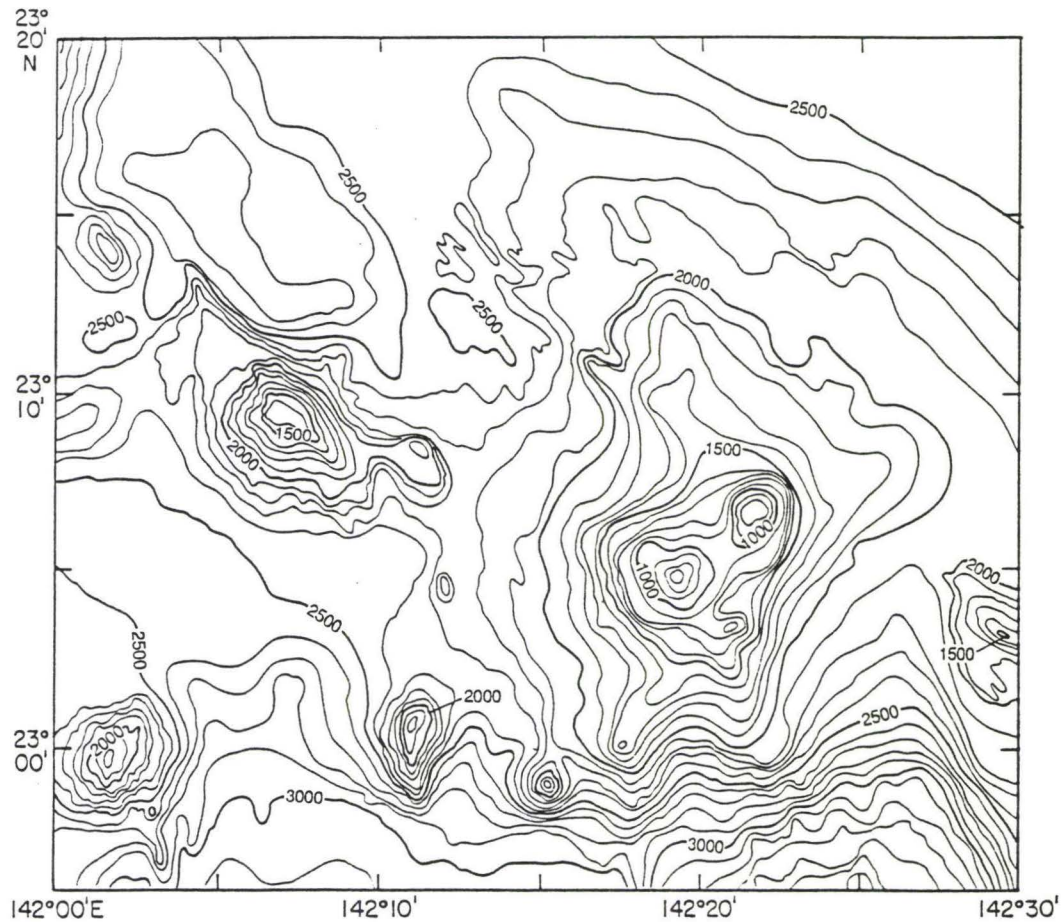


Figure 13A Bathymetry of Nikko Seamount and surrounding area. Nikko is located along the EBFZ, actively building between two large fault-bound graben. The morphology of this volcano is more complex than others along the arc, in response to tensional stresses as the backarc widens. A volcanic field of small cones and lava flows is aligned orthogonal to local fault trends. Contour interval is 100 meters. Map key explains symbols in Figure 13B. Location of this figure is shown in Figure 10 inset.

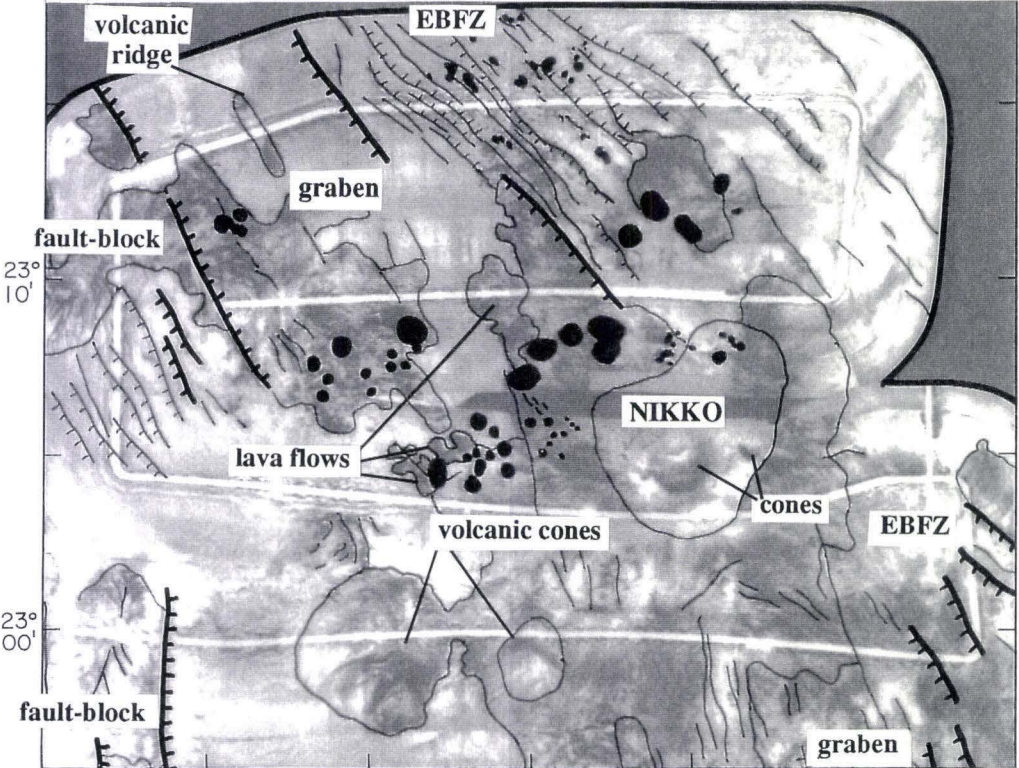
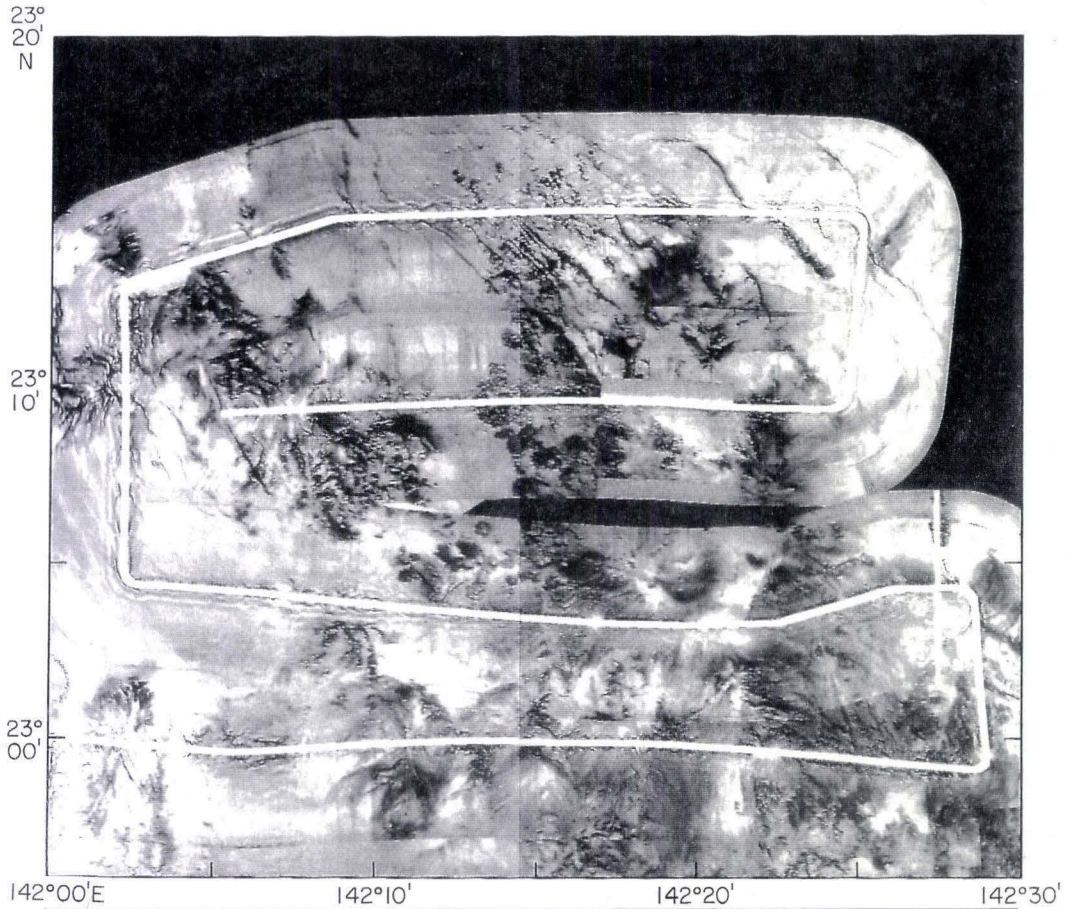


Figure 13B Side-scan and interpretation of Nikko Seamount and surrounding area.

shallow water resulted in large data gaps over the volcano. The data gaps were filled in using GSJ 3.5 kHz depths, with contours interpolated using the shape of the 1971 SASS survey and SeaMARC II acoustic characteristics as guides. The acoustic imagery, however, does depict the two peaks as distinct features (Figure 13).

Two subsidiary cones 10 to 15 km southwest of the summit have built up 200 to 300 meters above the surrounding platform, and exhibit radiating patterns with moderately high backscatter in the side-scan image that extend south toward the basin 1100m below (Figure 13). Dredges on the eastern of these two cones and the summit region recovered fresh basaltic to dacitic volcanic rocks (Fig 4b; Jackson, 1987, 1989; Bloomer et al. 1989a,b; Jackson and Fryer, 1991), the most common rock type dredged along the arc (Bloomer et al., 1989). On the northwest flank, a field of a total of 30 discrete, roughly circular high backscatter areas 100-2000m in diameter trends northeasterly, roughly parallel to the alignment of Nikko's twin peaks, and orthogonal to local fault strikes. Both lava flows and volcanic cones (distinguished by acoustic shadows on the side facing away from the shiptrack (Figure 13B) are present in this volcanic field. Most of these acoustic features are not observed in the bathymetry data, so if they are cones, they are less than 100m high (or occur in areas where we do not have swath bathymetry data coverage). Located at the southwest of the volcanic field, the largest cone ($142^{\circ}12'E$ $23^{\circ}N$) is visible in the bathymetric map (Figure 13A).

Lobate areas of high backscatter on the acoustic image appear to originate from this cone, and are interpreted to be young lava flows (Figure 13B,C). Two 100 m diameter cones 2 km east of the largest cone appear to be source vents for lava which flowed 1.5 and 2 km downslope to the northwest.

Northwest of Nikko's summit, a 12 km long ridge is bounded to the west by a 573m west-facing escarpment, which is a segment of the EBFZ (Figure 13). The block is intensely faulted; at least 23 lineaments trend 310° to 323° , parallel and subparallel to the EBFZ. These normal faults are 3 to 11 km along strike, and have offsets ranging from 19 to 46 meters. Most are antithetic, down-dropped toward the forearc. These faults cut the most recent sediments and are therefore currently or recently active. Distinct high backscatter "blotches," the largest measuring 300 to 500m across, are associated with hyperbolic diffractions on 3.5 kHz profiles, lie clustered around these small antithetic faults. These could be interpreted as small blocks and debris resulting from faulting and slumping off of this structural high, or as extrusive volcanic features. A seafloor magnetization map depicts a pronounced high in this area north of Nikko's summit (Martinez, 1991 pers. comm), indicating the latter interpretation is preferable.

Due west of this faulted block is a 2700m deep, 11 km wide graben lying more than 300m below the surrounding horsts. The sediments ponded in the basin floor have been intruded by a 5 km-long, 1 km wide rift-parallel volcanic

ridge (profile 21, Figure 6B). The 109m high ridge is visible as an area of high backscatter on the acoustic image (Figure 13). The tilted fault block on the west side of the graben is fractured by small antithetic faults similar to those on the eastern fault block. The strikes of these faults are more northerly than the ones on the east, measuring 320° to 330° . Small, high backscatter lava flows and cones are associated with the faults closest to the graben (Figure 13). The close association between lava flows and faults demonstrate that faulting patterns control the distribution of volcanism, possibly indicating the volcanic activity is a passive response to extensional processes.

Basin Floor

North Province

The floor of the trough southwest of Nikko appears as flat grey tones on the acoustic image (Figure 5), disrupted by local areas of variable backscatter. Seismic profiles (profile 15, Figure 6B) and 3.5 kHz data (profile D, Figure 7) reveal large backtilted fault blocks with steep east-facing scarps corresponding to the areas of variable backscatter (Figure 14). The blocks are 10 to 12 km long and 20 to 30 km wide, with east-facing escarpments as large as 944 m in relief.

An 85 km² area of high backscatter ($22^{\circ}50'N$, $142^{\circ}15'E$) is interpreted as a recent lava flow field (Figure 14B). Rock dredge KK8403 (Figure 4B) recovered a small volume (25 kg) of fresh, glassy porphyritic basaltic andesite,

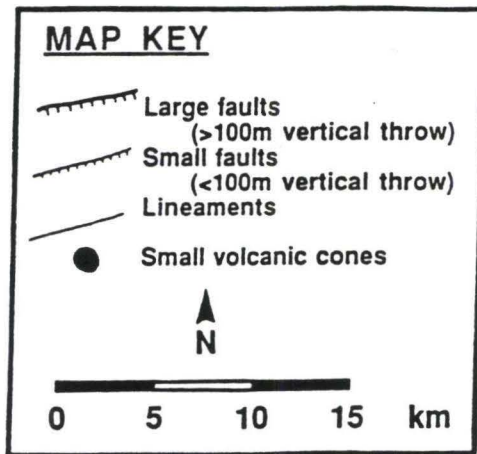
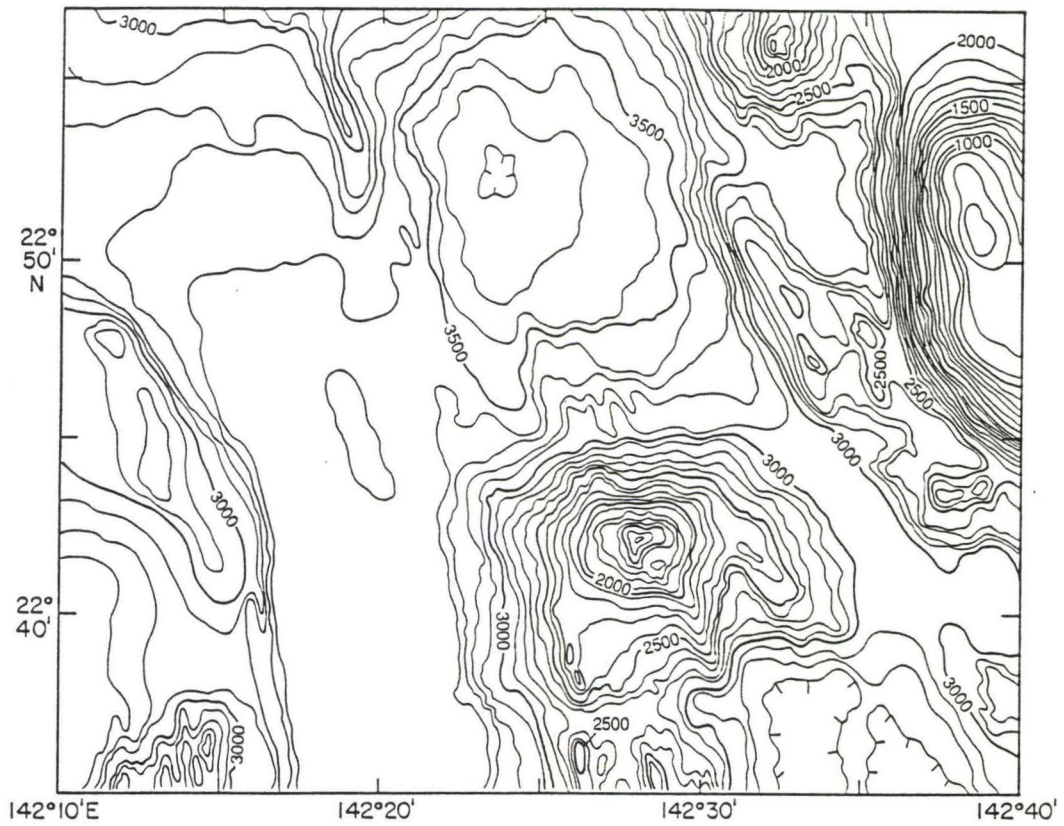


Figure 14A Bathymetry of North Province and Seamount A. The west side of North Province is characterized by sedimented areas between large tilted fault blocks. A lava flow field covers the recent sediments west of a 3700m deep graben, which has been intruded by a lava flow. Volcaniclastic debris and lava flows cover the flanks of Seamount A. Map key explains symbols in Figure 14B. Contour interval is 100 meters. Location of this figure is shown in Figure 10 inset.

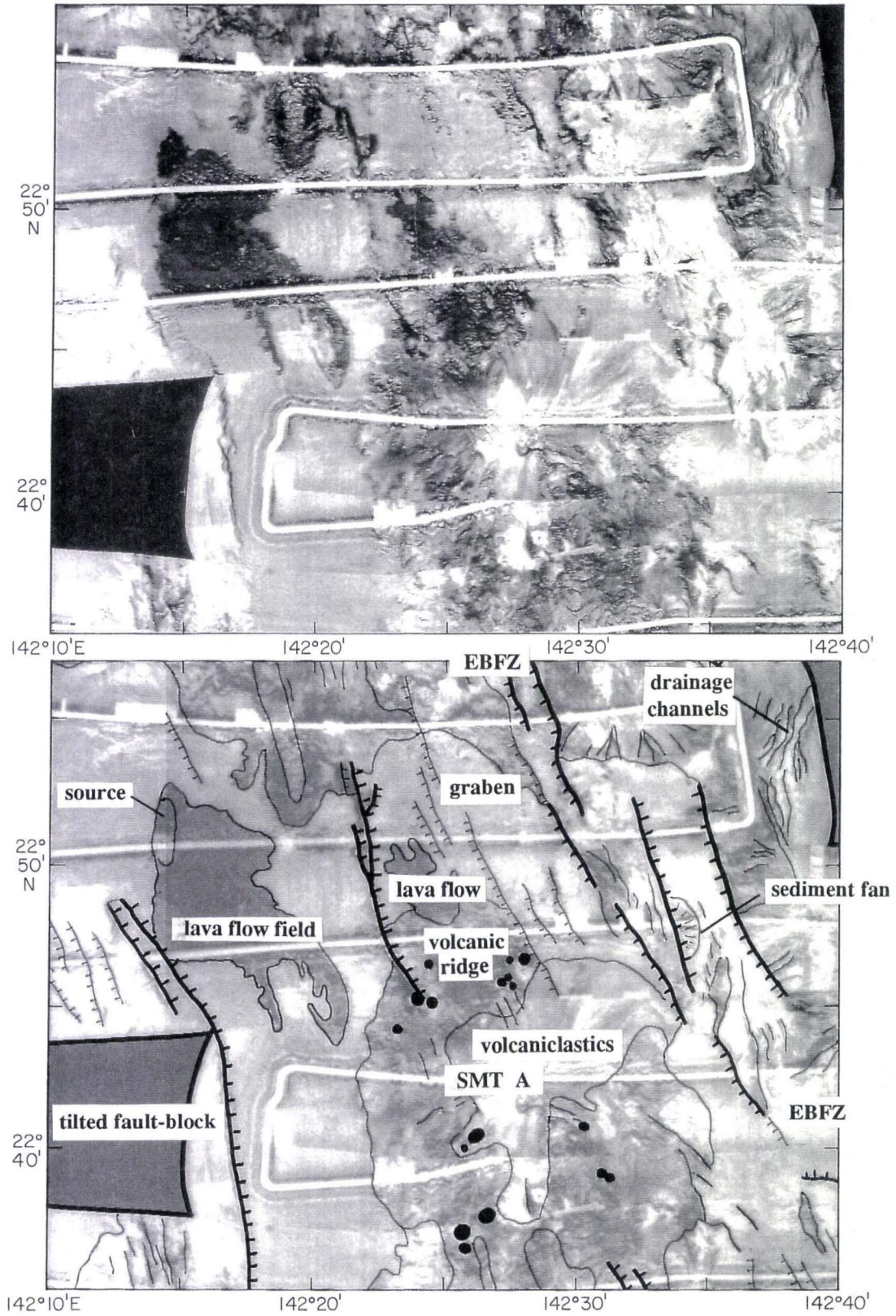


Figure 14B Side-scan and interpretation of North Province and Seamount A.

confirming this interpretation. Geochemical analyses of the lavas demonstrate the flows have affinities to Mariana Island Arc tholeiites (Jackson, 1989). A 4 km long 100m-high ridge is visible in the bathymetry (142°20'E 22°45'N, Figure 14A) at the northwest corner of the flow field. This 4 km ridge is the source of these lava flows, which then flowed downslope toward the southeast. Two arms of the flow extend 5 to 6 km southeast beyond the main flow field, their paths diverted around a small horst block. A subtle yet distinct difference in backscatter intensity indicates lavas from at least two separate eruptive events are present. The location of this flowfield about 15 km west of the volcanic-tectonic zone, is unusual. The occurrence of recent volcanic features outside of the volcanic-tectonic zone is uncommon within this survey region of the Mariana Trough.

The volcanic-tectonic zone in North Province is the site of recent faulting and volcanic activity. A 180 km² 3700m deep graben is broken by small (9 to 25m) rift-parallel faults (Figure 14). A 36km² area of hummocky, high backscatter with small (500m) diameter cones, is a volcanic ridge extending from the north flank of Seamount A (Figure 14). A 5 km long double-lobed (presumably) recent (~12 km²) lava flow appears to originate from the northern edge of this ridge.

Central Province

The west side of Central Province appears similar to North Province in the normalized side-scan image (Figure 5A). Primarily low backscatter intensities are presumably caused by sediment cover. Although the acoustic returns are low, the enhanced structural image reveals a mottled character near $142^{\circ}20'E$ $22^{\circ}N$, distinct from the smooth and featureless sedimented plain at $22^{\circ}30'$ (Figure 5B). Seismic profiles (west ends of profiles 5 and 7, Figure 6A) show the structure is clearly distinguishable from North Province. There are many faults in this region, yet the structural features are not well imaged in the side-scan data. An unfavorable angle of the survey pattern relative to the strike of structural features (see last section of Chapter 2), and/or a smoothing of the fault scarps by sediment cover, may have caused the observed backscatter characteristics. Sediment cover in this region is indicated by the character of 3.5 kHz bottom echoes.

In contrast to the sedimented terrain of the western side of Central Province, the volcanic-tectonic zone on the east side shows abundant evidence of recent faulting, three volcanic seamounts, and numerous volcanic ridges (Figures 14, 15). Seamount A is located 43km south and 15km east of Nikko, at the intersection of the scarp bounding North and Central Provinces, and the volcanic-tectonic zone (Figure 10). The volcano rises to a shoal depth of approximately 1500m from a basal depth of 2800m on the east side, and 3400m

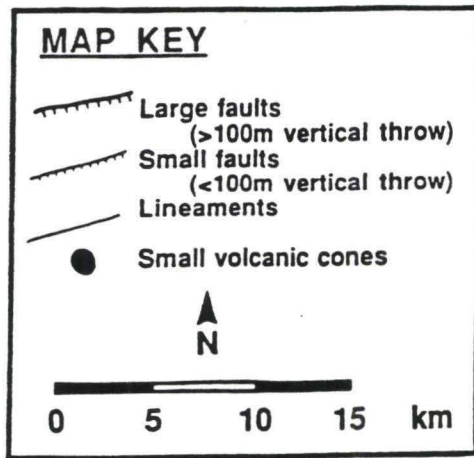
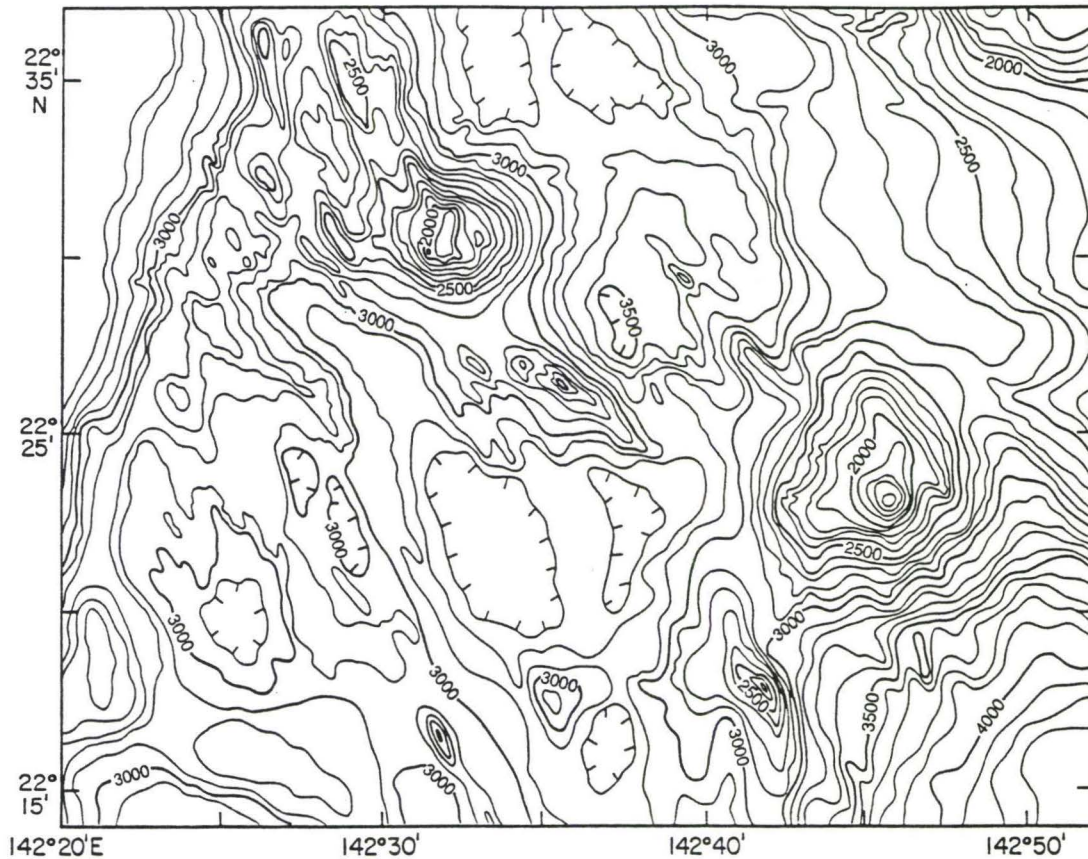


Figure 15A Bathymetry of Central Province volcanic-tectonic zone. Seamounts B and C, normal faulting and volcanic ridges characterize this structurally complex area. Contour interval is 100 meters. Map key explains symbols in Figure 15B. Location of this figure is shown in Figure 10 inset.

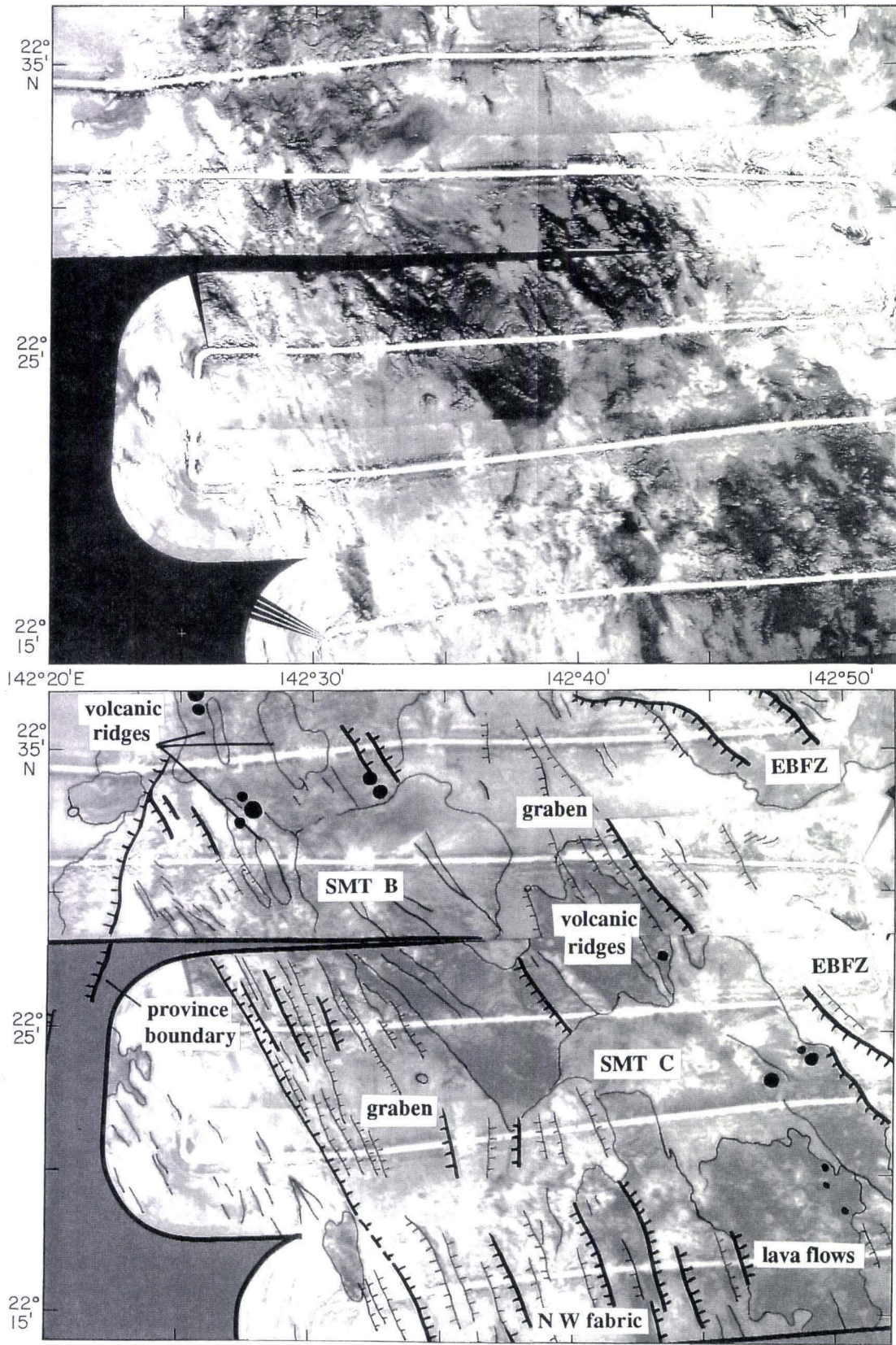


Figure 15B Side-scan and interpretation of Central Province volcanic-tectonic zone.

on the west (Figure 14). The diameter of the volcano is 18km; roughly circular on the north side, and has three ridges extending south and southeast. Wispy, radial patterns of low to medium backscatter intensity extend to the north and northeast from the summit (Figure 14B). These backscatter characteristics are similar to those observed from the Kasuga Seamounts (21°45'N, 143°40'E, Figure 10) described by Hussong and Fryer (1983). Dredging and ALVIN dive observations on the Kasuga Seamounts have confirmed that areas with this backscatter characteristic are covered with volcanoclastic debris and debris flows (Jackson, 1989; Stern et al., 1990).

The southern slopes of Seamount A are dominated by high backscatter intensities. A dredge at 2300m (Figure 4B) recovered fresh to slightly altered basalts, including slabs of frothy pahoehoe with glassy rims 1.5 km south of the summit (Jackson, 1989). These high backscatter intensities are therefore attributed to the presence of rough, young lava flows. The three ridges on these southern slopes (Figure 14A) are most likely formed by constructional volcanism rather than scars left from erosional processes. Whether the ridges have been produced by Seamount A (andesitic volcanism), or the intrusion of backarc basin basalt is subject to debate. Jackson (1989) reported two geochemically distinct lava types were present in the dredge haul; the first he classified as typical back-arc basin basalts (BABBs), and type two Jackson described as "vaguely akin" to boninites abundant in the forearc.

No matter which petrological origin is preferred, the orientations of the three ridges are likely the result of both local and regional stresses since they have differing trends. The shapes of volcanoes reflect the geometry of feeding conduits (Fiske and Jackson, 1972). In turn, dike injection patterns reflect the effect of regional non-magmatic stress superimposed on local magmatic pressures (Nakamura, 1977). The trends of volcanic features in extensional areas are concentrated normal to the minimum compression axis, resulting in elongation of volcanic edifices and alignment of subsidiary craters and cones parallel to fault strikes (Nakamura, 1977). The western ridge on the south flank of Seamount A has an azimuth of 348° , aligned with the boundary between North and Central Provinces (Figure 14A). The other two ridges trend 334° and 330° , sub-parallel to the trend of both the volcanic-tectonic zone, and the EBFZ.

Recent volcanic features are associated with the faults in the volcanic-tectonic zone, yet are largely absent from the EBFZ southeast of Nikko (Figure 14B). Although the acoustic image does not completely cover the EBFZ, well-developed drainage channels can be seen cross-cutting bathymetric contours and extending into the forearc (Figure 14). Small sediment debris fans have formed at the base of several faults. Thus the predominant features are indicative of erosion and sedimentary activity, supporting the general conclusions of Bloomer et al., (1989) that the eastern boundary of the Mariana Trough is volcanically inactive in this region.

The seafloor is very rugged south of Seamount A, with complex structures arising from both faulting and volcanism (Figure 15). Normal faults and lineaments spaced 1 km or less trend 330° . Several 4 to 6 km long volcanic ridges have been built along these faults, terminating at the boundary between Central and North provinces. A 10 km diameter volcanic edifice, named here as Seamount B, is located 25 km SSE of Seamount A (Figure 10). Radial, low to medium intensity backscatter patterns emanate from the 1900m deep summit at $22^{\circ}30'N$, $142^{\circ}32'E$ (Figure 15B). A 14 km long volcanic ridge southeast of Seamount B has an unusual local trend of 304° . Volcanic ridges northwest of Seamount C extend into a 3500 m deep graben (Figure 15), resembling the structural pattern north of Seamount A (Figure 14). Local magnetization highs are observed on the north flanks of Seamounts A and C (F. Martinez, pers. comm. 1991), correlating with these high backscatter ridges. Seamount C is 14 km wide, has a shoal depth of 1600m, and lies perched at the top edge of the greater than 700 m high dividing scarp between Central and South Provinces. High backscatter lava flows drape this scarp, extending 15 km southeast to the graben below. Although the general trend of the dividing scarp is roughly northeast, orthogonal to the active arc (Figure 4A,10,11), the structural fabric trends to the northwest (Figure 15B).

South Province

Southwest basin

The southwest basin is irregularly shaped, bounded to the north by the sinuous scarp between Central and South Provinces, and on the east by major (>300m) faults of the central fault-block terrain (Figure 10). The floor of southwest basin lies at depths greater than 4000m (Figures 4,11), and is visible on the acoustic image as an area of flat grey tones along its north and west edges (Figure 5B). High backscatter lineaments between 142°30'E 21°40'N and 142°40'E 22°N (Figure 5A) result primarily from block faulting. The west edge of a large fault block near (142°35'E 22°50'N, Figure 5A) rises abruptly out of the surrounding sediment ponds (profile 3, Figure 6A). The western half of the block corresponds to a local magnetization high (F. Martinez, pers. comm., 1991), suggesting that a volcanic ridge has been superimposed on the western edge of the fault block.

Central fault-block terrain

The northern and western extents of the central fault-block terrain are visible as large (>300m) scarps in the bathymetry (Figures 10,16). The side-scan image is characterized by predominantly low backscatter, broken by high backscatter lineaments (Figure 16). The lineaments in this area, spaced between 0.5 and 2 km apart, are interpreted to be the result of both high angle normal

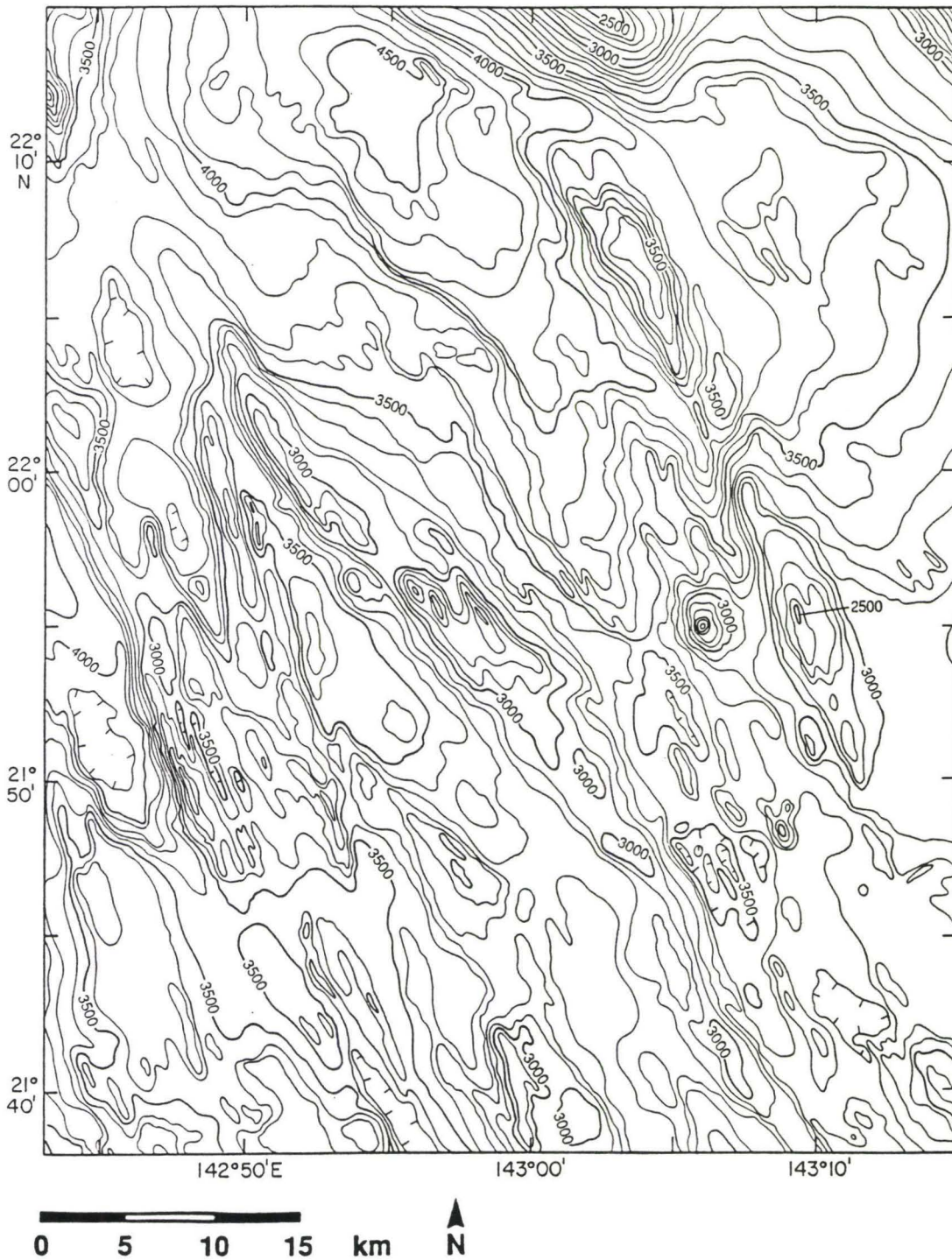


Figure 16A Bathymetry of South Province fault-block terrain and volcanic-tectonic zone. The fault-block terrain is a series of irregular ridges and valleys with predominantly low backscatter. Volcanism is concentrated in a fault-bound valley trending 330° which widens into a 4500m graben at the north end of this figure. Contour interval is 100 meters. Location of this figure is shown in Figure 10 inset.

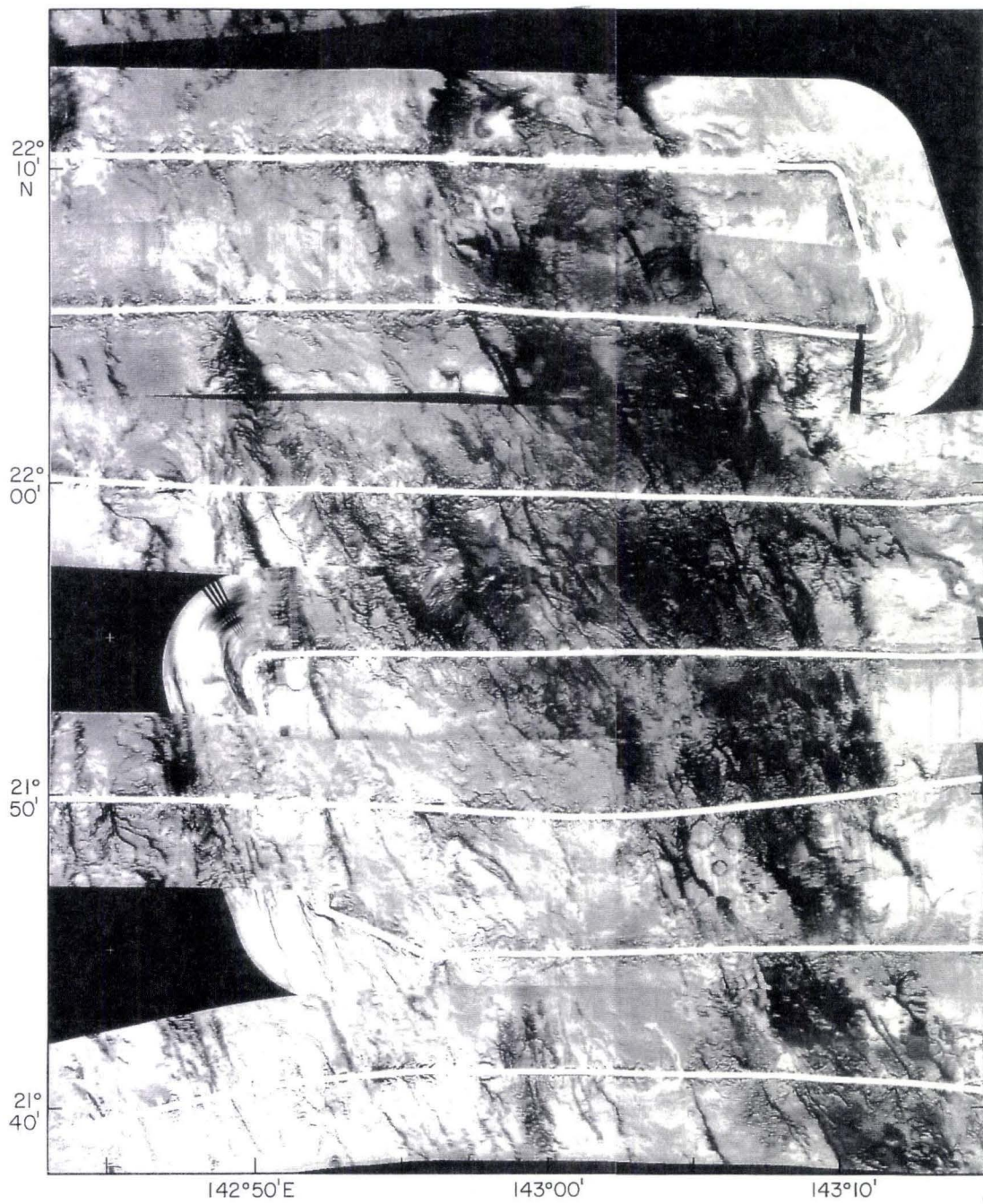


Figure 16B Side-scan of South Province fault-block terrain and volcanic-tectonic zone.

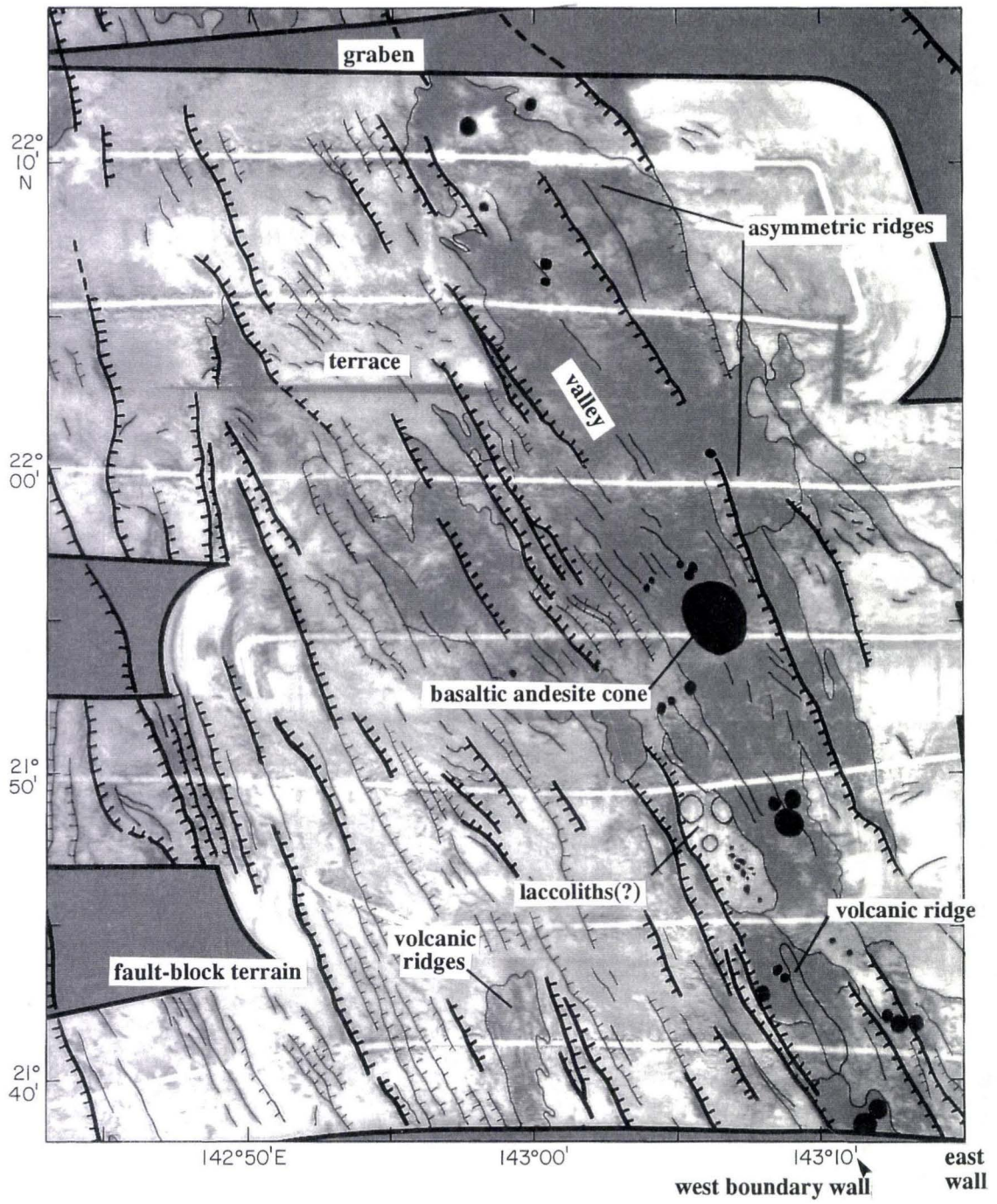


Figure 16C Interpretation of South Province fault-block terrain and volcanic-tectonic zone. Symbols are the same as Figures 12-15.

faulting and the construction of elongate volcanic ridges. 3.5 kHz echograms in this region are characterized by irregularly overlapping hyperbolae, a result of the rugged terrain (profile A, Figure 7). These characteristics are similar to abyssal hill fabric. The abyssal hill label is not used because of the inference that the topography was generated at a mid-ocean ridge spreading axis, rather than from extension and faulting of preexisting crust. The origin of these features will be discussed in more detail in Chapter 5.

Volcanic-tectonic zone

A 6 to 11 km-wide area of predominantly high backscatter is located on the east side of the trough in South Province (Figure 16B,C), and lies in a bathymetric low trending roughly 330° (Figure 16A). From southeast to northwest the low widens and deepens into a >4500m graben at the base of the scarp dividing the Central and South Provinces. The western boundary of the valley is defined by high angle east-facing normal faults (Figures 16B,C). *En echelon* fault segments step eastward in roughly 2 km lateral offsets along a 75 km length of this boundary. Individual fault segments measure 2 to 15 km in length; the longer segments have large vertical throws of 157 to 300m. Near 22°N, the steep valley wall is replaced by a 6 to 8 km wide east-stepping fault zone, creating a terrace to the northwest, and an inner valley to the north.

Fault traces are somewhat curved and anastamosing, with azimuths ranging from 310° to 340° .

The eastern boundary of the valley is also comprised of eastward stepping *en-echelon* fault segments. Segments south of $21^{\circ}50'N$ are laterally continuous along 12 to 20 km lengths. North of this latitude, a large fault can be followed along strike nearly continuously for 50km. This fault forms the steep western slope of two linear asymmetric ridges, interpreted to be fault blocks. The southern ridge is 25 km long, with its southern tip located near $21^{\circ}50'N$, $143^{\circ}10'E$. This ridge reaches a shoal depth of $<2600M$ at the widest section, measuring nearly 5km across. The acoustic image reveals high backscatter along the western escarpment and very subdued acoustic returns on the east side. The northern ridge measures 18km by 4km, with a shoal depth of 3300m.

The floor of the valley is 6 km wide across the southern swath of this survey, and lies at a depth of 3400 to 3500m (Figure 16A). Bathymetric data reveal six ridges ranging from 2 to 9 km in length, roughly 1 km wide and 100 to 300m high. The high backscatter area within side-scan image shows evidence of fissure eruptions, numerous cones, and volcanic ridges (Figure 16B,C). The largest of these ridges was dredged, as were two other locations in this area (Figure 4A) and fresh typical low-K backarc basin basalts (BABBs) and BABBs slightly enriched in K20 were recovered (Jackson, 1989). A fourth dredge, near the summit of the 4 km diameter cone located at $21^{\circ}54'N$ $143^{\circ}06'E$, recovered a

high volume of fresh basaltic andesite. This cone stands 600m above the surrounding floor of the valley. The lavas have been modeled geochemically as resulting from crystal fractionation of BABB (Jackson, 1989). Fresh pillow lavas were also collected during Alvin dive 1881 25 km SE of the southernmost of these four dredges (Stern et al., 1990).

Evidence of intrusive volcanic activity is also present on the valley floor. Circular rings of moderate backscatter intensity having one and two km diameters are found near 21°48'N, 143°05'E. The center of the rings have low acoustic returns, similar to the surrounding sedimented seafloor. These features are acoustically distinct from small extrusive volcanic cones, which exhibit high returns from the ensonified side and an acoustic shadow on the far side. These rings have bathymetric relief of approximately 100m. Unfortunately, none of the shiptrack data cross these features, so no profiles are available to confirm their shapes. Clusters of circular domes similar in size have been mapped by the Seabeam system on the flank of the East Pacific Rise (EPR) (Lonsdale, 1983) and also similar in acoustic character by SeaMARC II in the Manus Basin (Taylor, 1991). Lonsdale (1983) suggests the domes on the flanks of the EPR are actually laccoliths, raised by the intrusion of magma beneath the sediment blanket. Laccoliths are a plausible, though tentative classification for the high backscatter rings in the valley. Laccoliths are precursors to eruptive seamount volcanism (Lonsdale, 1983).

CHAPTER 4: Analysis of Faulting Patterns

Azimuth Orientations

Fault orientations were measured (as outlined in Chapter 2) in order to compare the geometry of the border and basin floor faults, and to estimate the extension direction. The survey area was divided into 8 zones: two each for the WBFZ and EBFZ (one zone north and one south of $22^{\circ}20'N$), North Province (one zone), Central Province (one zone), and South Province (two zones, southwest and south). Major ($> 100m$ vertical offset) and minor faults and lineaments ($<100m$ vertical offset) were measured separately. The large boundary scarps between Central and the adjacent provinces are interpreted as preexisting structures, and therefore not part of the same fault population. For this reason, they were not included in the analysis. The North, Central and each of the South province zones were analyzed separately in order to test whether a change in orientation of faults azimuths occurs along strike of the basin. Such a change would indicate that stress patterns within the trough are not uniform, and provide evidence for the presence of accommodation zones as described in continental rift systems (Morley, 1988; Rosendahl, 1987) and backarc rifts (Klaus et al., 1991; Taylor et al., 1991).

Fault azimuth and length results are reported in Table 1. Mean azimuths of the WBFZ are nearly due north (358° - 000°), and of the EBFZ are

Fault Azimuth Analysis Results (all zones)

Zone	Vertical Offset	N (segs)	N (faults)	Total Length (km)	Mean Azimuth (deg)	Var. (deg ²)	S.D. (deg)	mean R (norm)
NWBFZ	SML	165	22	42	000	971	31.2	0.606564
NWBFZ	LGE	527	18	262	358	1059	32.5	0.757862
SWBFZ	SML	1268	153	335	358	546	23.4	0.757862
SWBFZ	LGE	627	22	178	359	374	19.3	0.830978
NEBFZ	SML	274	51	100	322	541	23.3	0.776308
NEBFZ	LGE	354	16	92	320	492	22.2	0.738166
SEBFZ	SML	559	63	151	314	1183	34.4	0.566600
SEBFZ	LGE	260	10	102	318	301	17.3	0.842992
NBASIN	SML	852	103	342	329	300	17.3	0.848681
NBASIN	LGE	215	19	154	334	176	13.3	0.911926
CBASIN	SML	825	156	420	330	404	20.1	0.868556
CBASIN	LGE	173	23	133	338	165	12.8	0.923272
SWBASIN	SML	517	45	130	344	305	17.5	0.862302
SWBASIN	LGE	260	14	100	353	127	11.3	0.930552
SBASIN	SML	1743	291	778	328	443	21.0	0.816902
SBASIN	LGE	1399	65	530	335	189	13.8	0.918652

Table 1 Fault azimuth analysis results (8 zones). Zone abbreviations: NWBFZ, SWBFZ--north and south west boundary fault zone; NEBFZ, SEBFZ--north and south east boundary fault zone; NBASIN--north province; CBASIN--central province; SWBASIN--western half of south province; SBASIN--eastern half of south province. Vertical offsets: SML--faults < 100 m; LGE--faults > 100 m; N segs--total number of digitized straight-line segments; N faults--total number of faults; Total length--cumulative length of all faults in km; Mean azimuths--in degrees; Var-variance; S.D. standard deviation; mean R--normalized mean length of sector diagram bins.

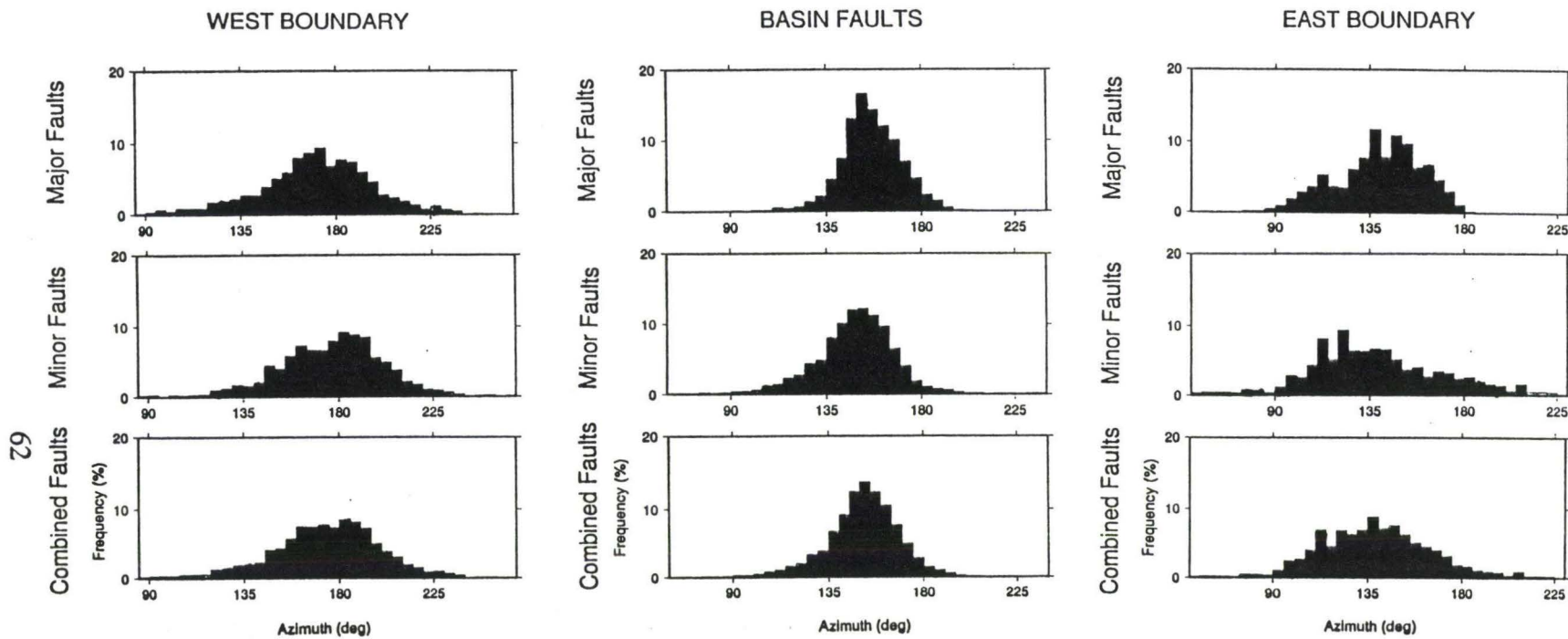
northwesterly (314° - 322°). Individual azimuths are highly variable, with standard deviations as high as 34° . In all zones except the northern half of the WBFZ, the minor fault azimuths have higher standard deviations than the major faults. Minor faults have more variable orientations because they alleviate small local stresses. The mean azimuths of three of the four basin floor zones are surprisingly uniform, ranging from 334° - 338° (large faults) and 328° - 330° (small faults). Mean orientations of faults in the southwest basin zone are more northerly (large faults 353° , small faults 344°). The range of mean fault orientations is smaller than their respective standard deviations (12° to 21°), indicating there is not a significant change in orientation of faults along strike of the basin floor.

The basin floor fault zones were combined for graphical presentation as they are not distinct populations statistically. The north and south halves of the border fault zones were combined as well, to ensure adequate sample sizes of these populations. The combined results are listed in Table 2. Histograms of the percent frequency of digitized straight-line fault segments in each 5° azimuth bin are shown in Figure 17. The distribution of basin floor fault azimuths is gaussian for both major and minor faults, forming clear, sharp peaks when plotted as histograms (Figure 17). The azimuths of faults from the WBFZ form a broad gaussian distribution, reflecting a higher variance in the data compared to the basin floor faults. Orientations of minor faults of the EBFZ form a very

Fault Azimuth Analysis Results (combined zones)

Zone	Vertical Offset	N (segs)	N (faults)	Total Length (km)	Mean Azimuth (deg)	Var. (deg ²)	S.D. (deg)	mean R (norm)
EBFZ	LGE	614	26	194	319	441	20.3	0.792619
EBFZ	SML	833	114	251	318	977	31.3	0.644698
COMBINED		1447	140	444	318	737	27.2	0.709105
WBFZ	LGE	1154	40	441	352	712	26.7	0.638184
WBFZ	SML	1712	175	378	358	591	24.3	0.740683
COMBINED		2866	215	819	355	647	25.4	0.681472
BASIN	SML	3657	595	1670	330	393	19.8	0.831125
BASIN	LGE	2047	121	917	337	186	13.6	0.901882
COMBINED		5704	716	2587	331	348	18.6	0.850340
total cumulative length of all faults				3850	km			

Table 2 Fault azimuth analysis results (combined zones). The north and south halves of the border fault zones were combined to increase the sample size of the fault populations. The basin floor zones were combined because statistically they are not distinct populations. These data are illustrated in the histograms of Figure 17, and sector diagrams in Figures 18-20. See Table 1 for explanation of abbreviations.

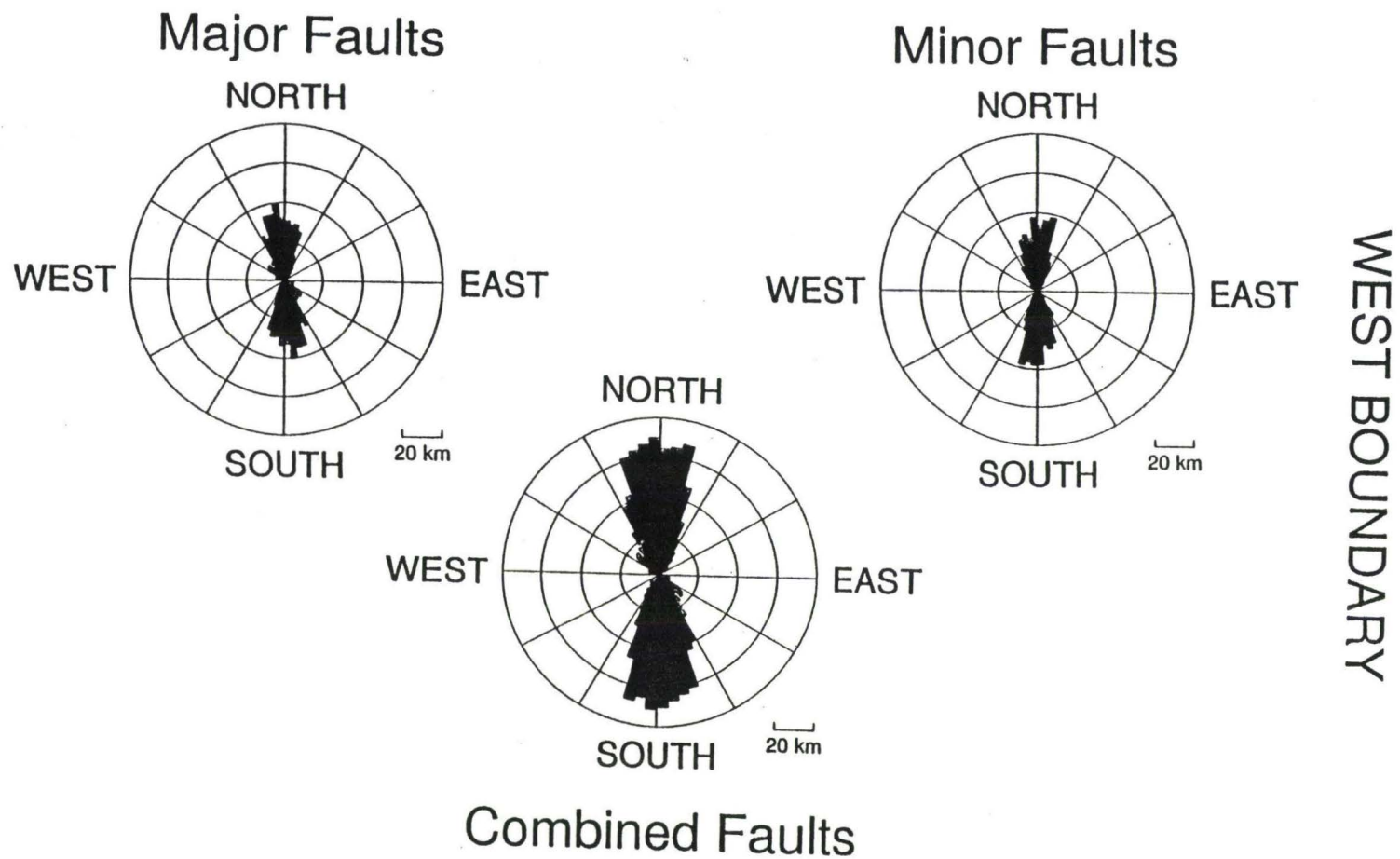


62

Figure 17 Percent frequency histograms of fault azimuth data, combined zones listed in Table 2. Major faults >100m vertical offset, Minor faults < 100m vertical offset. Note the broad distribution of border fault azimuths compared to the sharp peak of the basin floor fault azimuths.

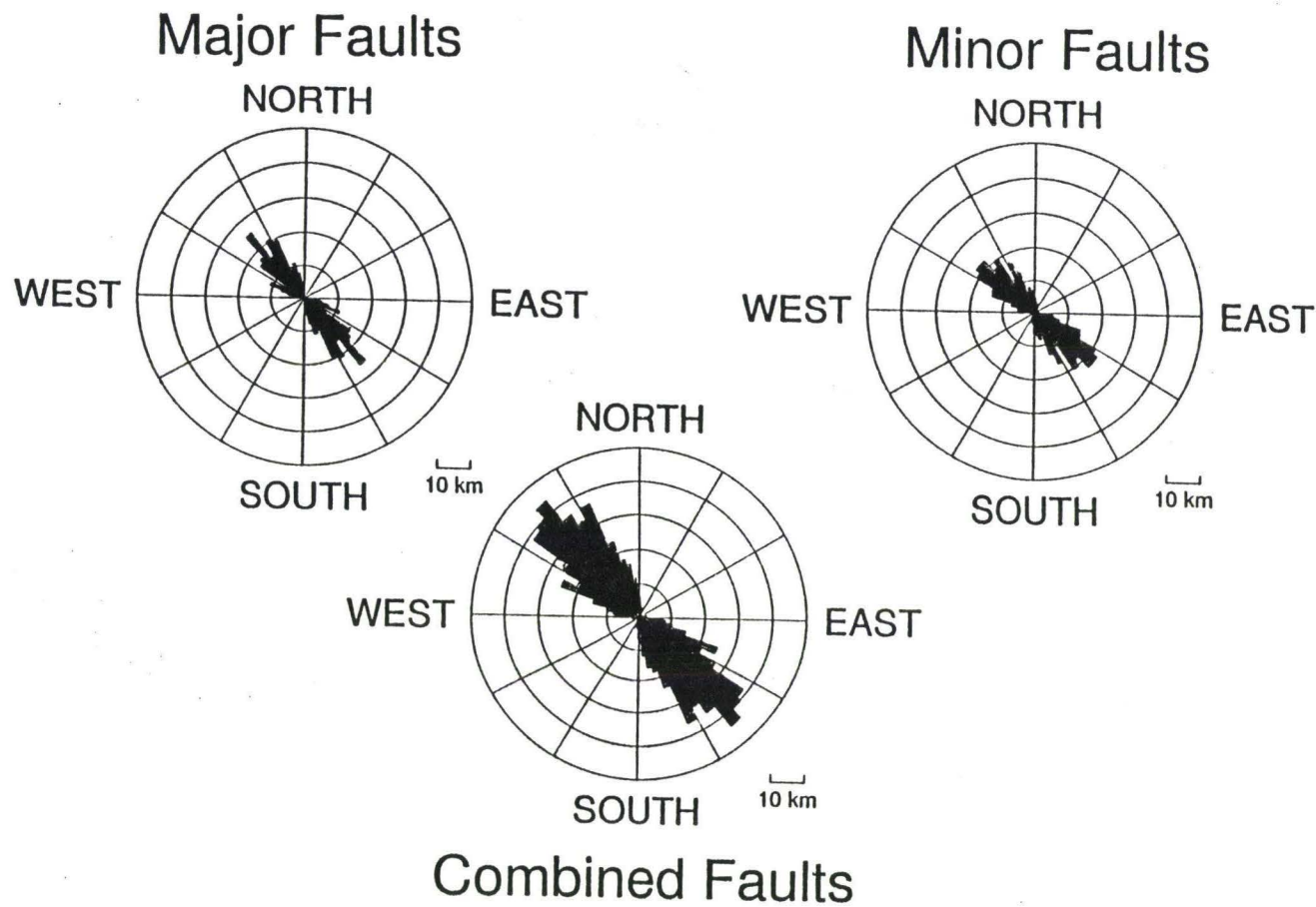
broad asymmetric peak, but when the major and minor populations are combined, a normal distribution results. The gaussian distributions of these histograms demonstrate the fault populations have been adequately sampled (Davis, 1986).

Linear faults are underrepresented by the histograms in Figure 17 because curved fault traces were digitized using points spaced more closely than straight fault traces. In order to eliminate this bias, the sector diagrams in Figures 18-20 are plots of cumulative fault lengths (rather than percent frequency of data points) at given azimuths. Data are separated into 5° bins, each plotted with the length of the bin proportional to cumulative length of faults with those azimuths. The mean orientations of the 40 major and 175 minor faults mapped in the WBFZ are 352° and 358° respectively (Table 2; Figure 18). The EBFZ is comprised of 26 major and 114 minor faults with mean orientations of 319° and 318° respectively (Table 2; Figure 19). The overall mean orientations of the WBFZ (355°) and the EBFZ (318°) are different, though statistically, high standard deviations (25° and 27° respectively) result in some overlap of azimuth orientations between the two populations. In contrast to the wide distribution of boundary fault orientations, sector diagrams of the basin floor faults display a narrow range of azimuths (Figure 20). Major, minor and combined basin floor fault azimuth data exhibit one preferred orientation, with an overall mean azimuth of 331° (Table 2).



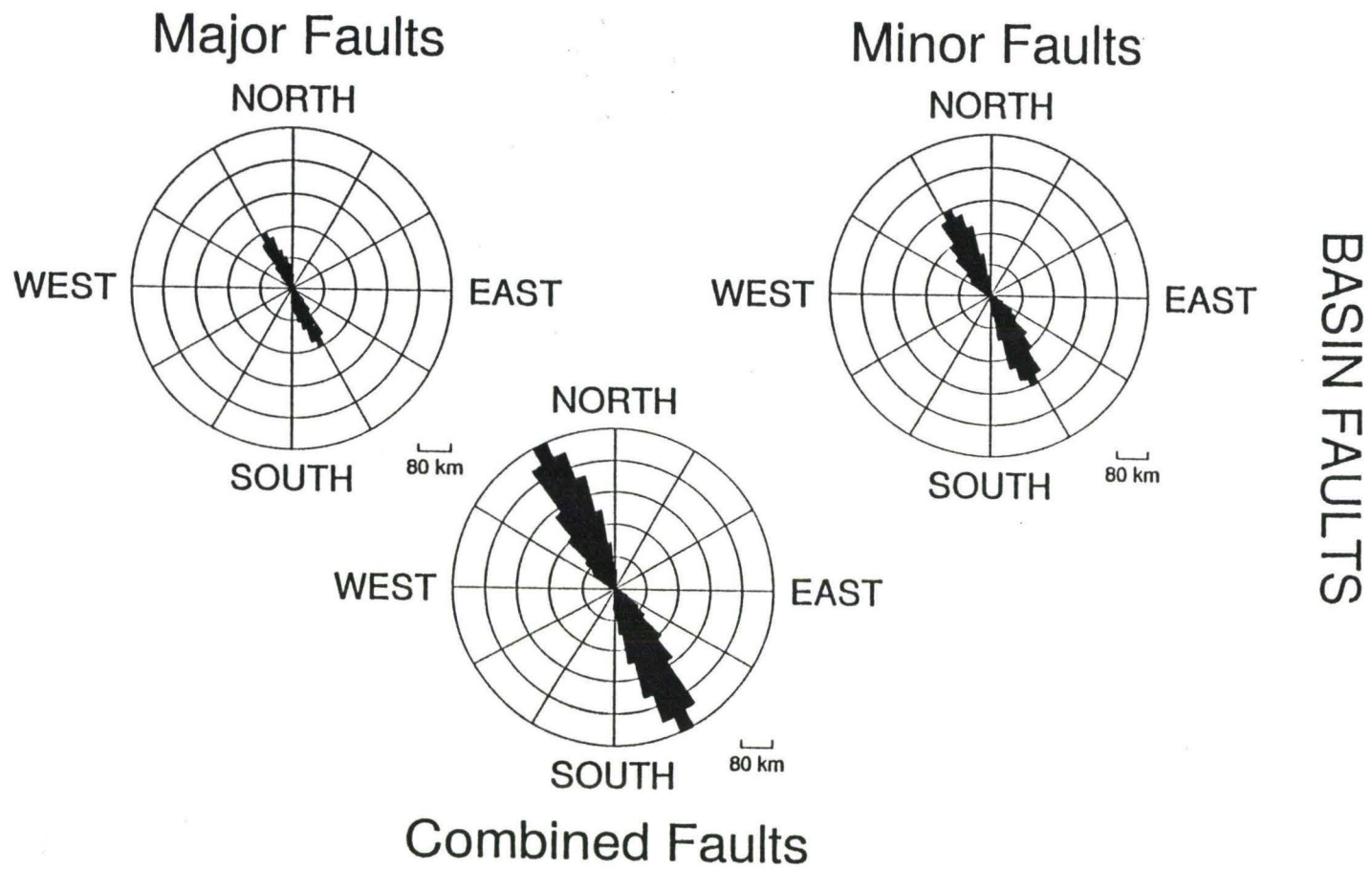
64

Figure 18 Sector diagrams of West Boundary Fault Zone (WBFZ) illustrating cumulative fault lengths in 5° azimuth bins. The mean azimuth of the WBFZ is 355°. Two dominant peaks are visually apparent (~346° and ~008°) when major and minor faults are plotted separately. However, these peaks disappear when all faults are combined, indicating further study is needed to determine whether the WBFZ meets criteria for orthorhombic symmetry statistically.



EAST BOUNDARY

Figure 19 Sector diagrams of East Boundary Fault Zone (EBFZ) illustrating cumulative fault lengths in 5° azimuth bins. The mean azimuth of the EBFZ is 318°. Two dominant peaks, indicative of orthorhombic symmetry, are not obvious in these data. Note the scale of these diagrams is not the same as in Figure 18, reflecting a contrast between the EBFZ (a small number of large offset faults resulting in low cumulative lengths) and the WBFZ (numerous small offset faults resulting in high cumulative lengths).



BASIN FAULTS

Figure 20 Sector diagrams of basin floor faults illustrating cumulative fault lengths in 5° azimuth bins. In contrast to the broad distribution of border fault azimuths, fault azimuths in the floor of the basin are dominated by a single sharp peak, with a mean azimuth of 331°.

Faulting Models

The development of faulting patterns can be described by several models. Anderson (1951) proposed the conjugate fault model, in which the faults are produced as a result of biaxial or plane strain; the axis of maximum extension is in the horizontal plane, perpendicular to the fault strike. Conjugate faults are recognized as two sets of faults of parallel strike, but opposing dip, producing a single dominant azimuthal trend. In order to explain the formation of multiple fault orientations with the conjugate model, temporally separate episodes of faulting with a different stress orientation for each azimuth are required.

Three dimensional (triaxial) strain fields may produce zig-zag fault patterns in a single episode, as predicted by both empirical and theoretical models (Oertel, 1965; Reches, 1983; Reches and Dieterich, 1983). These models predict the contemporaneous formation of four sets of normal faults arranged in orthorhombic symmetry; two faults with opposing dips and parallel strikes are separated by an acute angle less than 60° from a second pair of faults also having opposing dips and parallel strikes. Thus, contemporaneous zig-zag fault sets with equal and opposite senses of displacement can be explained by a single event of triaxial strain.

Zig-zag fault patterns with opposing dips are common in rift systems on both local and regional scales (Reches, 1983; Rosendahl, 1987; Taylor et al., 1991). As the Northern Mariana Trough is in a rifting stage of development

(Stern et al., 1984; Beal, 1987; Yamazaki et al., 1991; Martinez et al., 1992), structural similarities might be expected between this study area and Sumisu Rift, a backarc rift basin located about 1000 km to the north in the Izu-Bonin Arc (Figure 1). The boundary faults of Sumisu Rift have been described as displaying orthorhombic symmetry, indicative of triaxial strain (Klaus et al., 1991; Taylor et al., 1991). Sector diagrams of fault sets with orthorhombic symmetry should theoretically show two distinct peaks, indicative of two dominant trends. Visually, two peaks ($\sim 346^\circ$ and $\sim 008^\circ$) are apparent in the WBFZ sector diagrams when major and minor faults are considered separately (Figure 18). However, two peaks are not evident when large and small faults are combined. Distribution of the EBFZ fault azimuths is even less well-defined (Figure 19). A more rigorous statistical analysis would need to be conducted to determine whether two dominant modes truly exist. The border fault zones may have formed during the rifting of the arc in a triaxial strain field, but the evidence is not conclusive.

Faults in the basin floor apparently concur with the conjugate fault model, exhibiting one dominant trend (Figure 20), and have possibly formed under different conditions than the boundary faults (plane strain rather than triaxial strain). It is interesting that Taylor et al. (1991) did not recognize the dominance of a single trend in the floor of the rift basin in the analysis of faults in Sumisu rift, and state that "The zig-zag fault pattern is evidenced at all scales."

Klaus et al. (1991) recently reported a single dominant trend in faults and volcanic ridges in the floor of Hachijo and Aoga Shima Rifts in the Izu-Bonin Arc, and a zig-zag geometry of the boundary faults. Klaus et al. (1991) postulate that boundary fault formation modified the local strain field within the Izu-Bonin rifts from triaxial to plane strain. It is possible that the Northern Mariana Trough fault azimuth data concur with this hypothesis.

An alternative explanation for the broad distribution of boundary fault zone azimuths compared to the basin floor fault azimuths may simply be a matter of data type and scale. Boundary fault populations were mapped without full SeaMARC II coverage, and as a result, many minor faults within the boundary zones are likely to have been left out of the analysis because of the 100m resolution of the bathymetric data. In addition, the possibility exists that faults on the basin floor may have more variability than as mapped, but were not visible in the data as a result of the survey pattern (as mentioned in Chapter 2).

Estimating Extension Direction

The extension direction predicted by 3-D strain modeling is perpendicular to the bisector of the acute angle between the two fault trends in a given region (Reches and Dieterich, 1983). Wessel (1991) interpreted a zig-zag geometry of the EBFZ and the WBFZ from published bathymetric data and conducted a rigorous statistical analysis of the orientation the faults. The bisectors of the

acute angle between zig-zag fault strikes reported by Wessel (1991) are 349° and 314° for the WBFZ and EBFZ respectively. The extension direction predicted by the conjugate fault model is perpendicular to the mean strike of the faults in a given region (Anderson, 1951). The mean orientation of faults measured in the WBFZ and EBFZ in this study are 355° and 318° . Thus the extension direction predicted by Wessel (1991) and by this study are in close agreement (080° to 085°) for the opening of this region of the trough. If the EBFZ formed synchronously with the WBFZ, and under the same strain field, its orientation (315°) requires a subsequent rotation of 40° counterclockwise relative to the West Mariana Ridge during the opening of the basin. Alternatively, if the EBFZ formed more recently than the WBFZ, and no such rotation would be required. The steep, linear morphology of the scarps of the EBFZ may arise from a more youthful origin, whereas curved traces and lower slope angles of the WBFZ possibly reflect modification by erosional processes.

CHAPTER 5: Implications for Models of Structural Development

Two prominent regional scale features of the Northern Mariana Trough are revealed by this data set: (1) the volcanic-tectonic zone, a long narrow zone of high backscatter along the east side of the basin (Figure 5A); and (2) the elevated platform of Central Province (Figure 11). Understanding the tectonic implications of these features is essential to the development of a model of structural evolution for the region.

The volcanic-tectonic zone

Active faulting and volcanism within the survey area is concentrated along the volcanic-tectonic zone. A series of four isolated deeps alternate with volcanic edifices along strike of the zone (Figures 4,10,11). These graben are all similar in size (about 15 km wide and 20 km long), and are spaced 40 to 50 km apart. Although the basal depths of the graben vary (2700m to 4500m), they all lie roughly 300 to 400 m below their respective local platforms. High and variable heat flow values have been recorded in these deeps (Murakami et al., 1989). Small rift-parallel faults that disrupt the sedimented graben floors provide avenues for magma migration, resulting in the emplacement of volcanic intrusions and growth of elongate ridges (profiles 12,15,21, Figure 6B). The alignment, spacing and volcanic intrusions of these graben are remarkably similar to deeps

described in the Northern Red Sea, which are proposed to be the sites of future seafloor spreading cells (Bonatti, 1985; Martinez and Cochran, 1988; Cochran and Martinez, 1988). The volcanic-tectonic zone may be interpreted as an incipient plate boundary zone.

Three volcanoes (Nikko Seamount, Seamount A and Seamount C) are spaced equally in between the graben along the volcanic-tectonic zone. These volcanoes all lie at the intersection of major structural boundaries (Figures 4,10,11). Nikko Seamount is situated at the top of an east-west trending scarp, and the intersection of the volcanic-tectonic zone with the active volcanic arc. An orientation change in the trend of the volcanic-tectonic zone occurs across the area surrounding Nikko. Due south of Nikko, lineaments in the north wall of the graben trend 350° (Figure 13B). The walls of the graben north of Nikko have a more westerly trend of 320° . This evidence, combined with the differential subsidence between the platform on which Nikko lies, and the floor of North Province (Figure 11) imply that the volcanic cones southwest of Nikko and the northeast trending volcanic field (Figure 13B) are accommodating differential strain between segments of the rift basin. Strain related to the intersection of the volcanic-tectonic zone, and the EBFZ, is causing the complex morphology of Nikko's edifice.

Seamounts A and C are also located at major structural boundaries (Figures 10,11). These edifices are being constructed at the top of large scarps,

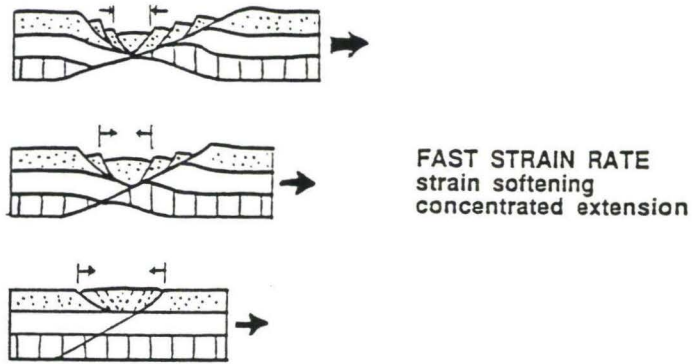
located at the intersection of the volcanic-tectonic zone and the boundaries of the elevated platform of Central Province. Seamount B lies on the edge of major east-facing faults bounding the graben in Central Province (Figure 11,15A). The locations of smaller volcanic features are also structurally controlled. Volcanic ridges, cones and lava flows within the volcanic-tectonic zone are distributed along faults, and at the tips and edges of large fault blocks. This suggests that faulting affects where volcanism is localized and distributed on the seafloor. Brittle deformation patterns therefore control the distribution of volcanic activity in the volcanic-tectonic zone.

Normal faults within the volcanic-tectonic zone are all sub-parallel to the trend of the zone (Figure 8). Minor changes in the overall orientation of the zone are primarily accommodated by *en echelon* offsets. Near 22°N, the volcanic-tectonic zone widens northward to 20 km, with *en echelon* faults forming an upper terrace and an inner valley (Figures 10,16A). Active volcanism is concentrated into the eastern valley (Figure 16B). However, the active volcanic-tectonic zone to the northwest is aligned with the upper terrace (Figures 5A,10). This offset of the active volcanic activity within the zone occurs near a 15 km west-stepping offset in the EBFZ (22°10'N, Figures 10,12). Although the style of faulting does not change north and south of this offset, the style of volcanism does. North of 22°10'N, the volcanoclastic aprons of Seamounts A,B and C are intermixed with elongate ridges and small cones. South of 22°10'N, such

seamounts are absent. This change in volcanic style may be related to the increased distance from the volcanic arc (Fukujin is 40 km east) or the development of a spreading center south of 22°N, and will be discussed in more detail later.

The location of the volcanic-tectonic zone on the arc side of the trough is probably related to lithospheric strength. Higher heat flow and thicker crust have been shown to weaken the continental lithosphere (Vink et al., 1984; Kusznir and Park, 1987). The lithosphere is appreciably weaker if the crust is thick because the quartz-feldspar rheology of the crust is weaker than the olivine rheology of the mantle. Taylor et al. (1991) infer that the locus of rifting in the Izu-Bonin Arc is controlled by a linear zone of lithospheric weakness caused by the arc volcanoes. The location of the volcanic-tectonic zone on the east side of the basin may result from the weaker lithosphere close to the arc, as Taylor et al. (1991) suggest for the Izu-Bonin rift basins.

The process of lithospheric extension causes a thinning of the crust (which strengthens lithosphere) and an increase in geothermal gradient (which weakens lithosphere) (Figure 21; Kusznir and Park, 1987). If the lithosphere is thinned slowly, the proportion of olivine-dominated rheology increases the overall strength of the lithosphere, and subsequent deformation will move laterally into weaker, previously undeformed crust (Kusznir and Park, 1987). A slow rate of extension in the Northern Mariana Trough may cause the zone of active faulting



Kusznir and Park, 1987
Extensional strength of the continental lithosphere depends on geothermal gradient, crustal composition and thickness.

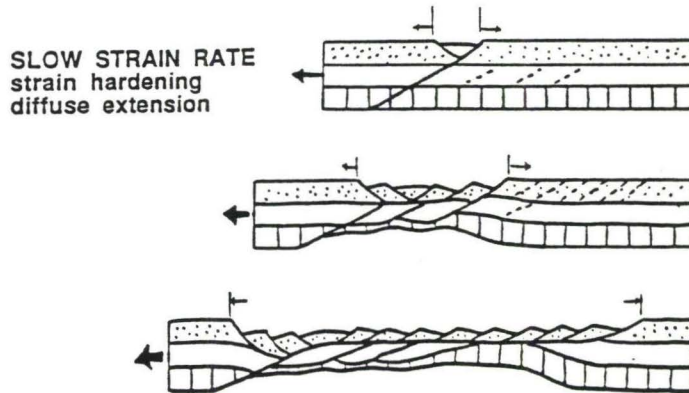


Figure 21 Lithospheric strength model of Kusznir and Park (1987). This model assumes the continental lithosphere is composed of three layers with differing rheologies. The top crustal layers are weak (dotted layer is quartz-dominated; white layer is feldspar-dominated) compared to the olivine-dominated rheology in the upper mantle (bottom layer with vertical lines). The upper three cross sections show that at fast strain rates extension remains localized because of the high geothermal gradient produced by rapidly thinning the lithosphere. The lower three cross sections illustrate diffuse extension that results from slow strain rates, as crustal thinning strengthens the lithosphere. Rheological and lithospheric strength factors may explain how the Northern Mariana Trough has widened by rifting without producing a spreading center.

to shift eastward (arcward) through time, inhibiting the formation of a spreading center. This model would apparently promote diffuse extensional deformation, however, and some other mechanism is required to explain why the active volcanic-tectonic zone is concentrated in a 20 km wide zone. This hypothesis might be tested by calculating the amount of extension (beta value, McKenzie, 1978) and constraining the strain rate. Multi-channel seismic data are needed in order to constrain the dip measurements required to perform this calculation.

Elevation of Central Province

As the Mariana Trough widens southward, changes in morphology might be expected to reflect successive stages of rifting. As the amount of extension increases, crustal thinning and subsidence should occur. The occurrence of the elevated platform of Central Province (Figure 11) is therefore an interesting problem. Bouguer gravity anomalies over the survey area reflect density anomalies that can be caused by large scale variations in crustal thickness, and partitioning of the basin into distinct tectonic domains (Martinez et al., 1991). A Bouguer low in the area of Central Province indicates that the crust may be thicker compared to the crust of the North and South Provinces. Thicker crust of Central Province may result from a smaller degree of extension, and thus less crustal thinning and subsidence by faulting, compared with the regions to the north and south. It may be argued that the width of the basin should be

narrower here if it has not been extended as far. However, this is not necessarily the case, as the initial configuration of the rift system is unknown.

An apparently smaller degree of extension in Central Province compared with the other provinces could result from (1) a temporal difference in the onset of extension between the regions, i.e., the onset of rifting in Central Province was later than the other two provinces, resulting in less total extension; or (2) a rate difference between the regions, i.e., Central Province is being extended at a slower rate than the other two.

If there is a temporal difference in the onset of rifting, and Central Province began rifting after North and South Provinces, rifting must be propagating from both the north and the south simultaneously, with Central Province caught in the middle. There is, however, no morphologic or structural evidence of a southward-propagating rift in North Province. Beal (1987) identified three northward propagating rifts in South Province that he suggested become progressively younger as they step eastward. The basin floor faults in South Province are overprinting large scarp that marks the southern boundary of Central Province (Figure 15B). Relative age relationships require that these faults propagated through the region after the formation of the scarp. However, these faults cross-cut features previously identified as pseudofaults by Beal (1987), and thus are inconsistent with the propagating rift hypothesis (Hey, 1977; Hey et al., 1980) and the model of Courtillot (1982). This evidence suggests that

either a temporal difference in the initiation of rifting between provinces is unlikely, or the progression of extension proceeds by a mechanism other than simple rift propagation.

If there is a difference in extension rates between Central Province and the adjacent provinces, evidence of shear stress between the regions would be expected. There is no clear evidence that the bounding scarps of Central Province are experiencing strike-slip motion. Rift-parallel fabric extends through the southern province boundary (Figures 5,15B) and seismic data show evidence of recent normal faulting on the northern boundary (profile 13, Figure 6B), contrary to a model requiring shear. Differential rates of extension within the survey area are implausible.

If Central Province has been extended the same amount as the other regions, either the crust of Central Province was originally thicker than the surrounding areas, or some other factor(s) has (have) prevented crustal thinning and subsidence. An increased magma supply to Central Province relative to the other two provinces is one possible explanation for the thicker crust. As the region is stretched, extension is accommodated by magma injection into fractures, in addition to brittle failure. Magma that fails to migrate upward into fractures may be underplated onto the base of the crust as well, further inhibiting crustal thinning. As long as the magma supply is high enough for intrusion and underplating to keep pace with faulting, crustal thinning will be inhibited.

A mechanism is required for a higher magma supply rate in the Central Province relative to the other two provinces. Bloomer et al. (1989) determined that the typical spacing of large edifices in the Volcano and Mariana arcs is 50 to 70 km. As Nikko and Fukujin are separated by 170 km, there is an anomalously large distance between them. It is plausible that point source conduits for magma generated in this vicinity have not developed because faulting continuously destroys the system as it evolves. Instead of producing one large arc volcano, smaller edifices and numerous elongate ridges develop as lava flows are extruded along faults. This mechanism fails to explain, however, why this platform has sharp tectonic boundaries.

On the rift to spreading transition

The large tilted fault-block morphology of North Province (profile 15, Figure 6B,11) is comparable to structures observed in Sumisu Rift in the Izu-Bonin Arc. Comprehensive mapping of the Sumisu Rift in the Izu-Bonin Arc has demonstrated that structures observed in backarc rift basins can be comparable both in scale and structural style to continental rifts (Brown and Taylor, 1988; Klaus, 1991; Taylor et al., 1991). Taylor et al (1991) propose a two-stage model for the formation of Sumisu Rift, which is based on a model proposed earlier by Cochran and Martinez (1988) and Martinez and Cochran (1988) to describe the transition from continental to oceanic rifting in the

Northern Red Sea. This Northern Red Sea model is discussed as a possible analogy for the northernmost part of the Northern Mariana Trough.

In the Northern Red Sea model, Cochran and Martinez (1988) and Martinez and Cochran (1988) propose that a series of linked, asymmetric half-graben can accommodate the first 35 km of extension (Stages A and B) (Figure 22). A more symmetric profile is then developed by widespread faulting across the rift (Stage C). Tectonic activity becomes concentrated in a well defined axial depression by Stage D. Intrusion of basaltic magma within the axial depression occurs in small deeps located halfway between rift segments, which eventually coalesce to form a continuous spreading center (Stages E and F). The pattern of faulting and crustal breakup is proposed to control the distribution of extension in the Red Sea (Martinez and Cochran, 1988; Cochran and Martinez, 1988); this mechanism is consistent with the features observed in this study area.

The concentration of volcanism and faulting within the volcanic-tectonic zone is compatible with stage D of the Northern Red Sea model. However, the fault-block morphology of North Province has an asymmetric profile (profile D, Figure 7). A central axial deep in the Northern Red Sea is the focused zone of extension and greatest subsidence. The greatest subsidence in the Northern Mariana Trough is not always along the volcanic-tectonic zone (profile A, Figure 7). The magmatic arc complicates modeling of the Mariana Trough. In the Red Sea, magmatic intrusions are emplaced in the center of the deeps, halfway

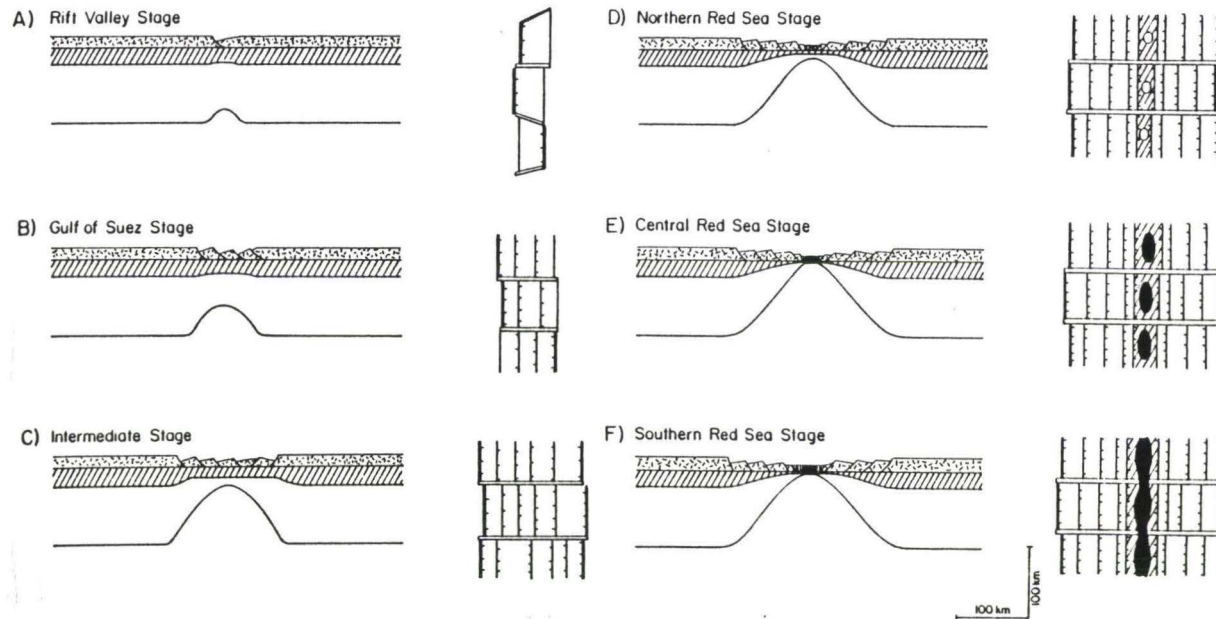


Figure 22 Rift to spreading transition model of the Northern Red Sea (Cochran and Martinez, 1988). Each stage is illustrated by a cross sectional view on the left and corresponding map view on the right. Initial rifting forms a series of linked asymmetric half graben which develop symmetric profiles by widespread faulting (A-C). Tectonic activity then becomes concentrated into an axial depression. Small deeps within the axial depression are intruded by basaltic magma (D). A continuous spreading center is eventually formed by coalescence of the basaltic intrusions (E-F). The structure of the volcanic-tectonic zone in the Northern Mariana Trough is consistent with stage D of this model, although the profile of the rift basin is asymmetric.

between segmented sections of the rift (Martinez and Cochran, 1988; Cochran and Martinez, 1988). This pattern is observed in the Northern Mariana Trough, but not exclusively. Intrusions are also initiated on the flanks of the seamounts located at major structural boundaries (Figures 14,15). The elevated platform of Central Province, possibly caused by an increased magma supply, is evidence that spatial variations exist in the mode of extension during the opening of the backarc. The North, Central and South structural provinces within this study area do not necessarily represent successive stages in the development of the basin.

The rugged morphology of South Province has been proposed earlier as seafloor spreading fabric, and the large scarp dividing Central and South Provinces as a transform fault (Beal, 1987). Because structural features analogous to continental rifts are observed in North Province, a transition from rifting to seafloor spreading across Central Province is required by Beal's model. Reprocessing of the side-scan data, the addition of 3.5 kHz data, and modeling of magnetics and gravity data (Martinez, 1991) have provided the opportunity to reevaluate whether the volcanic-tectonic zone has evolved into a true plate boundary south of 22°N.

If seafloor spreading generated the crust south 22°N, the volcanic-tectonic zone of South Province is the neovolcanic zone of a spreading axis, and the central fault-block terrain consists of abyssal hills generated at the axis. The

structures should be comparable to a slow-spreading axis such as the Mid-Atlantic ridge, where the spreading half-rate varies from 1.1 to 1.8 cm/yr (Malinverno, 1990). At the Mid-Atlantic Ridge, active faulting is restricted to the axial zone (Searle and Laughton, 1977; Macdonald and Atwater, 1978; Macdonald, 1983; Kong et al., 1988; Malinverno, 1990); faults are dominantly inward facing (Carbotte and Macdonald, 1990); median valley relief is observed to vary from 600 to 2100m; and abyssal hills are no larger than axial valley relief (usually about half) (Malinverno, 1990).

The volcanic ridges and small cones in the high backscatter zone of South Province are located in a long narrow valley (Figure 16), consistent with characteristics expected in the neovolcanic zone of a mid-ocean ridge spreading center. The valley is highly asymmetric in cross section (Figure 16). A 60 km long ridge forms the steep western boundary with relief of 400 to over 1000m. There is not a distinct eastern boundary of this valley near 21°45'. North of 21°50', the eastern boundary is formed by two elongate, discontinuous ridges. The resulting cross sections are 10 to 20 km wide and have alternating asymmetries along strike. In a qualitative sense, these structures resembles rifted fault-block topography. However, slow-spreading ridges may be structurally complex; cycles of alternating tectonic and volcanic activity have been proposed within a given location through time (Macdonald, 1986). The structures produced during tectonic cycles of a slow spreading ridge may not differ

significantly from those produced by rifting of preexisting crust. A qualitative structural description of the province does not adequately distinguish between a rifting and spreading models.

A quantitative method for distinguishing between structures originated through rifting and those originated by spreading was recently proposed by Cowie et al. (1991). These authors observe that faults in continental rifts follow power-law distributions in length and spacing. By contrast, faults on the East Pacific Rise follow exponential distributions (Cowie et al., 1991). Based on these observations, Cowie et al. (1991) suggest that there is a fundamental difference in the process by which faults in oceanic ridges and continental rifts are generated. Faults at mid-ocean ridges form in a very narrow zone at the ridge axis, are active for a short period of time, and are subject to a consistent stress field (Cowie et al., 1991). Whereas the structural morphology of mid-ocean ridges is strongly dependant on spreading rate (e.g. Macdonald, 1983), and spreading rates calculated for the Mariana Trough at 18°N are 2.15 cm/yr or less (Bibee et al., 1980; DSDP Leg 60), it is not known whether faults generated by a slow spreading center in the Mariana Trough would follow the same exponential pattern as EPR faults. If comparable studies are conducted on the Mid-Atlantic Ridge and yield similar results, this characteristic may become a viable test for the origin of these faults in the future, and provide justification for collecting new side-scan data suitable for a quantitative structural study. Until such time,

other lines of evidence must be examined to distinguish between rifting and spreading models.

Increasing sediment cover causes a gradual decrease in backscatter intensity with distance from the East Pacific Rise spreading axis (Macdonald et al., 1989; Hagen et al., 1990; Perram and Macdonald, 1990). A SeaMARC II swath across the southern Mariana Trough also reveals a gradual decrease in backscatter to the west of the proposed spreading axis (Hagen et al., 1992). Contrary to these observations, the zone of high backscatter in the South Province volcanic-tectonic zone ends abruptly in the normalized side-scan image (Figure 5A). An abrupt decrease in backscatter to the east can be attributed to rapid cover by volcanoclastic sediments shed from the Mariana arc (Hagen et al., 1992); however, an abrupt change to the west is apparently inconsistent with a spreading model.

Active faulting along a mid-ocean ridge is restricted to a narrow zone about the spreading axis, at both low and moderate spreading rates (e.g. Searle and Laughton, 1977; Macdonald and Atwater, 1978; Kong et al., 1988; Edwards et al., 1991). Faults along the WBFZ and EBFZ disrupt recent sediments (Fig 6, 7), indicating that these border fault zones are still active. Faulting patterns in the Mariana Forearc near 22°N are also consistent with current activity of the EBFZ (Wessel, 1991). Continental rifting models propose a progressive focussing of extensional deformation to a narrow region during the transition to

seafloor spreading (Chorowicz et al., 1987; Cochran and Martinez, 1988; Martinez and Cochran, 1988; Buck, 1990). Active deformation in the border fault zones suggests that seafloor spreading has not developed at this latitude; extensional strain would be accommodated by the spreading axis rather than a zone broad enough to encompass the border faults (Wessel, 1991).

If seafloor spreading is assumed in South Province, the width of the central fault-block terrain would represent the width of spreading-derived crust. Assuming half rates of 1-2 cm/yr, spreading has occurred for about 1 to 2 million years to produce this amount of crust. Yamazaki et al. (1991) interpret lineated magnetic anomalies in the trough between 21°N and 22°N as seafloor spreading anomalies. Martinez (pers. comm, 1992) offers an alternative interpretation of the magnetic data; lineated magnetic anomalies may be the result of structurally controlled intrusions, rather than seafloor spreading. Magnetization highs correlate with high backscatter areas in the side-scan, and the edges and tips of faulted blocks. These correlations are observed in North Province, which is in a rifting stage of development. The character of the magnetization data does not change significantly north and south of 22°N. It does not seem plausible for the same magnetization characteristics to be caused by a different mechanism (i.e. rifting north of 22°N and spreading south of 22°N).

Bouguer gravity data in the Northern Mariana Trough are dominated by positive anomalies which imply the crust has been thinned (Martinez et al.,

1991). There are places within the trough where Bouguer lows occur near bathymetric deeps, suggesting low density material (possibly partial melt zones) may underly them. These lows are discontinuous however, and lead Martinez (pers. comm. 1991) to conclude they are not organized in the form of a spreading axis between 20°N and 24°N.

In a petrologic study of the rocks dredged in the Northern Mariana Trough (locations indicated by circles, Figure 4A), backarc basin basalts (BABBs) were discovered both north and south of 22°N (Jackson, 1989). Jackson (1989) concluded that these rocks were formed by a similar degree of melting, but at higher temperatures and pressures than MORBS and rocks collected at 18°N. Many diverse rock types occur in close proximity of each other, leading Jackson to conclude that any generalization correlating petrochemistry with tectonic setting may not rigorously apply. The coexistence of BABB with the andesite cone in the high backscatter zone of South Province (Figure 16) indicates that isolated pockets of magma are accumulating long enough for crystal fractionation to occur, but is not conclusive evidence that area is spreading like a mid-ocean ridge.

The structural evidence presented in this paper does not conclusively discriminate between a rifting or spreading model for the origin of the features in South Province. However, when considered along with magnetics, gravity and petrologic data, a rifting origin is preferred. The rift to spreading transition is

now proposed to occur more than 100 km south of this study area, between 19°N and 20°N (Martinez et al., 1992; Fryer et al., 1992). The location of the transition has recently been identified using magnetic, gravity and SeaBeam data collected during a December 1991 sampling cruise, and preexisting SeaMARC II data. The remarkable aspect of this discovery is that the width of the Mariana Trough is over 200 km near 19°30'N, yet seafloor spreading appears to be a recent development there (Martinez et al., 1992).

A tectonic cartoon

An asymmetric extension model for the Northern Mariana Trough is consistent with the steep scarps of the EBFZ, asymmetric heat flow (Murakami et al., 1989), location of the volcanic-tectonic zone on the arc side of the basin, and lack of a well-developed spreading center. Predominantly low backscatter intensities on the west side of the trough indicate sediment cover, and presumably age, is greater to the west. A band of negative seafloor magnetization along the west side of the trough, and positive magnetization along the volcanic-tectonic zone on the east side support this interpretation (Martinez, pers. comm. 1991).

Figure 23 is a tectonic cartoon illustrating the rifting of the Northern Mariana Trough. This sketch is based on a model developed for the Central Volcanic Region of New Zealand (Stern, 1987). Land-based observations of the

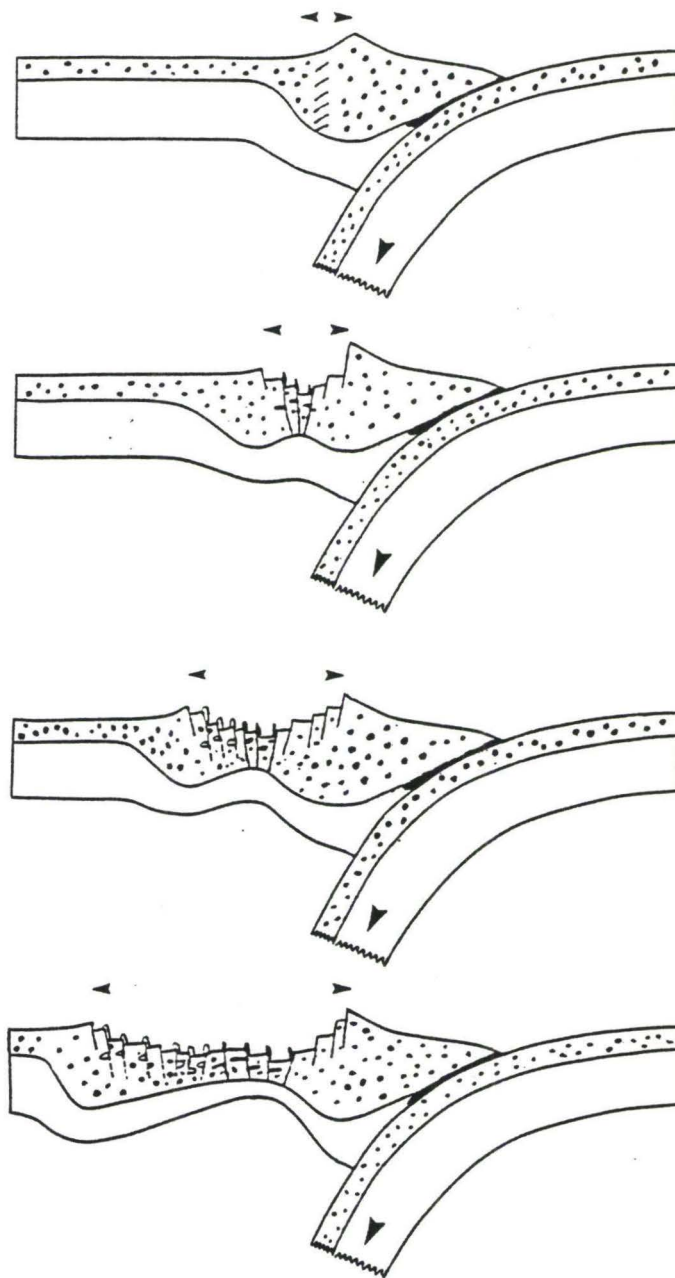


Figure 23 A tectonic cartoon of the rifting of the Northern Mariana Trough, based on a model proposed by Stern (1987) for the rifting of the Central Volcanic Region in New Zealand. Large arrows show the motion of the Pacific lithosphere being subducted underneath the Philippine Sea Plate. The crust is represented by the dotted layer, and the lower layer is the upper mantle. Rifting is initiated near the arc line, as indicated in the top cross-section by the diagonal lines. Progressive extension of the backarc is represented by the small arrows. Normal faulting results in extension and thinning of the crust. Active faults provide conduits for magmatic intrusions, shown in black. The active zone shifts laterally toward the arc through time. The reduction of faulting in the west results in waning of magmatic activity there.

structure and heat flow within the continental lithosphere led Stern (1987) to formulate a model of asymmetric backarc extension. In Stern's model, the western edge of the platelet between the trench and the backarc is progressively faulted toward the forearc, inhibiting the development of a simple, symmetrical spreading center. The cartoon in Figure 23 illustrates the rifting of the Mariana Arc and extension of the trough through time. Normal block faulting causes subsidence and thinning of the crust. Active faults provide conduits for the emplacement of dikes, sills, and lava flows, illustrated in black. At some later time, the active zone of extension shifts laterally toward the arc, possibly because of the increased strength of the lithosphere from thinning of the crust. The reduction in faulting activity to the west results in the waning of magmatic activity there. This process produces a complex, heterogeneous crustal section composed of rifted blocks of preexisting crust and intruded material.

Conclusions

The Northern Mariana Trough is in a rifting stage of development between $21^{\circ}30'N$ and $23^{\circ}N$. The trough widens from 70 km near $23^{\circ}N$ to 135 km near $21^{\circ}30'N$. The cartoon in Figure 24 summarizes the major tectonic elements in this survey area. Fault zones bounding both sides of the trough are active. The orientation of boundary fault azimuths is highly variable compared to faults in the basin floor, which exhibit a preferred orientation of 331° . The

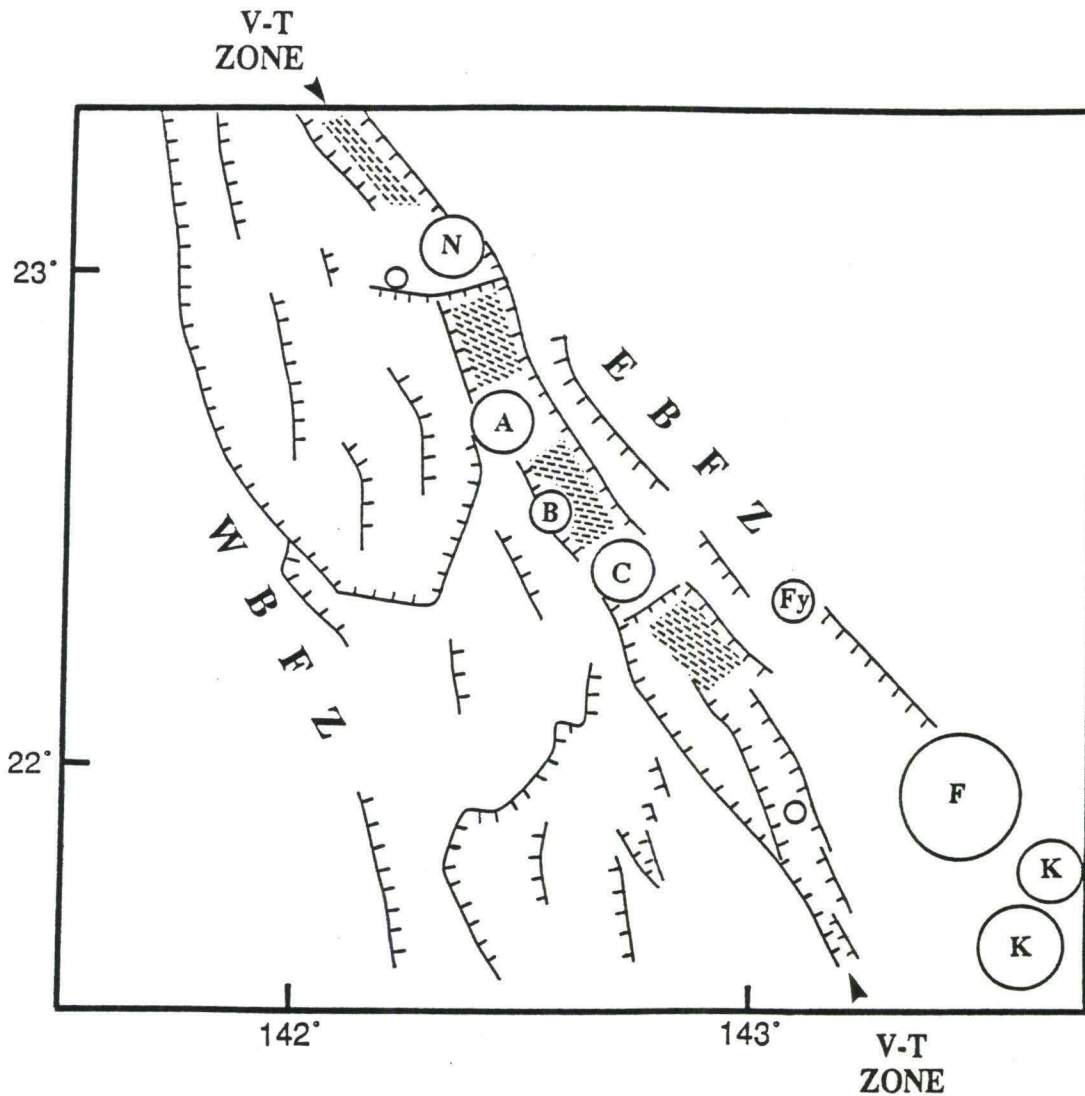


Figure 24 Tectonic sketch map of the survey area. Major faults are shown with ticks on the down-dropped side, fault-bound graben are illustrated with a diagonal pattern, and volcanoes are represented by circles. Abbreviations are the same as Figures 10 and 11. The distribution of volcanic features within the volcanic-tectonic zone is controlled by major structural trends and faulting. If extensional activity remains concentrated in this zone, it may eventually evolve into a backarc spreading center.

varying morphologies of three structural provinces along strike of the basin may represent a spatial variation in the style of extensional response rather than time-successive stages in the opening of the trough.

Active faulting and volcanism is concentrated into a 6 to 20 km wide zone along the arc side of the basin. This zone intersects the active volcanic arc at Nikko Seamount, and is 40 km from the arc near Fukujin Seamount. A series of fault-bound graben alternate with volcanic edifices along strike of this zone; volcanic seamounts, which are intermixed with elongate ridges and small volcanic cones north of 22°N , are absent south of this latitude. The change in volcanic style with latitude may be related to increased distance from the magmatic arc. Brittle deformation patterns are responsible for the distribution of volcanic activity along this zone, which may be an incipient plate boundary. Structural features in this area of Northern Mariana Trough are consistent with asymmetric extension models, and rift to spreading transition models that predict the initiation of seafloor spreading by the coalescence of discrete cells.

References

- Anderson, R.N. (1975) Heat flow in the Mariana marginal basin, *J. Geophys. Res.*, 80, 4043-4048.
- Anderson, E.M. (1951) The dynamics of faulting, Oliver & Boyd London 183 pp.
- Barone, A.M., P.F. Lonsdale and D. Puteanus (1990), Formation of axial volcanic ridges of the Mariana slow spreading center from spatial magma sources, *EOS Trans. AGU* 71: 1637-1638.
- Baker, N, P. Fryer and G. Brown, (1989) Rifting in the northern Mariana backarc basin, *EOS Trans. AGU* 70: 1313.
- Beal, K.L., (1987) The opening of a backarc basin: Northern Mariana Trough, M.S. Thesis, University of Hawaii, pp 56.
- Bergersen, D.D., (1991) A synopsis of SeaMARC II side-scan processing techniques, *Oceans 91 Proceedings*, v2: 921-926.
- Bibee, L., G.G. Shor, and R.S. Lu, (1980) Inter-arc spreading in the Mariana Trough, *Marine Geology*, 35: 183-197.
- Blackinton, J.G., (1986) Bathymetric Mapping with SeaMARC II: An Elevation-Angle Measuring Side-Scan Sonar System, Ph.D. Dissertation, University of Hawaii, 145 pp.
- Blackinton, J.G., D.M Hussong, and J. Kosalos, (1983) First results from a combination side-scan sonar and seafloor mapping system (SeaMARC II). Offshore Technology Conference, OTC 4478, p. 307-311 (+ 10 Figures).
- Bloomer, S.H., R.J. Stern, and N.C. Smoot, (1989a) Physical volcanology of the submarine Mariana and Volcano Arcs, *Bull. Volcanology* 51: 210-224.
- Bloomer, S.H., R.J. Stern, E. Fisk, and C.H. Geshwind, (1989b) Shoshonitic volcanism in the northern Mariana Arc 1. Mineralogic and major and trace element characteristics, *Jour. Geophys. Res.* 94(B4): 4469-4496.
- Bonatti, E., (1985) Punctiform initiation of seafloor spreading in the Red Sea during transition from a continental to an oceanic rift, *Nature* 316: 33-37.

- Brown, G. et al., (1988) Geological Map of Sumisu and Torishima Rifts, Izu-Ogasawara Arc, Marine Geological Map Series 31, Geol. Surv. of Japan.
- Brown, G. and B. Taylor, (1988) Seafloor mapping of the Sumisu Rift, Izu-Ogasawara (Bonin) island arc, *Bull. Geol. Surv. of Japan* 39: 23-38.
- Brown, G., (1991) Rifting of the Bonin Island Arc, Ph.D. Dissertation, University of Hawaii.
- Buck, W.R., F. Martinez, M.S. Steckler, and J.R. Cochran (1988) Thermal consequences of lithospheric extension: pure and simple, *Tectonics*, 7, 213-234.
- Carbotte, S. and K.C. Macdonald, (1991) Comparison of Sea Floor Tectonic Fabric Created at Intermediate, Fast, and Ultra-fast Spreading Ridges, EOS Transactions AGU, 456.
- Carbotte, S.M. and K.C. Macdonald, (1990) Causes of variation in fault-facing direction on the ocean floor, *Geol. Soc. Am. Bull* V 18: 749-752.
- Chorowicz, J., J. Le Fournier, and G. Vidal, (1987) A model for rift development in Eastern Africa, *Geological Journal* 22: 495-513.
- Cochran, J.F. and F. Martinez, (1988) Evidence from the northern Red Sea on the transition from continental to oceanic rifting, *Tectonophysics* 153: 25-53.
- Courtillot, V., (1982) Propagating rifts and continental break up, *Tectonics* 1: 239-250.
- Cowie, P.A. , A. Malinverno, C.H. Scholz, M.H. Edwards, (1991) Fault Strain on the East Pacific Rise: Implications for the Mechanics of Faulting at Mid-Ocean Ridges, EOS Trans. AGU, 466.
- Davis, J.C., (1986) Statistics and Data Analysis in Geology, John Wiley & Sons, 550 pp.
- Davis, E.E., R. G. Currie, B.S. Sawyer, and J.G. Kosalos, (1987) The use of swath bathymetric and acoustic image mapping tools in marine geoscience. *Marine Technology Society Journal* 20(4): 17-27.
- Ebinger, C.J., (1989) Tectonic development of the western branch of the East African rift system, *Geol. Soc. Am. Bull.* 101: 885-903.

Edwards, M.H., D.J. Fornari, A. Malinverno, and W.B.F. Ryan (1991) The regional tectonic fabric of the East Pacific Rise from 12°50'N to 15°10'N, *Journ. Geophys. Res.* 96, 7995-8017.

Eguchi, T. (1984) Seismotectonics around the Mariana Trough, *Tectonophysics* 102, 33-52.

Fiske, R.S. and E.D. Jackson, (1972) Orientation and growth of Hawaiian volcanic rifts: the effect of regional structure and gravitational stresses, *Phil. Trans. Roy. Soc. London*, 329: A, 299-325.

Fryer, P., Martinez, F., S.H. Bloomer, and R.J. Stern (1992) The Northern Tip of the Mariana Trough Spreading Axis: 19-20°N, *EOS Trans. AGU*, in press.

Fryer, P. and D.M. Hussong, (1981) Seafloor spreading in the Mariana Trough: results of Leg 60 drill site selection surveys, in D.M. Hussong et al., *Initial Reports of the Deep Sea Drilling Project 60*: 45-55, U.S. Government Printing Office, Washington D.C.

Hagen, R.A., A.N. Shor, and P. Fryer, (1992) SeaMARC II Evidence for the Locus of Seafloor Spreading in the southern Mariana Trough, *Marine Geology* 103:311-322.

Hagen, R.A., Baker, N.A., Naar, D.F., and Hey, R.N., (1990) A SeaMARC II survey of recent submarine volcanism near Easter Island, *Marine Geophys. Res.* 12, 297-315.

Hey, R.N. (1977) A new class of pseudofaults and their bearing on plate tectonics: A propagating rift model, *Earth Planet. Sci. Letters*, 37, 321-325.

Hey, R.N., F.K. Duennebieer, and W.J. Morgan, (1980) Propagating rifts on mid-ocean ridges, *J. Geophys. Res.*, 85, 2647-2658

Hussong, D.M., and P. Fryer (1983) Back-arc seamounts and the SeaMARC II seafloor mapping system, *EOS Trans. Amer. Geophys. Union*, 64, pp. 627-632.

Hussong, D.M. and P. Fryer, (1982) Structure and tectonics of the Mariana arc and forearc: drill site selection surveys, in Hussong, D.M., Uyeda, S., et al., *Init. Repts DSDP 60*: Washington (US Govt Printing Office).

Hussong, D.M. and S. Uyeda, (1981) Tectonic processes and the history of the Mariana Arc: A synthesis of the results of deep sea drilling project leg 60, in

initial Reports of the Deep Sea Drilling Project, 60: 909-929, U.S. Government Printing Office, Washington D.C., 909-929.

Jackson, M.C., (1989) Petrology and petrogenesis of recent submarine volcanoes from the northern Marian arc and backarc basin, Ph.D. Dissertation, University of Hawaii, 277 pp.

Jackson, M.C. and P. Fryer, (1991) Comment on The growth rate of submarine volcanoes on the South Honshu and East Mariana Ridges by N.C. Smoot, *Jour. of Volcan. and Geothermal Res.*, 45: 335-345.

Jackson, M.C., (1987) Petrology of Fukujin Seamount: a tholeiitic arc-front volcano of the northern Mariana island arc. *Geol. Soc. Am. Abstr. Programs*, 19: 714.

Karig, D.E., R.N. Anderson, and L.D. Bibee, (1978) Characteristics of backarc spreading in the Mariana Trough, *Journ. Geophys. Res.* 83:1213-1225.

Karig, D.E. (1971) Origin and development of marginal basins in the western Pacific, *Jour. Geophys. Res.* 76: 2542-2561.

Klaus, A, B.Taylor, G.F. Moore, F. Murakami, and Y. Okamura, (1991) Structural Evolution of Hachijo and Aoga Shima Rifts: Backarc Rifting in the Izu-Bonin Island Arc, EOS TRansactions AGU, 243.

Kong, L.S., R.S. Detrick, P.J. Fox, L.A. Mayer, and W.B.F. Ryan, (1988/89) The morphology and tectonics of the MARK area from Sea Beam and SeaMARC I observations (Mid-Atlantic Ridge 23 N), *Marine Geophysical Researches* 10, 59-90.

Krantz, R.W., (1988) Multiple fault sets and three-dimensional strain: theory and application, *Jour. of Structural Geol.* 10(3): 225-237.

Kusznir, N.J. and R.G. Park (1987) The extensional strength of continental lithosphere: its dependence on geothermal gradient, and crustal composition and thickness, from Coward, M.P., Dewey, J.F. and Hancock, P.L. (eds), *Continental Extensional Tectonics*, Geol. Soc. Special Pub. 28, pp. 35-52.

Lonsdale, P. and J. Hawkins, (1985) Silicic volcanism at an off-axis geothermal field in the Mariana Trough backarc basin, *Geol. Soc. Am. Bull* 96:940-951.

Lonsdale, P. (1983) Laccoliths(?) and small volcanoes on the flank of the East Pacific Rise, *Geology*, 706-709.

- Macdonald, K.C., (1986) The crest of the Mid-Atlantic Ridge: Models for crustal generation processes and tectonics, in The Geology of N. America Vol. M, P.R Vogt & B.E. Tucholke eds., Geological Society of America, p 51-68.
- Macdonald, K.C., R. Haymon and A.N. Shor, (1989) A 220² km recently erupted lava field on the East Pacific Rise near Latitude 8 S, *Geology* 17, 212-216.
- Macdonald, K.C. and T.M. Atwater, (1978) Evolution of rifted ocean ridges, *Earth and Planet. Sci. Letters*, 39, 319-327.
- Malinverno, A., (1990) A quantitative study of the axial topography of the Mid-Atlantic Ridge, *Journ. Geophys. Res.* V95 B3, 2645-2660.
- Martinez, F. N.A. Baker, P . Fryer, and T. Yamazaki, (1991) Rifting and Magmatism in the Northern Mariana Trough,: A 3-D gravity and magnetics study, *EOS Trans. Amer. Geophys. Union*, v72(44), p. 247.
- Martinez, F., P. Fryer, S.H. Bloomer, and R.J. Stern (1992) Rift to Spreading Transition in the Northern Mariana Trough, *EOS Trans. AGU*, in press.
- Martinez, F., and J.R. Cochran, (1988) Structure and tectonics of the northern Red Sea: Catching a continental margin between rifting and drifting, *Tectonophysics* 150: 1-32.
- Matsumoto, H., (1990) Characteristics of SeaMARC II Phase Data, *IEEE Jour. of Oceanic Engineering* 15(4): 350-360.
- McKenzie, D., (1978) Some remarks on the development of sedimentary basins, *Earth Planet. Sci. Lett.* 40, 25-32.
- Moore, G.W. (1984) Plate motion vectors illustrated on the Plate Tectonic Map of the Circum-Pacific Region, Pacific Basin Sheet, from *Circum-Pacific Map Project*, directed by J.A. Reinemund, Amer. Assoc. Petrol. Geol.
- Morley, C.K., R.A. Nelson, T.L. Patton, and S.G. Munn, (1988) Transfer Zones in the East African Rift System and Their Relevance to Hydrocarbon Exploration in Rifts, *Amer. Assoc. Petrol. Geol. Bull.*, 74(8): 1234-1253.
- Murakami, F., T. Yamazaki, E. Saito, and M. Yuasa, (1989) Rifting and spreading processes at the northern Mariana Trough, *EOS Trans. AGU* 70(43): 1313.

- Nakamura, K., (1977) Volcanoes as possible indicators of tectonic stress orientation--principle and proposal, *Journ. of Volc. Geotherm. Res.*, 2: 1-16.
- Oertel, G., (1965) The mechanism of faulting in clay experiments, *Tectonophysics*, 2, 343-393.
- Perram, L.M., and Macdonald, K.C., (1990) A one-million-year history of the 11° 45'N East Pacific Rise discontinuity, *J. Geophys. Res.*, 95, pp. 21363-21381.
- Reches, Z. (1983) Faulting of rocks in three-dimensional strain fields II. Theoretical analysis, *Tectonophysics* 95: 133-156.
- Rosendahl, B.R., (1987) Architecture of continental rifts with special reference to East Africa, *Ann. Rev. Earth Planet. Sci.*, 15: 445-503.
- Searle, R.c. and A.S. Laughton, (1977) Sonar studies of the Mid-Atlantic Ridge and Kurchatov Fracture Zone, *Journ. Geophys. Res.* 82: 5313-5328.
- Sender, K.L., A. Shor and R. Hagen, (1989) SeaMARC II side-scan processing techniques, *EOS Trans. AGU* 70(43): 1304.
- Shor, A.N., (1990) SeaMARC II seafloor mapping system: Seven years of Pacific research, *Proc. Pac. Rim 90 Congress*, III pp.49-59.
- Smoot, N.C., (1990) Mariana Trough by multi-beam sonar, *Geo-Marine Letters*, 10, pp. 137-144.
- Smoot, N.C., (1988) The growth rate of submarine volcanoes on the South Honshu and East Mariana Ridges, *Jour. Volcan. Geotherm. Res.* 35: 1-15.
- Stern, T.A. (1987) Asymmetric back-arc spreading, heat flux, and structure associated with the Central Volcanic Region of New Zealand, *Earth Planet. Sci. Lett.*, 85, 265-276.
- Stern, R.J., P.N. Lin, J.D. Morris, M.C. Jackson, P.Fryer, S.H. Bloomer, and E. Ito, (1989) Enriched back-arc basin basalts from the northern Mariana Trough: Implications for magmagenesis at convergent margins, *Earth and Planetary Science Letters* 100: 210-225.
- Stern, R.J., Smoot, N.C., and Rubin, M. (1984) Unzipping of the volcano arc, Japan, *Tectonophysics*, 102, 153-174.

Taylor, B., A. Klaus, G.R. Brown and G.F. Moore, (1991) Structural development of Sumisu Rift, Izu-Bonin Arc, *Jour. Geophys. Res.* 96 B10: 16,113-16,129.

Taylor, B., and G.D. Karner, (1983) On the evolution of marginal basins, *Rev. of Geophys and Space Phys.* 21: 1727-1741.

Taylor, B. , G.R. Brown, D. Hussong, and P. Fryer, (1988a) SeaMARC II Side-scan Acoustic Imagery of Sumisu and Torishima Rifts, Izu-Ogasawara Arc, *Marine Geological Map Series 31*, Geol. Surv. of Japan.

Tyce, R. C., (1987) Deep seafloor mapping systems--a review, *Marine Technology Society Journal* 20(4): 4-16.

Vink, G.E., W.J. Morgan and W.-L. Zhao, (1984) Preferential rifting of continents: a source of displaced terranes, *J. Geophys. Res.*, 89, 10072-10076.

Vogt, P.R., and B.E. Tucholke, (1986) Imaging the ocean floor: History and state of the art, in Vogt, P.K., and B.E. Tucholke, eds., The Geology of North America, Volume M, The Western North Atlantic Region: Geological Society of America.

Wessel, J.K., (1991) A structural analysis of the Mariana inner forearc at 22°N, M.S. Thesis, University of Hawaii, 104 pp.

Wood, D.A., Marsh, N.G., Tarney, J., Joron, J.L., Fryer, P., and Treuil, M., (1981) Geochemistry of igneous rocks recovered from a transect across the Mariana Trough, arc, forearc and trench, sites 453-461, DSDP Leg 60, in Hussong, D.M. (ed) Init. Rep. Deep Sea Drilling Proj., 60, p. 611-633.

Yamazaki, T., T. Ishihara, F. Murakami, (1991) Magnetic anomalies over the Izu-Ogasawara (Bonin) Arc, Mariana Arc and Mariana Trough, *Bull. Geol. Survey of Japan*, 42(12), pp. 655-686.